NASA CONTRACTOR REPORT

LUNAR ORBITER II

PHOTOGRAPHY

Prepared by
THE BOEING CO.
Seattle, Wash.
for Langley Research Center

NATIONAL AERONAUTICS AND SPACE ADMINISTRATION • WASHINGTON, D. C. • NOVEMBER 1967

LUNAR ORBITER II

PHOTOGRAPHY

Issued by Originator as Report No. D2-100752-2

Prepared under Contract No. NAS 1-3800 by
THE BOEING COMPANY
Seattle, Wash.

for Langley Research Center

NATIONAL AERONAUTICS AND SPACE ADMINISTRATION

For sale by the Clearinghouse for Federal Scientific and Technical Information
Springfield, Virginia 22151 – CFSTI price $3.00

CONTENTS

*The section number 2 signifies only that this report is the second in a series of numbered volumes submitted by the contractor on the Lunar Orbiter II Project. Publication of the complete series by NASA is not necessarily contemplated.

CONTENTS

ILLUSTRATIONS

ILLUSTRATIONS

ILLUSTRATIONS

TABLES

LUNAR ORBITER II

2.0 PHOTOGRAPHY

2.1 INTRODUCTION

This volume of the Lunar Orbiter Mission II final report contains a description of mission photographic planning and conduct, and analysis of the photographs. Data pertinent to analysis and interpretation of the photographs are included. A functional description of the spacecraft photo subsystem and ground reconstruction is not included but may be found in Lunar Orbiter Mission I Final Report, Boeing Document D2-100727-2 (Volume II). However, changes made on the basis of Mission I results will be discussed.

Mission II was designed to provide data on sites located in the northern portion of the Apollo landing zone. Because of the value of oblique photography for interpretation of lunar topography demonstrated on Mission I, additional photographs of this type were scheduled and taken during Mission II.

All scheduled photography was accomplished and 98.5% of the planned coverage was read out before failure of the traveling-wave-tube amplifier (TWTA) to turn on terminated the photographic phase of the mission.

2.1.1 PROJECT OBJECTIVES

Lunar Orbiter's primary objective is to provide information necessary to locate sites that meet the requirements for Apollo manned lunar landings. These requirements include the following:

- Certification of multiple sites providing for accessibility during different Apollo launch windows and recycle times (at least 2 days between launch attempts and three launch attempts each month);
- Location of areas – free of protuberances, depressions, or slopes constituting a hazard to landing – that are large enough to accommodate LM guidance errors and maneuver capabilities;
- The locations must be within the zone of ±5° latitude and ±45° longitude.

Secondary objectives are to provide data regarding the lunar environment, including energetic radiation and meteoroid flux, and selenodesy and the Moon's gravitational field by determination of spacecraft orbit characteristics and perturbations.

2.1.2 MISSION II OBJECTIVES

The objectives of Mission II, as stated in NASA Document LOTD 107-1, are:

- Primary – To obtain, from lunar orbit, detailed photographic information of various lunar areas, to assess their suitability as landing sites for Apollo and Surveyor spacecraft, and to improve our knowledge of the moon.
- Secondary – To provide precision trajectory information for use in improving the definition of the lunar gravitational field.
- To provide measurements of micrometeoroid flux and radiation dose in the lunar environment, primarily for spacecraft performance analysis.

2.1.3 PHOTOGRAPHIC MISSION SUMMARY

Injection of the spacecraft into the first ellipse was accomplished on November 10, 1966. Orbital parameters were: apolune, 1871 km; perilune, 196.26 km; and inclination, 11.95 degrees. The spacecraft was held in this ellipse for 22 orbits to permit tracking and determination of orbital parameters. Photographs were not taken from the first ellipse. Transfer to the second ellipse, having an initial perilune of 50.51 km, was successfully accomplished on November 15 at 22.52.42 GMT during Orbit 23. Following the initial camera operations to move the film leader onto the takeup reel and photographic film into the camera, photography was started over Site II P-1 on November 18 at 15:24:53 GMT during Orbit 52. Upon completion of photography, Bimat was cut on November 26 (Day 330) at 08:58 GMT. All mission photography was accomplished from the second ellipse. Mission II photography is summarized in Table 2.1-1.

Table 2.1-1: Summary Of Mission II Photography

Numerical Summary Primary Sites	No. of Sites	Frames Exposed
Three passes, eight-frame sequence per pass	1	24
Two passes, eight-frame sequence per pass	7	112
Single pass, one eight-frame sequence	4	32
Single pass, one 16-frame sequence	1	16
Secondary Sites		
Two passes, four-frame sequence each pass	1	8
One pass, four-frame sequence	1	4
Single-frame exposure	15	15
Total	30	211

Areal Coverage	
Nearside Area	
Vertical, Wide Angle	48,000 km^2
Telephoto	12,000 km^2
Oblique, Wide Angle Only	200,000 km^2
Total nearside coverage: 0.05% of hemisphere	
Farside Area	
Total	3,000,000 km^2*
Newly photographed	2,000,000 km^2

*Without overlapping coverage

Multiple-frame sequences were exposed in the fast mode to provide contiguous high-resolution coverage except for Site IIP-5, where the camera axis was tilted to point at the target. The camera axis was aligned for near-vertical photography at all primary sites. Single-frame oblique photography at four secondary sites produced photographs of exceptional interest and value, as well as including areas beyond the range of a vertical field of view.

All Mission II photographs (except for Site IIS-10.2) depict target areas selected prior to flight. All photographs taken to satisfy constraints on time between camera operations and processing were planned as secondary sites of specific targets.

All photography planned for the mission was successfully accomplished. After 98.5% of the planned photography had been read out, failure of the TWTA to turn on at 01:16 GMT December 7, 1966 terminated final readout of the photographs.

2.1.4 PHOTOGRAPHIC SUBSYSTEM DESCRIPTION

A description of the Lunar Orbiter photographic subsystems and their functions, together with the ground support equipment necessary for photographic reconstruction, has been included in Lunar Orbiter Mission I Final Report, Volume II. Discussion here will be limited to changes made prior to Mission II that are pertinent to the photographic results, to significant factors specific to Mission II, and to procedural changes in preparation of the photographs.

Problems encountered during Mission I photography and readout indicated the need for modification of the photographic subsystem to improve photograph quality and reliability of operation. Changes pertinent to photography are summarized below; a detailed description of all changes is included in the data package, compiling all premission testing that has been submitted to NASA.

- Changes were made in electrical and electronic circuitry to prevent incorrect operational timing of the focal-plane shutter that had resulted in image smear in most telephoto photographs of Mission I. These changes reduced the susceptibility of the shutter triggering circuit to spurious pulses or other electromagnetic interference (EMI). A filter was added to the 28-volt line to minimize the possibility of triggering other photographic subsystem circuits.
- The platen clamping spring tension was increased to improve film clamping. This change ensures that no motion of the film relative to the platen occurs during the exposure. It also improves flatness of the film in the lens focal plane to enhance focus and resolution.
- Following Bimat cut, tension on the film is reduced as the processor continues to run to clear the Bimat from the processor. The reduced tension had been observed (in final assembly tests) to result in the film not separating properly from the Bimat, and both being pulled through the diffusion channel toward Bimat takeup. To prevent such an occurrence:
  1) Tension on the Bimat supply drum was increased;
  2) Diffusion channels were widened;
  3) Springs were added to the readout looper to increase film tension.

  Addition of the springs to the readout looper increased the possibility that the looper-empty encoder would stop in the switch transition region, causing the command-control-and-program (CCP) circuit to act as an amplifier instead of a switch. This could possibly result in:
  1) The supply brake failing to release;
  2) The supply motor stalling and causing the switch transistor to overheat and go into thermal runaway.

  A trigger circuit that will be either "on" or "off" was incorporated to compensate for possible logic ambiguity that could result in the above operational anomalies.
- In Mission I, the optical-mechanical scanner, using the best state-of-the-art techniques, introduced image distortion affecting image match between adjacent framelets and precise stereo evaluation. However, in Mission II, reseau marks preexposed on the spacecraft film permit correction or compensation to be made to metrical data. Details of these marks are given in Paragraph 2.3.1.3.

2.1.5 CALIBRATION

Tests and calibrations performed on the photographic subsystem were essentially the same as those described in Volume II of the Mission I final report.

Test and calibration data specific to the Mission II subsystem has been submitted to NASA.

2.2 PHOTOGRAPHIC SITES

All photographic targets for Mission II were scheduled prior to flight as either "primary sites" or "secondary sites." Primary sites were selected potential Apollo mission landing areas. Selection of secondary sites was governed by two factors.

- Scheduling of primary site photography established the orbits during which photography was required by filmset and Bimat-stick constraints.
- The most desirable target from the standpoint of obtaining supplementary terrain information or special scientific information, such as photography of thermally anomalous locations. Oblique photography was included.

No deviations from planned photographic sites occurred during the mission except for Secondary Site IIS-10.2.

2.2.1 PRIMARY SITES

The criteria for selection of primary sites are detailed in Lunar Orbiter Mission II Description, NASA Document LOTD-107-1, October 26, 1966. Major criteria are summarized here for convenience.

- Zone of interest — Sites must lie within $\pm 5°$ latitude and $\pm 45°$ longitude.
- Site characteristics — Sites must be smooth enough for a lunar module landing and with topographic features during approach adequate for landing radar.
- Site locations — Longitude selections are based upon Apollo launch considerations requiring opportunities on alternate days for each month of 1968. This requires that sites be separated by $23 \pm 3°$ longitude. Selection is governed by Apollo performance constraints. Mission I provided preliminary data on the southern portion and Mission II was planned to cover the northern portion of the zone of interest. Additionally, the Ranger VIII impact area was to be photographed and certain Mission I sites were to be re-examined. The primary-site locations and the approximate spacecraft altitude during photography are shown in Figure 2.2-1.

Preliminary analysis of Mission I photographs (refer to NASA Document LOTD-107-1) showed that the darker mare areas appeared to be the smoothest terrain, thus the most promising areas for Lunar Module (LM) landing. Mission II Primary Sites IIP-1, -7, -8, -9, -12, and -13 are within or contain areas of this terrain type. Areas of average mare are included in Primary Sites IIP-3, -8, -9, and -11. The presence of ray structure is believed to correlate with surface roughness. Primary Sites IIP-1, -3, -4, -8, -9, -10, -11, -12, and -13 include varying amounts and types of rays to provide additional data on the above correlation. Mission I photographs showed evidence of volcanic-type formation, particularly Frame I-48M. This area was selected as Site IIP-2 for re-examination. Site IIP-9 also contains positive relief features suggestive of volcanic origin. Evaluation of the area in southern Mare Tranquillitatis photographed in Site I-3 showed it to be the smoothest area found on the first mission. Re-examination of this area was desired and thus designated as Site IIP-6. The area of Ranger VIII impact was selected as Site IIP-5.

The locations and albedos specified for the primary sites are listed in Table 2.2-1. The albedo to be used in determining choice of shutter speed for a site was selected to optimize photography of the overall site or of the particular area of interest within the planned coverage.

2.2.2 SECONDARY SITES

Targets selected as secondary sites are tabulated in Table 2.2-2. Selection of the secondary sites was constrained by availability of a suitable target within range on the designated orbit. Site IIS-10 was originally planned as a westerly oblique of Sinus Medii with the camera axis within 4 degrees of the sunline to investigate terrain appearance with near-zero phase illumination. Premission illumination studies to predict exposure and signal-to-noise ratios for the photography showed that the planned photograph would grossly exceed exposure limitations. The photograph could not be taken, however, because photography with the vehicle 45 degrees off sunline violated a photo-subsystem power constraint.

The albedos specified for each of the secondary sites are listed in Table 2.2-3.

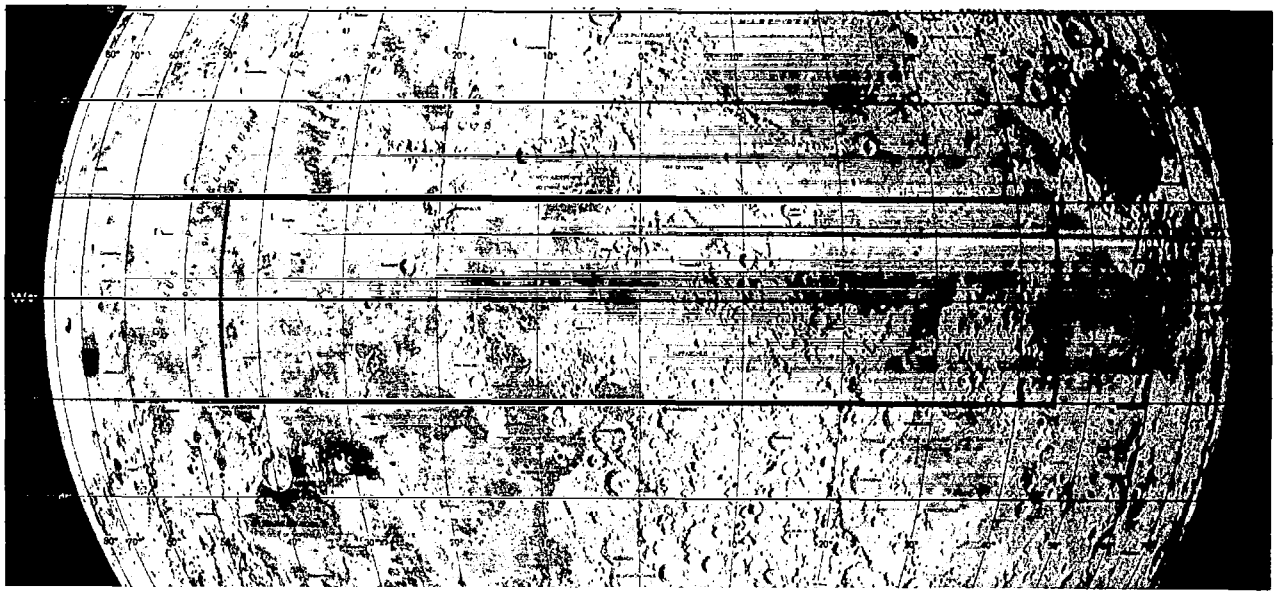

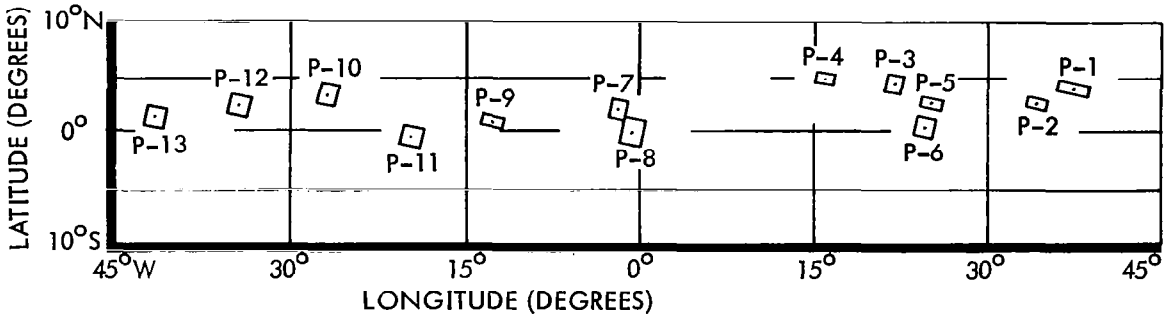

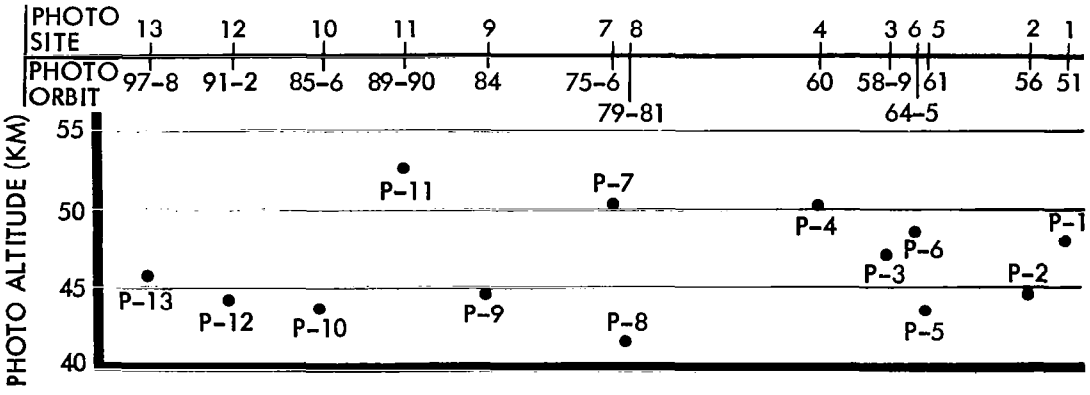

Figure 2.2-1: Primary-Site Distribution

Table 2.2-1: Primary-Site Locations and Albedos

Site	Location		Albedo		
	Latitude	Longitude	Maximum	Minimum	Selected
IIP-1	4°10'N	36°55'E	0.091	0.086	0.088
-2	2°45'N	34°00'E	0.091	0.086	0.088
-3	4°20'N	21°20'E	0.086	0.080	0.084
-4	4°45'N	15°45'E	0.120	0.098	0.111
-5	2°42'N	24°38'E	0.091	0.080	0.086
-6	0°45'N	24°10'E	0.098	0.086	0.087
-7	2°10'N	2°00'W	0.111	0.091	0.098
-8	0°05'N	1°00'W	0.105	0.091	0.092
-9	1°00'N	13°00'W	0.098	0.091	0.093
-10	3°28'N	27°10'W	0.105	0.086	0.091
-11	0°05'N	19°55'W	0.120	0.091	0.105
-12	2°25'N	34°40'W	0.091	0.086	0.087
-13	1°30'N	42°20'W	0.080	0.072	0.073

Table 2.2-2: Planned Secondary Sites

Site Number	Planned Position		Principal Feature	V/H Sensor	Remarks
	Latitude	Longitude			
IIS-1	4°10'N	36°55'E	Mare Tranquillitatis	On	Following IIP-1 as soon as possible. No intervening maneuvers.
IIS-2	3°36'N	36°25'E	Site IIP-1	On	Converging stereo for telephoto. Two four-frame sequences centered midway between Orbits 52 and 53. Three-axis maneuver.
IIS-3	Not specified	176°E	Farside	Off	Vertical. Centered 20 degrees before PM terminator. Roll maneuver only.
IIS-4	Not specified	174°E	Farside	Off	Northerly oblique. Horizon included in wide-angle frame.
IIS-5	Not specified	158°E	Farside	Off	Southerly oblique. Horizon included in wide-angle frame.
IIS-6	4°15'N	4°30'E	Triesnecker	On	Vertical. Three-axis maneuver.
IIS-7	0°05'N	1°00'W	Flammarion Herschel	Off	Southerly oblique from point of closest approach. Three-axis maneuver.
IIS-8	0°30'N	12°50'E	Sinus Medii	On	Vertical. North of Site I-4. Three-axis maneuver.
IIS-9	2°20'N	0°30'E	Sinus Medii	On	Vertical. Southwest of Triesnecker. Northwest of Site IIP-7a. Three-axis maneuver.
IIS-10.2	3°20'N	11°00'W	Gambart C	On	Crater identified as a thermal anomaly.
IIS-11	4°40'N	27°04'W	Copernican ray	On	Vertical. Three-axis maneuver.
IIS-12	8°00'N	20°00'W	Copernicus	Off	North oblique. Three-axis maneuver.
IIS-13	3°20'N	43°50'W	Braided ridge	On	Vertical. Three axis maneuver. Area southwest of Kepler.
IIS-14	Not specified	100°E	Farside	Off	Vertical. Roll maneuver only. Centered 20° before PM terminator.
IIS-15	11°00'N	53°00'W	Marius	On	Northerly oblique. Three-axis maneuver.
IIS-16	2°40'N	54°30'W	Smooth mare	On	Vertical. Three-axis maneuver.
IIS-17	7°25'N	59°00'W	Bright ray structure west of Reiner	On	Northerly oblique. Three-axis maneuver.

Table 2.2-3: Albedos Specified for Secondary Sites				
Site	Albedo Maximum	Albedo Minimum	Albedo Selected	
II-S-1	0.098	0.091	0.096	
-2	0.091	0.086	0.088	
-3	-	-	0.120	
-4	-	-	0.120	
-5	-	-	0.120	
-6	0.158	0.120	0.137	
-7	-	-	0.092	
-8	0.147	0.137	0.139	
-9	0.137	0.098	0.105	
-10.2	-	-	0.092	
-11	0.111	0.091	0.105	
-12	-	-	0.120	
-13	0.075	0.072	0.074	
-14	-	-	0.120	
-15	-	-	0.070	
-16	-	-	0.072	
-17	-	-	0.100	

Note: No measurements were available for farside sites. Selected albedos are estimated. Maximum and minimum values are not listed for limited near-side areas of near-uniform albedo or where data was uncertain.

2.3 PHOTOGRAPHS

Assessment and analysis of mission photography has been based upon second-generation copies of the GRE 35-mm reconstructed record and upon paper prints of reassembled photographs prepared by NASA and by the Army Map Service. Assessment of photographic quality was based principally upon the GRE film. All 35-mm reconstructed film could not be examined in detail for analysis because of the amount of film involved. A sampling technique was used. Frames at the start, middle, and end of each sequence of primary-site photographs were examined, and framelets near each end and the center of these frames were examined in detail.

Because of the sensitometric characteristics of photographic paper emulsions and the various control techniques used in the photographic printing processes involved, the prints were used only for assessing site coverage, to relate the overall effects of gross topography and illumination to photography, and to screen the photographs for processing anomalies.

2.3.1 GENERAL CHARACTERISTICS

The telephoto and most of the wide-angle photographs from Mission II are of good quality. In many cases, however, the exposure used for a site was selected to optimize telephoto coverage at the expense of overexposure of the wide-angle photographs and resultant degradation of their quality. The enhancement technique – developed at Langley Research Center – in which an amplified video tape record was used as GRE input, was used successfully on many of the overexposed wide-angle photographs. Resolution requirements were met at all sites in telephoto photographs, and in wide-angle photographs that were enhanced or not degraded by overexposure.

No major operational problems or failures affecting overall mission photography occurred.

Lunar Orbiter photographs exhibit certain occasional blemish characteristics, some of which, such as the processor stop and pull-off lines, are defects inherent in the film processing system due to the start-and-stop processing requirements of the mission. The properties and characteristics of Mission II photographs are described in the following paragraphs. Refer to Lunar Orbiter Mission I Final Report, Boeing Document D2-100727-2, Volume II, Paragraph 2.2.1.1, for discussion and description of those characteristics common to both missions.

2.3.1.1 Exposure

Correction of or compensation for the difference in light transmission between the telephoto (610-mm) lens and the wide-angle (80-mm) lens described in the Mission I final report, Volume II, could not be completed in time for Mission II. Therefore, the difference in exposure between telephoto and wide-angle photographs, noted for Mission I, is present in those from Mission II. At most primary sites, the telephoto coverage was considered to be of greatest importance and shutter speeds were selected to more nearly optimize these exposures. Because of the light transmission difference between the two camera lenses, the expected consequence was overexposure of the wide-angle photographs. In some cases, the wide-angle coverage was severely overexposed and the subsequent enhancement technique using an amplified video tape input to the GRE was not adequate to recover the photographic detail. In some cases, where overlapping coverage of a primary site was obtained on successive orbits, a different exposure was used on each pass to more nearly optimize both telephoto and wide-angle coverage. Surface topography resulted in localized areas of extreme over- and under-exposure in nearside photographs.

Quantitative determination of spacecraft film density cannot be used as a measure of exposure evaluation since direct measurement is impossible. Determination of spacecraft film density from the edge-data gray scale on the GRE film is difficult because each step in the reconstruction – from spacecraft readout scanning through production of the GRE film record or copy being used – must be considered and evaluated. The edge-data gray scale was calibrated using Bimat-processed flight film during preflight testing at ETR. The density readings are listed in Table 2.3-1 and the location of each step on the H&D curve is shown in Figure 2.3-1. The densities determined at ETR are ASA visual densities. The equivalent values in terms of readout density are listed in Table 2.3-1. Edge data densities have a tolerance of $\pm$ 0.05.

Table 2.3-1:
Flight Film Edge Data Gray Scale Densities

Step No.	ASA Visual Density	Readout Density
1	0.35	0.29
2	0.37	0.31
3	0.43	0.38
4	0.50	0.45
5	0.65	0.62
6	0.91	0.93
7	1.19	1.22
8	1.49	1.34 (Estimated)
9	1.72	

Most of the exposure evaluation of each site in subsequent paragraphs is based upon a visual comparison of image density of a second-generation copy of GRE record with a calibrated 21-step gray scale. The determination is approximate. Evaluation of exposure, with respect to over-, under-, or satisfactory, is largely subjective.

More precise determination, using microdensitometer measurements, has been made on a limited number of framelets from some sites. This evaluation has shown that the noise pattern of the photographs, described in Mission I final report, Volume II, Paragraph 2.2.1.1, is such that it is the limiting factor in resolution. The presence of detail equivalent to 100 microns on the GRE film (nominal system resolution), where the image is of moderate contrast, could not be distinguished from the noise on the trace from a microdensitometer employing a 10-micron aperture. On the other hand, an experienced observer frequently could recognize, with some assurance, small features in the size range of the noise pattern on the GRE film by visual examination at a magnification of about 10 diameters. Such recognition became more sure where contrasts were higher. It has been found that detection of very small surface detail appeared to be related to the type of terrain photographed. This is evident particularly in rock-strewn areas near craters where much fine detail is expected.

No anomalies or operational failures of either shutter affecting mission photography were noted.

2.3.1.2 Processor-Dryer

Processing defects that are inherent in the system and that are described and illustrated in the Mission I final report were present. A more detailed discussion and description, reflecting analysis of photographs from both missions, follows.

The increase in processing defects noticed in Mission II over Mission I was largely attributable to the increased number of times that the processor-dryer was stopped and started during this mission. The defects were divided into two groups – those expected due to processor stops and those for which no explanation is presently known. The expected defects as observed in Missions I and II correspond to known dimensions from the Bimat-film lamination point, Figures 2.3-2 and 2.3-3. The other defects, "Queen Anne's lace" or "freckles," are as yet unpredictable and are not really explained even though attempts to duplicate the phenomena under controlled conditions have been performed at Eastman Kodak Company.

Subsequent to this flight, a procedure had been developed by which repetitive processing defects would occur outside a few frames. For subsequent missions, certain frames or photographs would be defined as critical for a given mission so that mission planning and conduct could proceed accordingly to eliminate or at least minimize the possibility of a blemish in a critical area to be photographed.

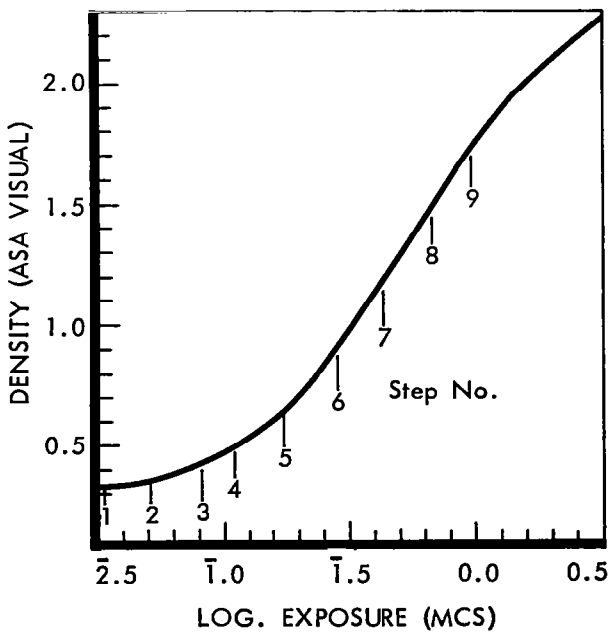

Figure 2.3-1: Edge Data Gray Scale Calibration

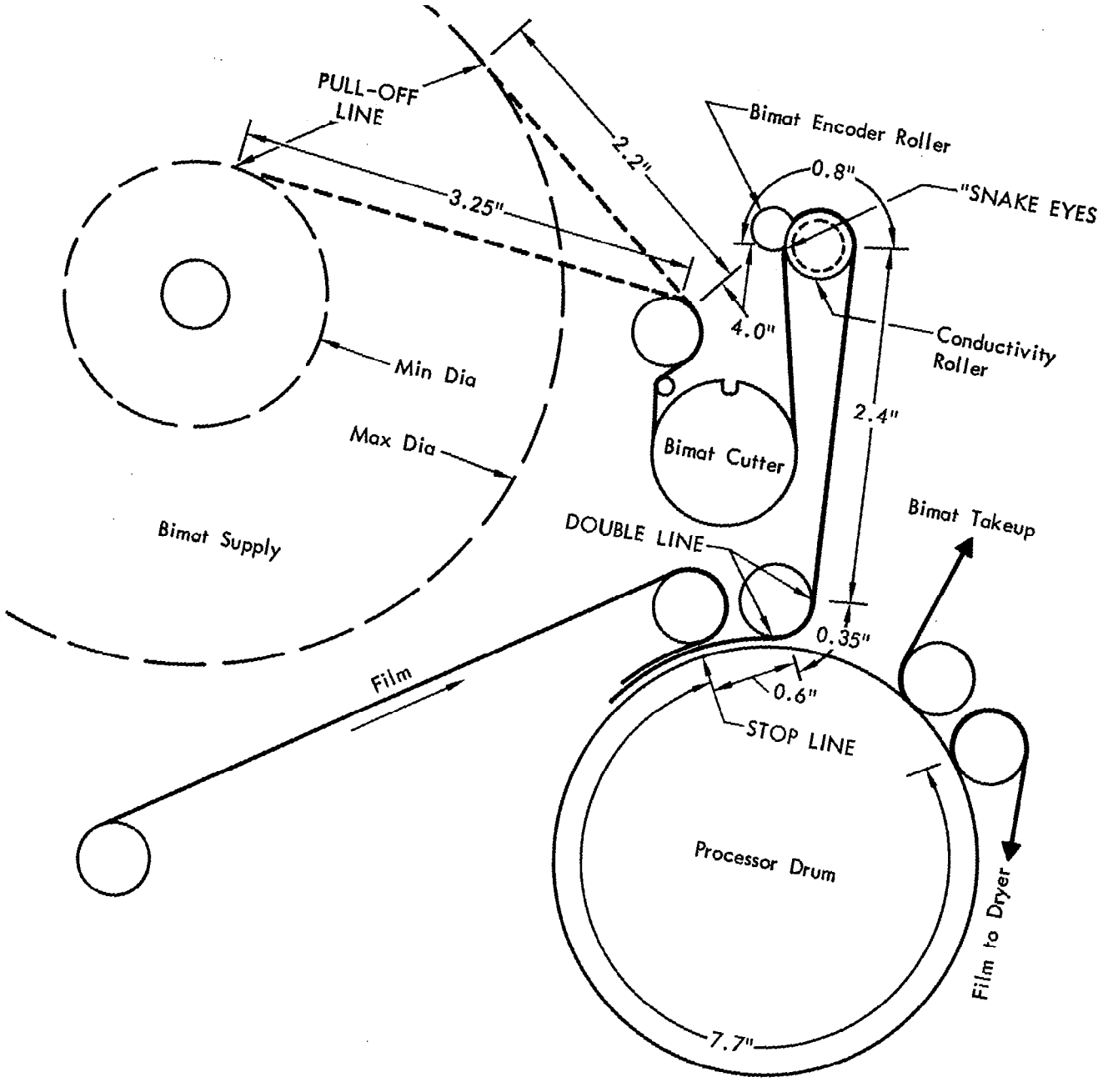

Figure 2.3-2: Processing Mark Sources

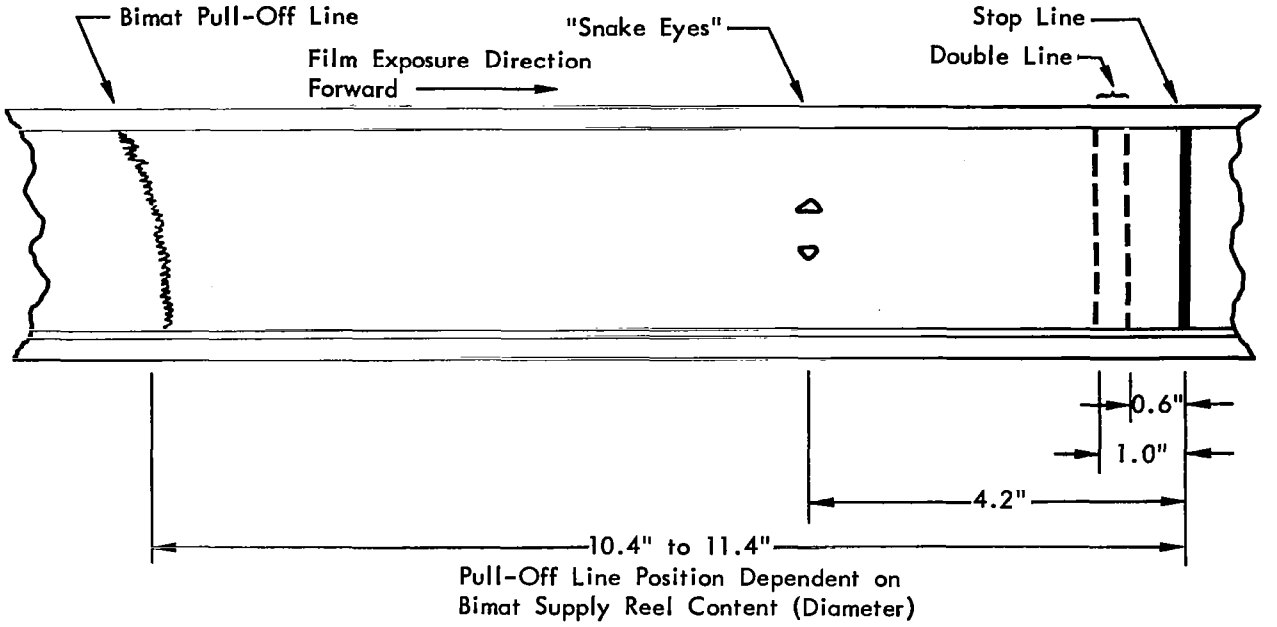

Figure 2.3-3: Relative Locations of Processing Marks — Spacecraft 70-mm Film

Discussion of Defects

- Bimat Stop Line
  This line normally is approximately ½ framelet wide and crosses the film at an angle of 90 degrees to the direction of film motion. The Bimat stop line is caused by the pressure differential at the lamination point of the film and the Bimat. This pressure differential and possible dryout effects result in displacement of the Bimat emulsion and cause improper or no processing. The Bimat stop line is usually closely followed by two lesser defect lines parallel to the stop line. These lines, approximately six and ten framelets away, are evidently due to pressure at the tangent points of the Bimat contact on the first roller prior to lamination. The emulsion side of the Bimat contacts this roller for about an 80-degree wrap. Two other rollers contact the emulsion side of the Bimat in the same manner; however, corresponding defects have not been observed. This is no doubt due to the decreasing Bimat tension in this area. These lines are associated with the location of the Bimat at the start of each processing-on period and can be predicted following location of the first Bimat stop line during readout. There is no operating technique that would prevent this condition other than continuous processing.

- Bimat Pull-Off Line
  This generally appears as a curved line that crosses the entire Bimat processed area. It normally starts at a slope of roughly 15 degrees off right angles to the film and then ends up as a curve. The Bimat pull-off line is often associated with a partial line of defective processing spots. This combination of lines is normally located on the film about 11 inches following the Bimat stop line. The Bimat pull-off line appears to be related to the variances in adhesion between the emulsion and the backside of the Bimat as it just starts to pull away from the Bimat wraps on the supply spool. The location of this defect is subject to some variation due to variation in Bimat unrolling tensions. No known method of eliminating this defect is known; however, it is lessened as the processor-off time is decreased.

- "Snake Eyes"
  These appear as two oval-shaped spots near the center of the film. They are generally spaced about 0.375 inch apart, are associated with the location of the Bimat

stop line, and follow it by about 4.2 inches. Pressure of the Bimat cut encoder roller on the back of the Bimat forces the emulsion against the cutout area edges of the conductivity roller during the processor-off time. Because the size and degradation of this condition seems to vary with processor-off time, no known solution is available other than continuous processing. This condition does not always appear following a processor-off period.

- Longitudinal Lines
  Two, three, or four longitudinal lines of varying density are present at times on the film. Tests have been made to determine the cause of the streaks. It was found that, as the film passed into the camera storage looper, a static charge was generated when the film rubbed against the first teflon separator in the looper end. The streaks were caused by static discharge onto the film, which produced localized fogging. The separator has been relocated and covered with aluminized mylar tape to correct this problem in photo subsystems for missions following Mission III.

- "Freckles" or "Queen Anne's Lace"
  This appears as a spotted area of unprocessed film arranged in a random manner. The areas vary in size and location on the film and do not follow any repeating pattern. No known reason for these defects has been found; they could be attributed to bubbles in the Bimat, an unknown reaction of an area of the Bimat, or processing characteristics when the tension of the film and Bimat is varied due to the frequent starting and stopping of the processor-dryer. At present there is no known way to prevent this condition.

A significant area of defective processing occurs between wide-angle Frames 99 and 102. The defects appear as lace-like loops and spots as shown in Figure 2.2-4 of the Lunar Orbiter Mission I final report, Volume II. Telephoto Frame 215 is also affected to some extent by this problem. Processing defects of minor extent occur occasionally throughout mission photography. Also noted in the area of Frames 99 to 102 was an effect similar in appearance to the noise pattern but of a much larger scale. This pattern is believed to be due to the same cause as the "lace" effect but not as intense.

Avoidance of Processing Defects in "High-Value Frames"

There are no known changes to present operating techniques that will reduce the number of defects when the mission is programmed with photos and processing spread out through so many orbits.

- Freckles or lace appearance cannot be predicted; however, they seem to be associated with the Bimat stop line. It is hopefully believed that longer processing-on time would help minimize their occurrence.
- The quality of processing has not shown obvious degradation at the end of the processing period; therefore, it is believed that no improvement would be possible by shortening the time to completion of processing.
- Priority readout to the extent used in Mission II does not seem to affect processing quality.
- The practice of processing at least two frames every 4 hours or each orbit as a minimum is still recommended. Fewer defects would be present if more frames were processed at one time.
- Bimat emulsion peeling or failure of the film and Bimat to delaminate has not been noted.

2.3.1.3 Readout

Small marks that may have originated at the readout section appear as a repeating pattern at and near the edge of each framelet. The occurrence of these thin, scratch-like marks was found to increase as readout progressed. Accumulation of Bimat or film elusion particles at the readout gate has been suggested as a possible cause. Similar marks were observed on Mission I photographs.

Longitudinal density variations within the framelets, due to the halo effect described in the Mission I final report, were prevented by GRE masking. Transverse density variations were controlled by control of the line-scan-tube focus.

The noise pattern, described in the Mission I final report, was present in the Mission II GRE film. The cause of this pattern has not been established conclusively.

Some variations in readout film advance occurred. This effect occasionally resulted in a

small amount of incorrect overlap of adjacent framelets. In one case, during priority readout sequence 052, a temporary failure of film advance resulted in one framelet (769) being read out 18 times. No other similar occurrence was noted.

Nonlinearity of the optical-mechanical scanner was present. However, reference ("reseau") marks in the form of small crosses, illustrated in Figure 2.3-4, have been included. These reseau marks were exposed on the spacecraft film at the time the edge data was pre-exposed, and thus occur in a fixed relationship to the edge data format. Any dimensional changes subsequent to imaging by the spacecraft cameras, including readout, can be determined and corrections made.

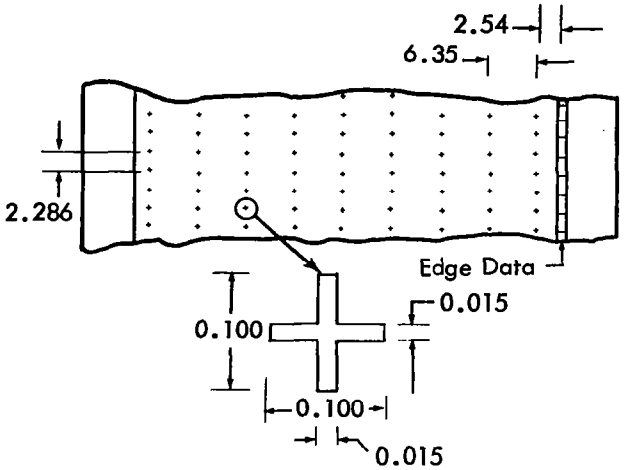

Figure 2.3-4: Pre-exposed Reseau Mark Placement and Detail of Cross

2.3.1.4 Reassembly

Mission II photographic reassembly was accomplished by NASA at the Langley Research Center, by the Army Map Service, and by Eastman Kodak Company at Rochester, New York.

Photographs were hand reassembled at the Langley Research Center and by the Army Map Service to enable rapid analysis of the photographs by NASA Apollo landing-site screening group, and to obtain high-quality paper prints to enable early systems performance analysis and interpretation. Paper prints were prepared at the same scale as the GRE film record. Control techniques were used in the photographic printing process to enhance print quality by both agencies. For example, LogEtronics printers were used to compensate for large density variations within the photographs and thus produce prints more easily interpreted. Printing control also compensated for density differences between wide-angle and telephoto pictures to produce greater similarity in appearance of the two types of photographs. While these control techniques do not increase the information content of the photography, they do increase the information within the prints by effectively lowering the density range capability inherent in the film to more nearly match the range capability of the paper.

The video tape enhancement technique also was used by Langley Research Center to prepare prints of overexposed wide-angle photographs. Photographic detail was retrieved that was obscured by the high image density of the spacecraft negative and corresponding low video signal. However, information loss occurred in some darker or shadowed areas of such photographic prints.

The Army Map Service reassembled telephoto frames in three sections. Facing in the direction of flight, No. 1 is the left side, No. 2 is the center section, and No. 3 is the right-hand third. Not all wide-angle photographs were reassembled but, where done, the full frame was reassembled as a single photograph rather than as subframes.

The reassembly accomplished at Eastman Kodak Company was done on the reassembly printer as described in the Mission I final report, Volume II, Paragraphs 2.1.1.5 and 2.2.3. No paper prints were prepared by Eastman Kodak.

The combination of spacecraft camera optical train and readout process results in changes in image orientation. Proper orientation of the Lunar surface image occurs when the edge data image appears normal on wide-angle photographs and as a mirror image on telephoto frames.

2.3.2 PRIMARY-SITE PHOTOGRAPHY

All primary sites were photographed with the camera axis near vertical except for Site IIP-5. That is, the spacecraft was maneuvered, prior to photography, to direct the camera axis to nadir at the center of the target area. Attitude was held constant ($\pm$0.2 degree) in inertial space during the photographic sequence.

Thirteen primary sites were planned. Analysis of the photographic coverage of Mission I sites indicated the desirability of modifying the previously selected sites for Mission II area coverage. Site IIP-1 was photographed by a single 16-frame sequence; Sites IIP-2, -4, -5, and -9 were photographed by single 8-frame sequences; for Sites IIP-8, three eight-frame sequences on successive orbits were used. The remaining seven primary sites were photographed by two eight-frame sequences on successive orbits. Photographic parameters for primary sites are summarized in Table 2.3-2. Site-dependent characteristics of photography are discussed in the following paragraphs.

In the evaluation of mission photographic resolution, the scan lines provide a convenient unit of measure independent of copying processes used in preparing the film being examined. This criterion also is independent of the spacecraft altitude at the time of photography, as opposed to actual ground measure. For these reasons, resolution has been estimated and reported in the following discussions largely in these terms.

The resolution requirement for Lunar Orbiter photography has been stated as that necessary to detect a 1-meter object with the telephoto lens and an 8-meter object with the wide-angle lens from an altitude of 46 kilometers. This requires a resolution of 76 lines per millimeter on the spacecraft film or 10 lines per millimeter on the 35-mm GRE reconstructed record. There are approximately 40 scan lines per millimeter on the GRE record. Thus, the resolution requirement is equivalent to detection of objects whose images span four scan lines.

Table 2.3-2: Photographic Parameters — Primary Sites

Site No.	Terrain Type	Albedo	Phase Angle (deg)	Shutter Speed (sec)	Altitude Range (km)	Photo Orbit	Frame No's.
IIP-1	Average mare	0.088	72.95	0.04	48.1 - 46.0	52	5 - 20
IIP-2	Smooth mare	0.088	67.83	0.02	44.5 - 44.7	57	35 - 42
IIP-3a	Mare. Ridges and rilles	0.084	75.56	0.04	47.9 - 47.0	59	43 - 50
b			74.38	0.04	46.0 - 45.3	60	51 - 58
IIP-4	Upland plains	0.111	77.69	0.04	49.7 - 48.6	61	59 - 66
IIP-5	Average mare	0.086	69.05	0.04	42.9 - 43.1	62	67 - 74
IIP-6a	Smooth mare	0.087	62.59	0.02	46.5 - 47.6	66	76 - 83
b			61.13	0.02	48.5 - 49.6	67	84 - 91
IIP-7a	Mare-upland contact	0.098	70.21	0.02	41.0 - 41.1	76	96 - 103
b			68.74	0.02	41.5 - 41.8	77	104 - 111
IIP-8a	Rayed mare	0.092	63.15	0.02	46.6 - 47.7	80	113 - 120
b			61.69	0.02	49.0 - 50.5	81	121 - 128
c			60.23	0.02	51.8 - 53.6	82	129 - 136
IIP-9	Dark and light mare	0.093	66.10	0.02	44.4 - 45.2	85	138 - 145
IIP-10a	Diffused ray on mare	0.091	76.93	0.04	44.7 - 44.0	86	146 - 153
b			75.47	0.04	43.6 - 43.1	87	154 - 161
IIP-11a	Mare and upland	0.105	62.92	0.02	51.4 - 52.9	91	163 - 170
b			61.47	0.02	54.6 - 56.5	92	171 - 178
IIP-12a	Ray-covered mare	0.087	72.84	0.04	44.2 - 44.3	93	179 - 186
b			71.39	0.02	44.8 - 45.1	94	187 - 194
IIP-13a	Dark mare with rays	0.074	71.83	0.04	45.2 - 45.4	98	197 - 204
b			70.35	0.02	46.2 - 46.7	99	205 - 212

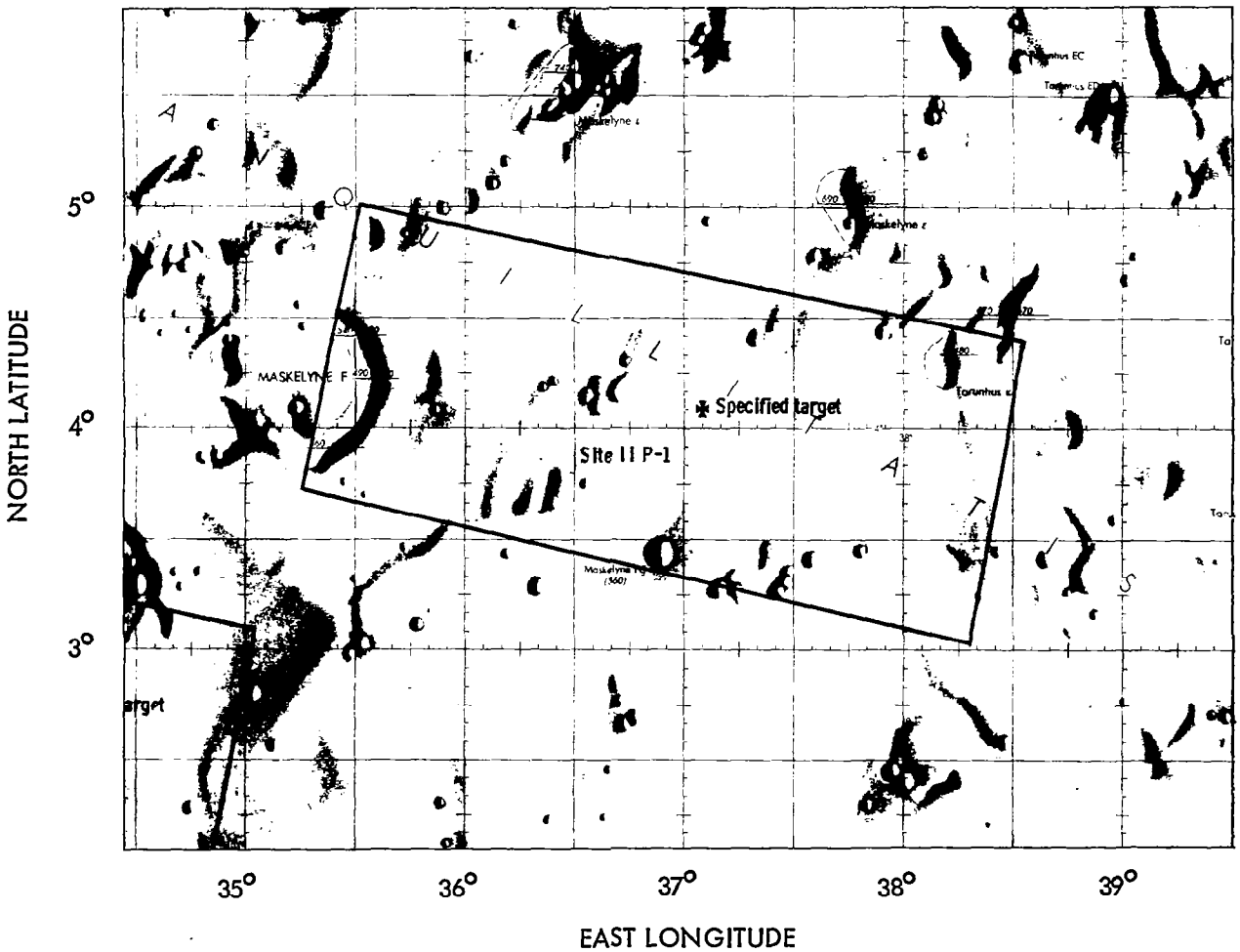

Figure 2.3-5: Site IIP-1 Coverage

Since ground resolution is directly proportional to the spacecraft altitude (or slant distance), it is related to scan lines by the expression:

$$\text{Ground resolution in meters} = \frac{N}{4} \times \frac{H}{46}$$

where N is the number of scan lines spanned by the smallest objects detected, and H is the spacecraft altitude in kilometers. (This applies to the telephoto coverage; wide-angle resolution must be increased by a factor of 8.)

2.3.2.1 Site IIP-1

Coverage of Site IIP-1, 4°10'N latitude, 36°55'E longitude, is shown in Figure 2.3-5. Note that the "specified target" is shown in this figure and in following figures showing site coverage. This marks the point location specified by NASA as the site target and used in mission planning. The obtained mission photographic coverage is not always centered on this position because of operational limitations. The closest orbit did not always pass directly over the position, and additional factors such as timing of the initial exposure of a sequence, variations in spacecraft attitude and altitude, uncertainities in predicted orbital parameters, and chart errors contribute to the apparent offset. Failure of the TWTA terminated final readout before the last eight frames had been read out. Portions of this site photography read out in priority mode included some frames not reached in final readout. Although three complete wide-angle frames were not read out (Frames 6, 8, and 10), the other frames completely overlap their coverage. Therefore, wide-

angle coverage is complete. Lack of telephoto frame overlap resulted in loss of coverage of most of six and all of two telephoto frames. The area for which no telephoto coverage was obtained is illustrated by shading in Figure 2.3-6.

The predicted exposure of 0.04 second appears to be satisfactory for both wide-angle and telephoto photographs of the mare area of this site. Inspection of second-generation ground reconstruction electronics (GRE) positive 35-mm film indicated that the wide-angle frames had exposures ranging from good to overexposed, while the corresponding telephoto frames tended towards underexposure. This difference in average image densities was anticipated since the photo subsystem wide-angle lens has greater white-light transmission than the telephoto lens. It should be noted here that GRE positive 35-mm film offers the most direct means of evaluating the suitability of spacecraft 70-mm film exposures. The correctness of photo system exposure times is especially difficult to evaluate from reassembled positive prints on opaque materials because of the many additional variables introduced in the various printing processes and the nature of the medium. Positive transparencies viewed by transmitted light can present an image with a greater contrast range and better definition than opaque positive viewed by reflected light. An example of Site IIP-1 wide-angle photography is shown in Figure 2.3-7. In this figure and subsequent photographic illustrations, the complete frame is not necessarily reproduced.

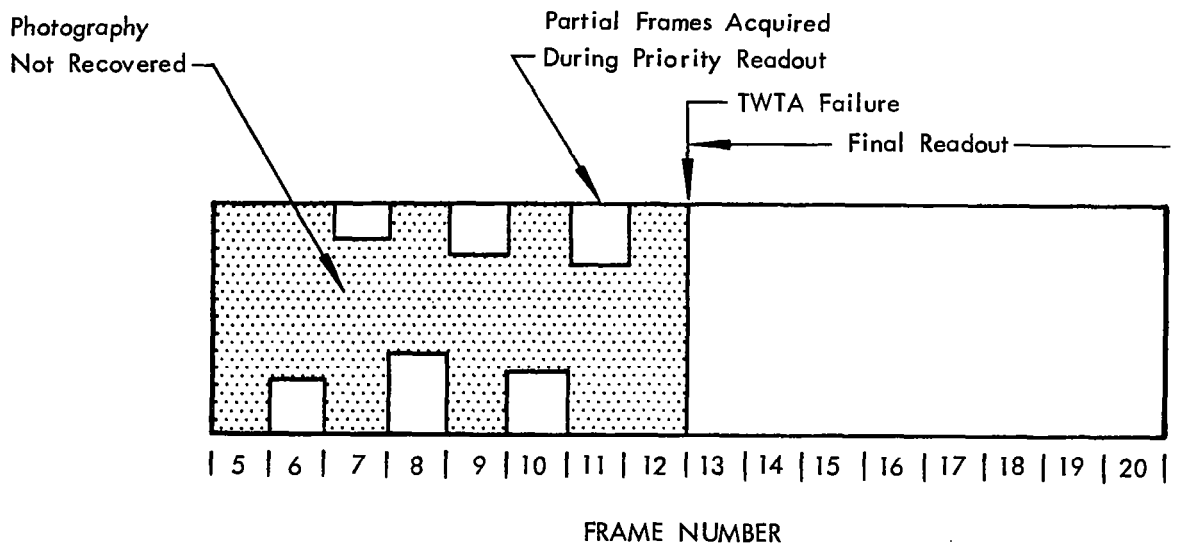

Figure 2.3-6: Telephoto Coverage of Site IIP-1

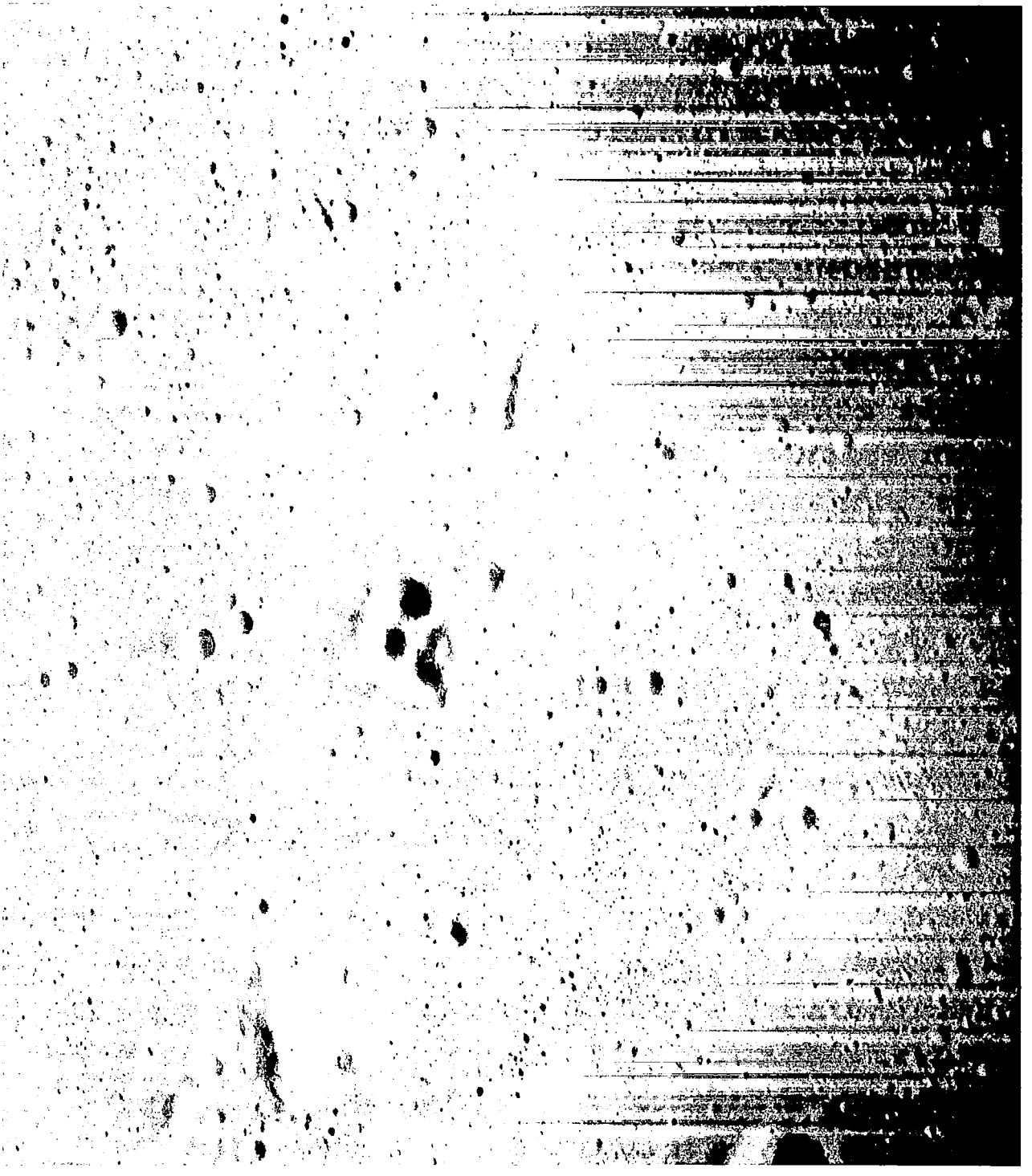

Figure 2.3-7: Wide-Angle Photography of Site IIP-1

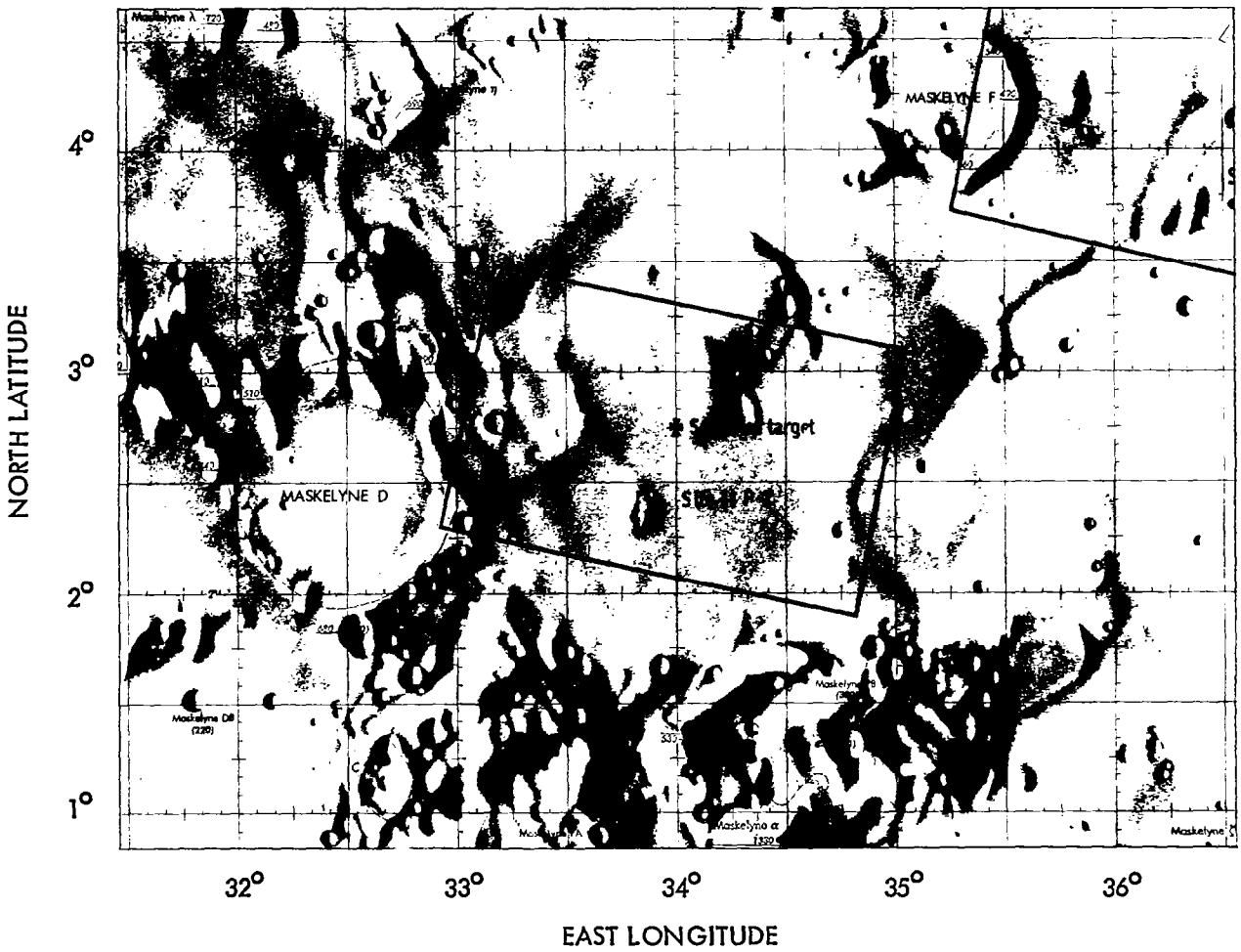

Figure 2.3-8: Site IIP-2 Coverage

2.3.2.2 Site IIP-2

This site, shown in Figure 2.3-8 and 2.3-9, is located at the southern boundary of Mare Tranquillitatis about 100 kilometers east of Maskelyne. Portrayal on ACIC charts LAC 61, Taruntius, and ACI 61D, Maskelyne D, shows a few craters 1 to 2 km in diameter and low dome structures in the central and eastern portion of the area. The entire area is depicted as flat or low-relief mare.

Correlation of aeral coverage in the photographs with the computed corners was difficult because of the limited number of well-defined features on the charts that could reliably be identified in the photographs. Some uncertainty exists with respect to certain small craters.

Wide-angle photographs show the circular dome structure in the south-central portion, although it is barely discernible as a luminance change resulting from the small slope change. The wide-angle photographs show excellent detail throughout, indicating that the shutter speed of 0.02 second was satisfactory. The telephoto frames are somewhat underexposed as judged by the GRE film. However, the underexposure does not appear to have resulted in loss of image detail. Craters spanning three and one half to four scan lines were detected, indicating acceptable resolution. Prints of telephoto frames prepared by the Army Map Service show very good detail and little apparent loss of information.

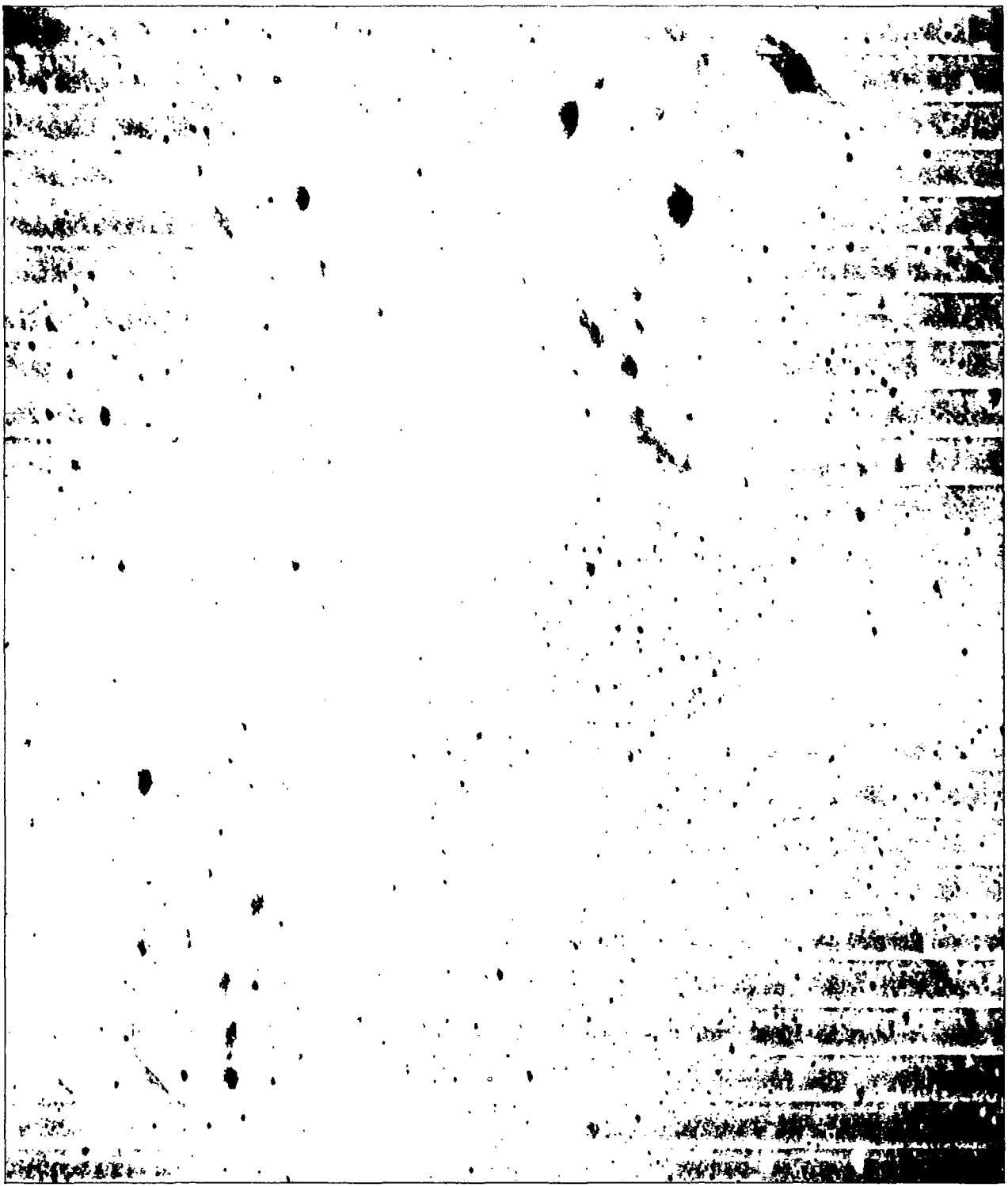

Figure 2.3-9: Wide-Angle Photography of Site IIP-2

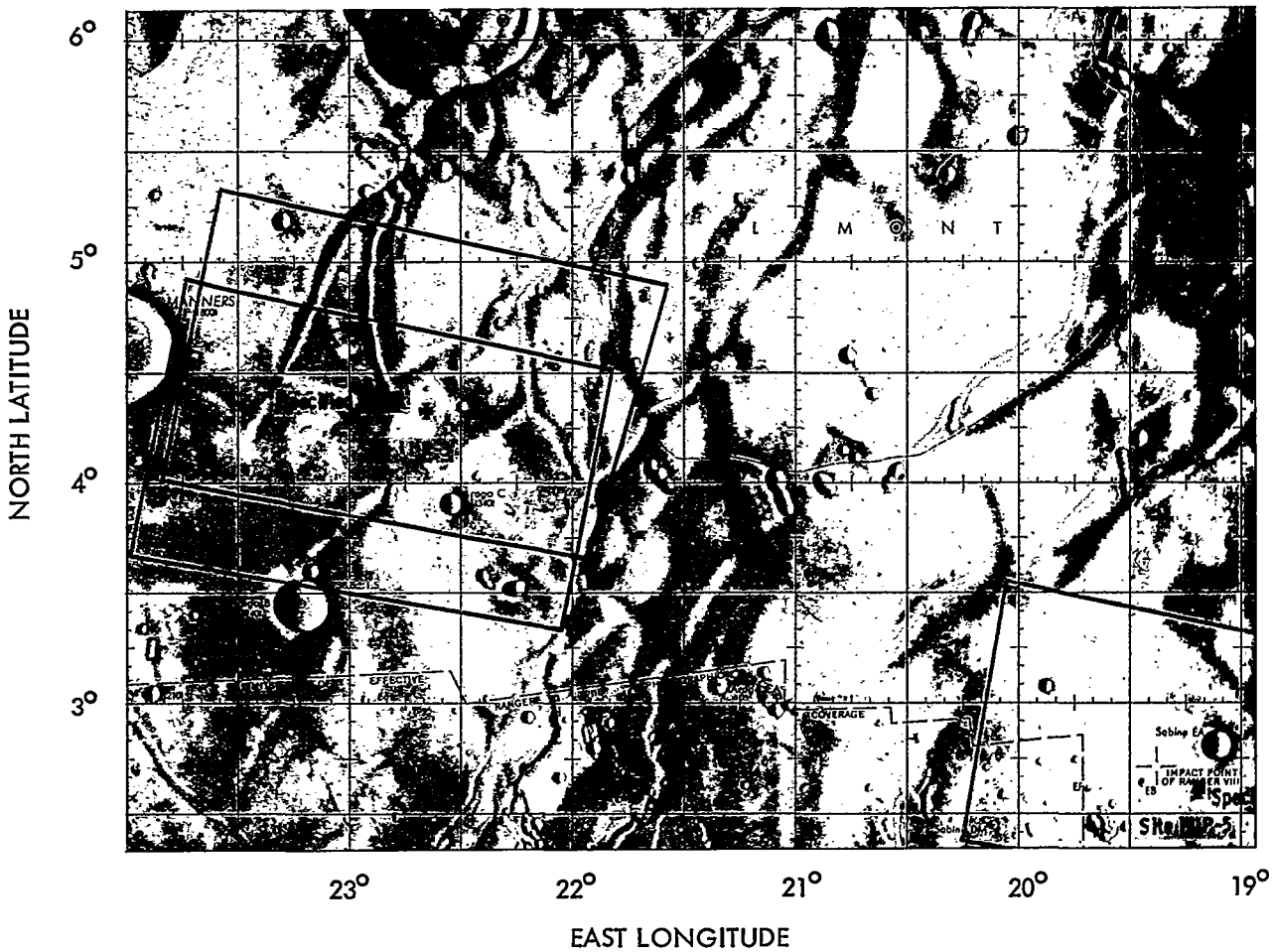

Figure 2.3-10: Sites IIP-3a and IIP-3b Coverage

2.3.2.3 Site IIP-3

This site, Figure 2.3-10, is south of Arago and east of Manners, in western Mare Tranquillitatis. The mare area of the site shown on AIC 60C, Arago, and in Figure 2.3-11, includes a prominent fan-shaped rille system extending south from Arago and a system of low ridges associated with the premare crater Lamont. Arago C, 3.5 kilometers in diameter, is the only named feature within the area photographed by the two eight-frame sequences.

Since the site was photographed on two successive orbits with eight-frame sequences in the fast mode, both forward and side overlap is provided for stereo examination of the wide-angle coverage. Side overlap of the telephoto exposures permits stereo examination of a limited area at high resolution. The amount of side overlap can be seen in Figure 2.3-10.

Exposure of the wide-angle frames appeared to be slightly more than for Site IIP-2 but not excessive. The telephoto frames were exposed somewhat less than desirable, which indicates that selection of 0.04 second was correct. Prints of both wide-angle and telephoto frames were of good quality, showing detail in all areas except hard shadows or brightly illuminated slopes facing the Sun.

Examination of GRE film showed many craters and features spanning three or four scan lines, equivalent to the required system resolution. Resolution capability of the system is shown dramatically in the rock-strewn summit of the prominent ridge and several craters included in the telephoto frames of the eastern portion of the area (Figure 2.3-12).

Figure 2.3-11: Wide-Angle Photography of Site IIP-3a

Figure 2.3-12: Telephoto Photography of Site IIP-3a

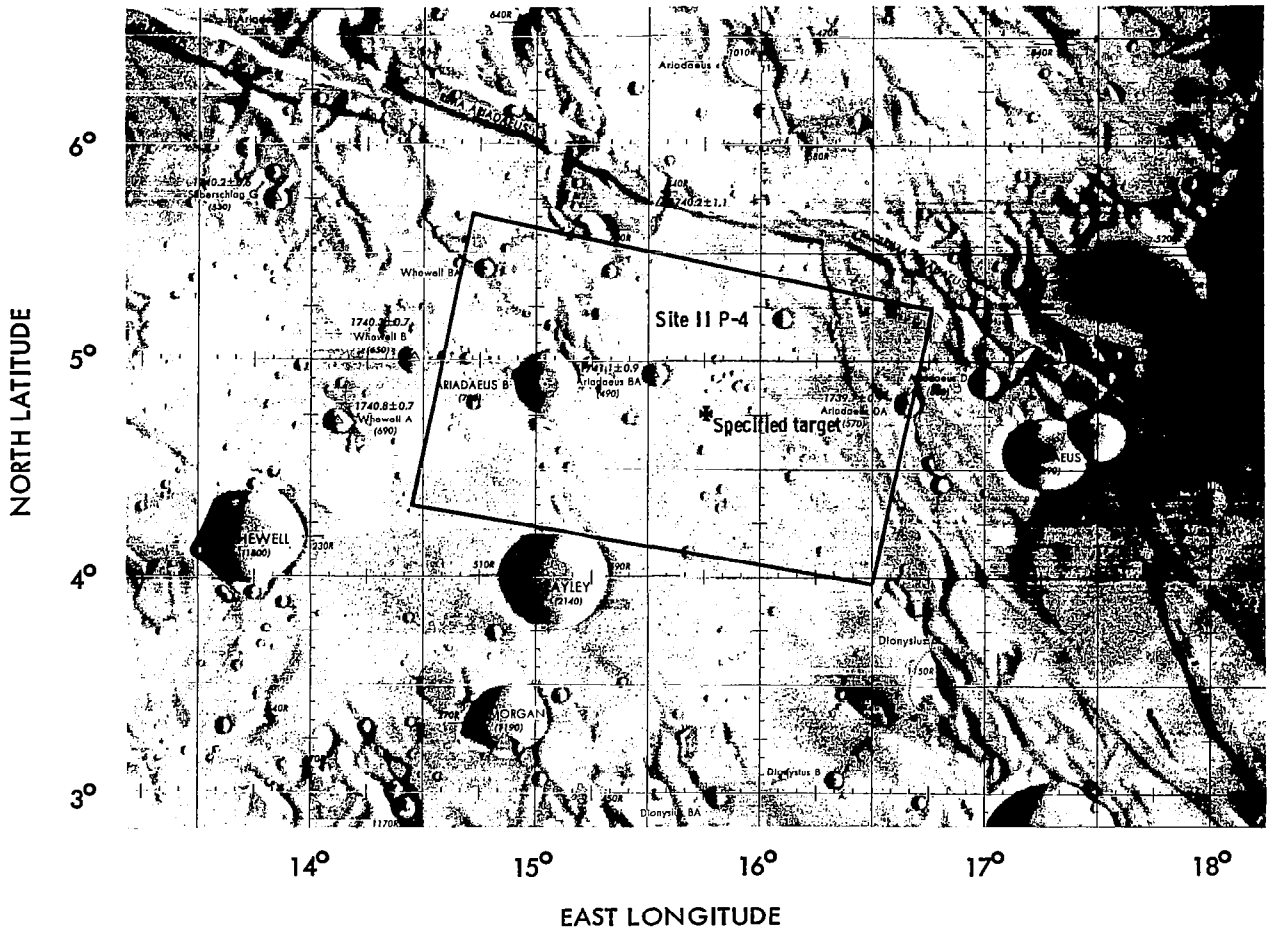

Figure 2.3-13: Site IIP-4 Coverage

2.3.2.4 Site IIP-4

Site IIP-4, Figure 2.3-13, is located just south of the eastern part of Rima Ariadaeus and includes the crater Ariadaeus B and the flat upland-type area to the east. The site is within the area of AIC 60D, Agrippa. In addition to several prominent craters, a portion of Rima Ariadaeus I is included in the wide-angle photography. The area has a relatively high albedo of 0.111. Figure 2.3-14 is an example of the wide-angle photograph of this site.

Although the area has a high albedo, the large phase angle resulted in a predicted shutter speed of 0.04 second. Exposure of the wide-angle photographs appeared good, with a GRE film density, in level areas, in the range of 0.7 to 0.9. Telephoto exposures were slightly less than optimum in spite of the slowest shutter speed being used. GRE film density was about 1.0 in level areas near the center of the frames. Prints of telephoto frames prepared by the Army Map Service appeared to be of good quality although the effects of underexposure are apparent in darker areas.

Wide-angle resolution of surface features spanning three to four scan lines was observed in the central area of the frames examined. Resolution equivalent to three to five scan lines was attained on some telephoto frames although in darker (underexposed) areas, particularly off the camera axis, features spanning less than 8 to 10 scan lines were not observed.

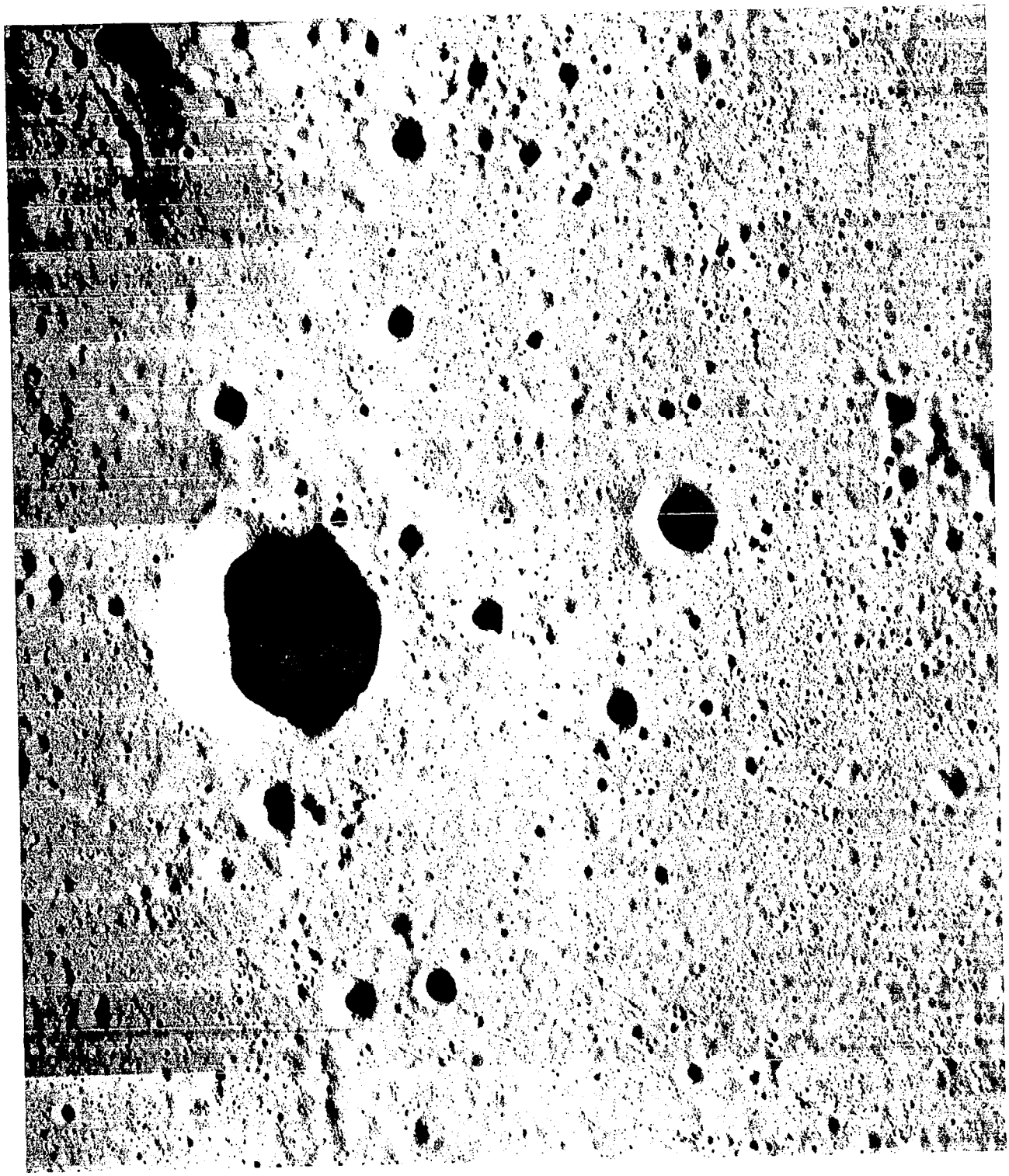

Figure 2.3-14: Wide-Angle Photography of Site IIP-4

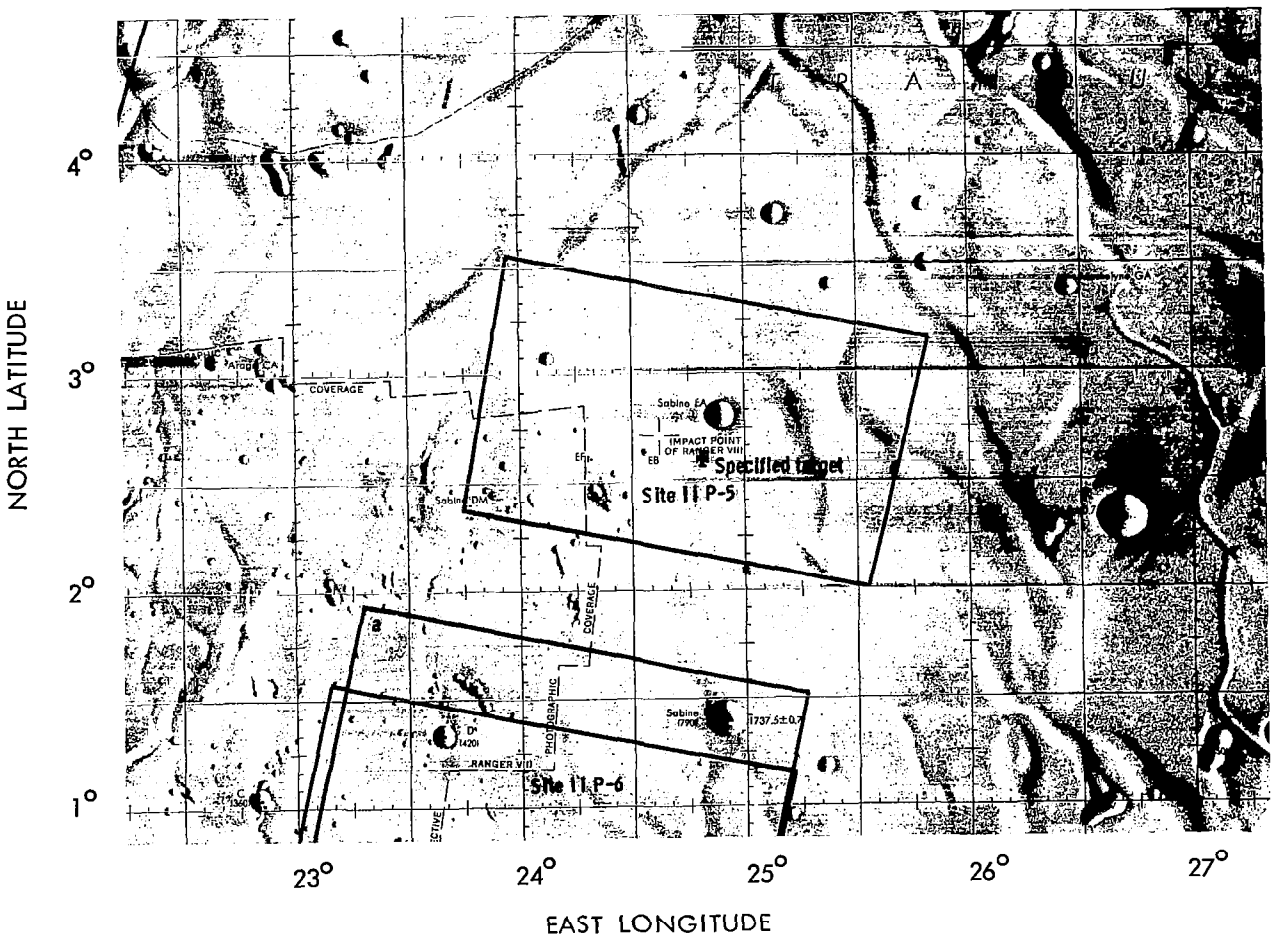

Figure 2.3-15: Site IIP-5 Coverage

2.3.2.5 Site IIP-5

Site IIP-5 was positioned to include the impact point of Ranger VIII in Mare Tranquillitatis. The area was photographed by a single eight-frame sequence.

The photographic coverage computed from post-mission data is shown in Figure 2.3-15. Location of the southwest corner of the photographic coverage was determined to be 23° 38.0' E longitude, 2° 21.0' N latitude by comparison of Wide-Angle Frame 67 with the ACIC chart Sabine DM, RLC9 having a scale of 1:50,000. Charts of this series do not include all of the area photographed at this site and AIC 60-C, Arago, does not include sufficient data to permit location of the remaining corners.

The shutter speed of 0.04 second used at this site was the correct choice. Wide-angle frames are exposed slightly more than optimum, while the telephoto frames are slightly underexposed. Image density for apparently smooth and level areas was estimated to be 0.7 to 0.8 in wide-angle photographs and 0.9 to 1.0 in telephoto frames as determined from GRE film. These values correspond to 0.8 to 0.9 and 0.6 to 0.7, respectively, on the spacecraft film. The photography is represented by a portion of Wide-Angle and Telephoto Frame 70, Figures 2.3-16 and 2.3-17, respectively.

Resolution of the wide-angle photographs was equivalent to four scan lines near the frame center. Telephoto frames were found to resolve features spanning four to five scan lines.

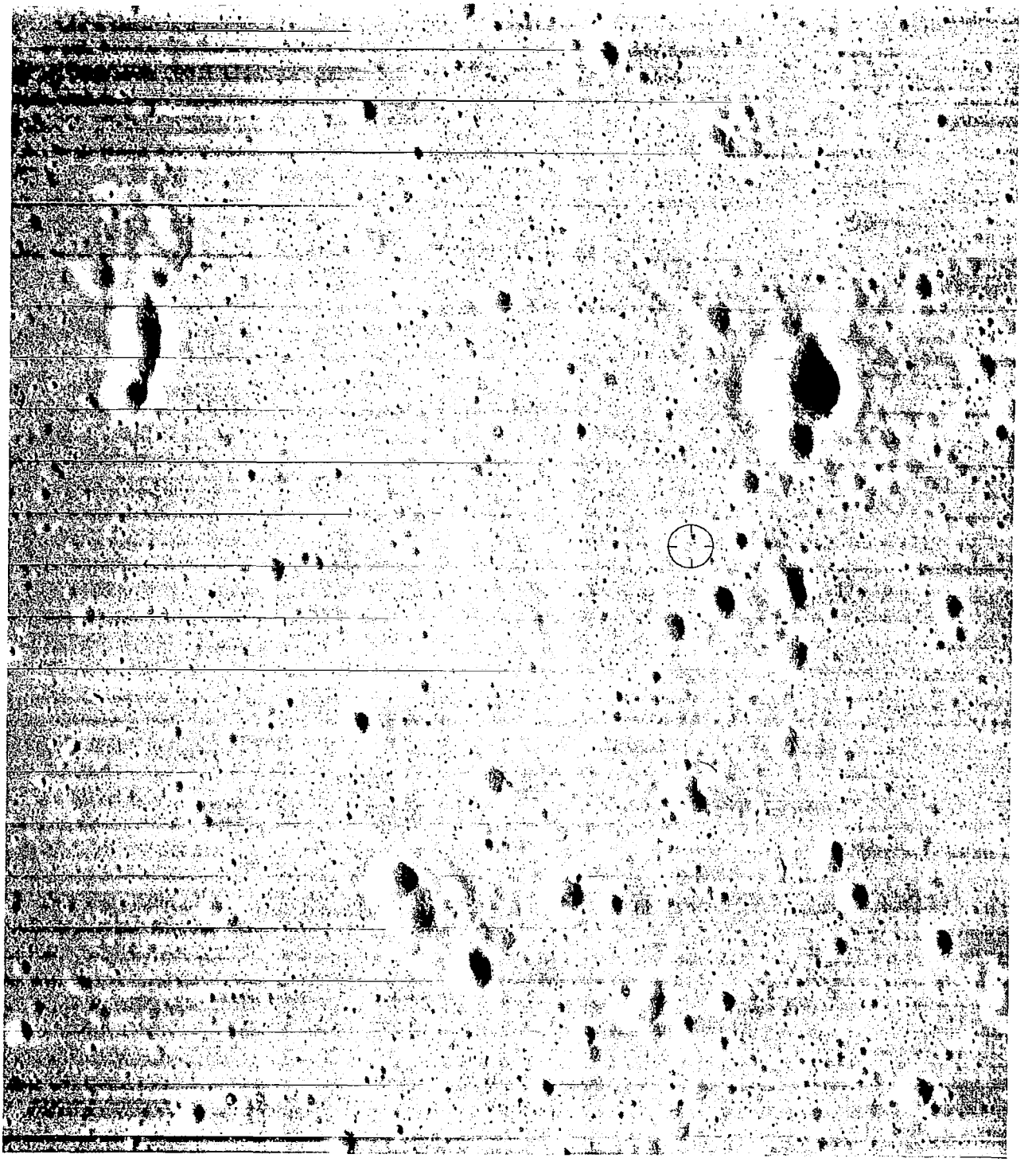

Figure 2.3-16: Wide-Angle Photography of Site IIP-5, Frame 70

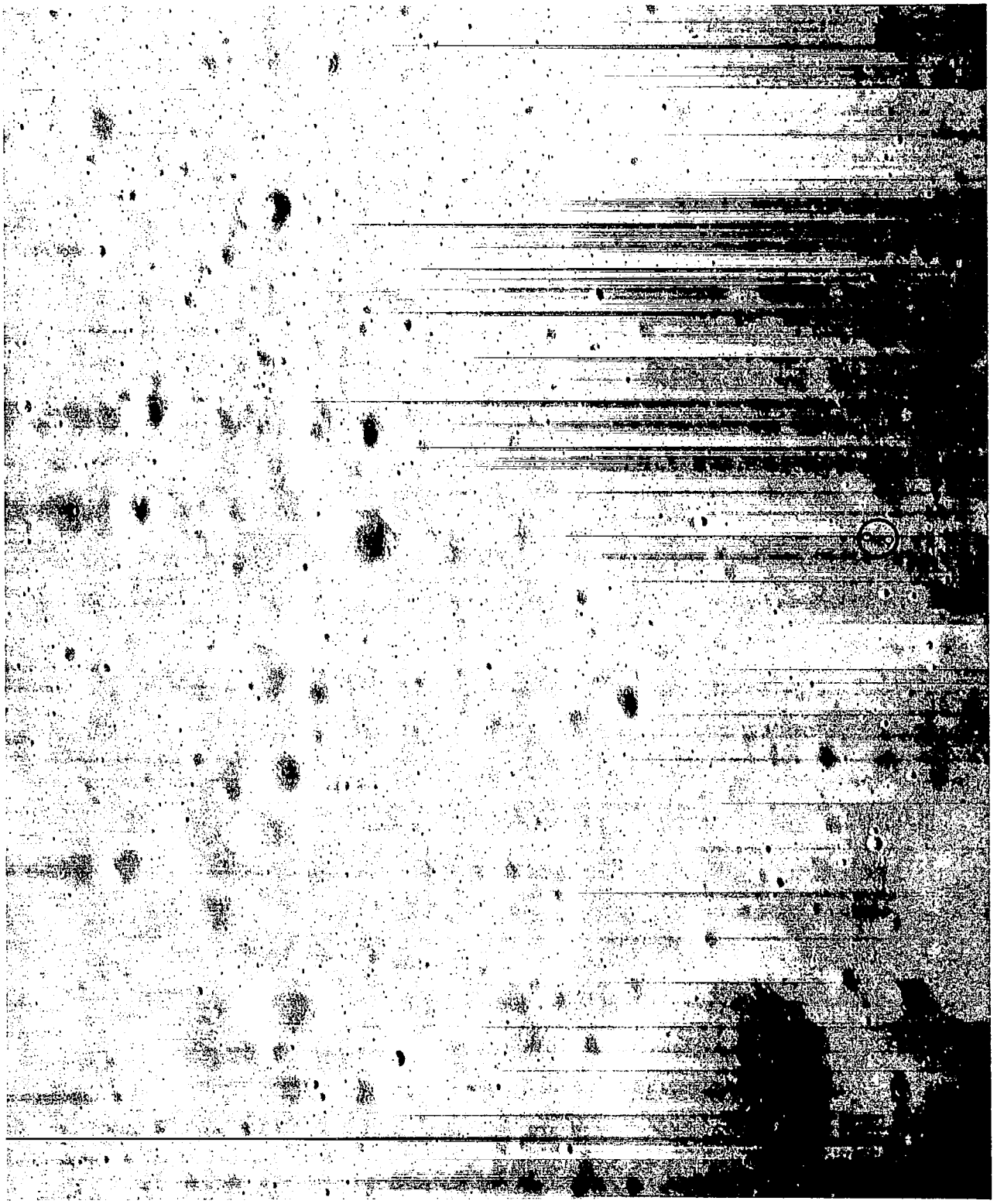

Figure 2.3-17: Telephoto Photography of Site IIP-5, Frame 70

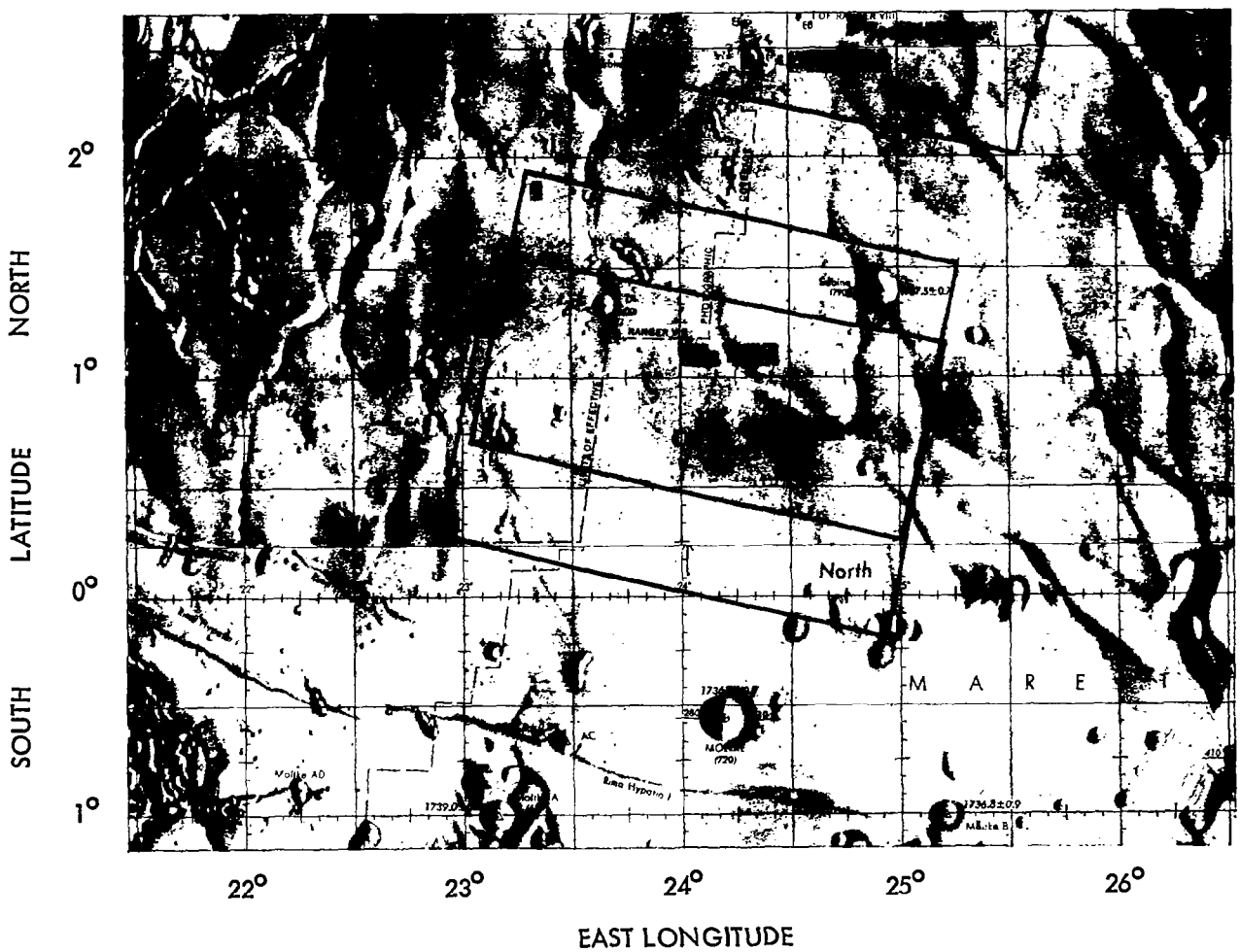

Figure 2.3-18: Sites IIP-6a and IIP-6b Coverage

The impact point of Ranger VIII has been identified on Telephoto Frame 70 as one of two small, bright craters. The craters have diameters of approximately 7 and 15 meters, lie close to the projected trajectory track, and have the appearance of recent formation. Since Ranger VIII did not photograph its impact point, positive identification of the crater by comparison of small photographic detail obtained by the two spacecraft cannot be made. However, results of impact studies by USGS geologists and others indicate the smaller of the two craters is the most likely candidate for the Ranger VIII impact point. The location of the craters is indicated on Figures 2.3-16 and 2.3-17.

2.3.2.6 Site IIP-6

Site IIP-6 was photographed with two eight-frame sequences on successive passes, providing the coverage shown in Figure 2.3-18. The area is south of Site IIP-5 and includes the western portion of the area photographed as Site I-3 on Mission I. The entire area is level mare, with crater Sabine E, 5 kilometers in diameter, the largest topographic feature. Computed positions of photograph corners agree within about 2 to 3 km of positions determined by comparison of the photographs with Ranger VIII charts (RLC 7, Sabine).

The quality of site photographs was good to fair based upon a subjective assessment of the GRE film. The relatively small phase angle (61.1 to 62.6 degrees), together with the smooth mare surface of the site, resulted in photographs that lack pronounced contrasts, although surface detail is shown (Figure 2.3-19).

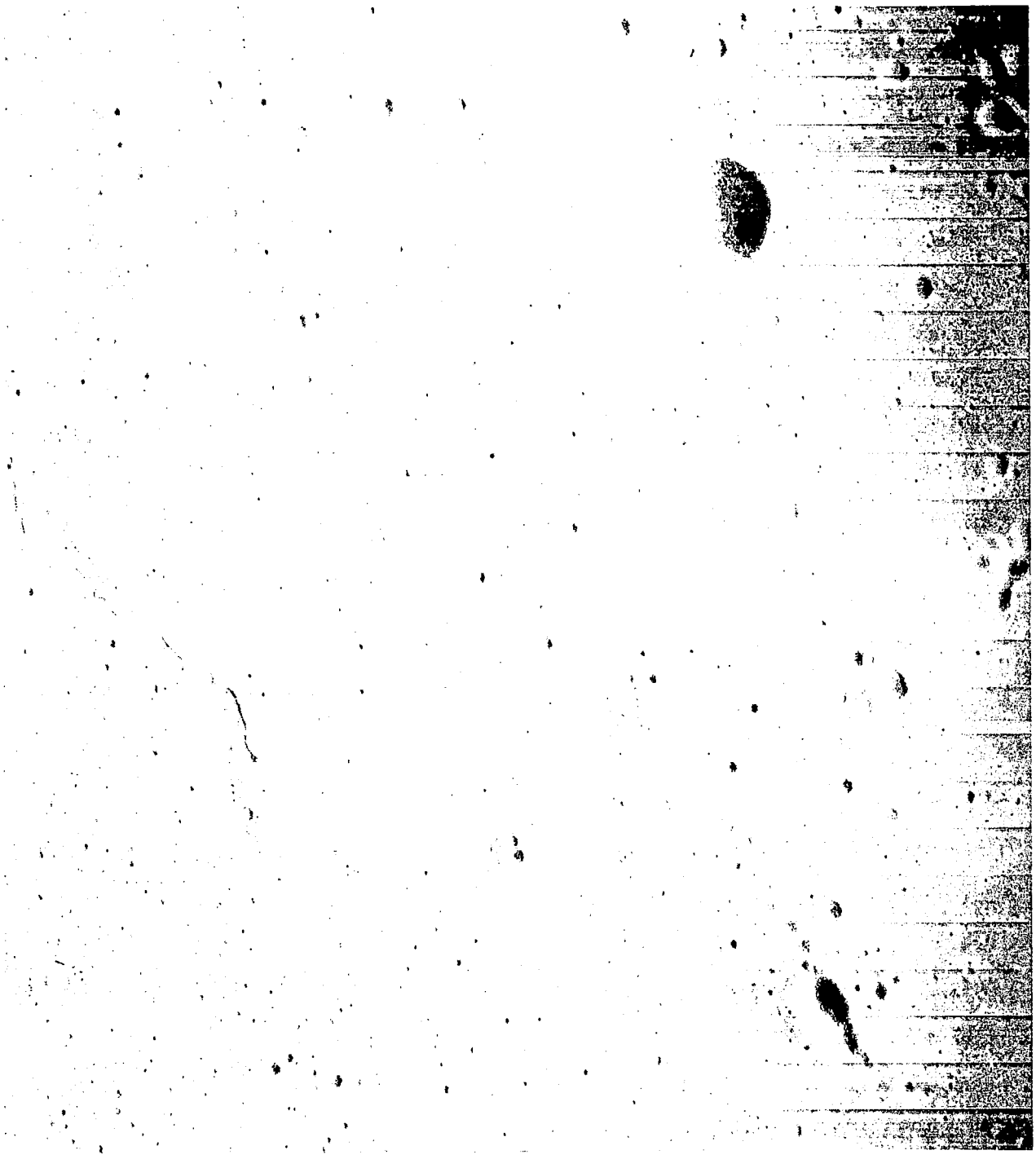

Figure 2.3-19: Wide-Angle Photography of Site IIP-6a

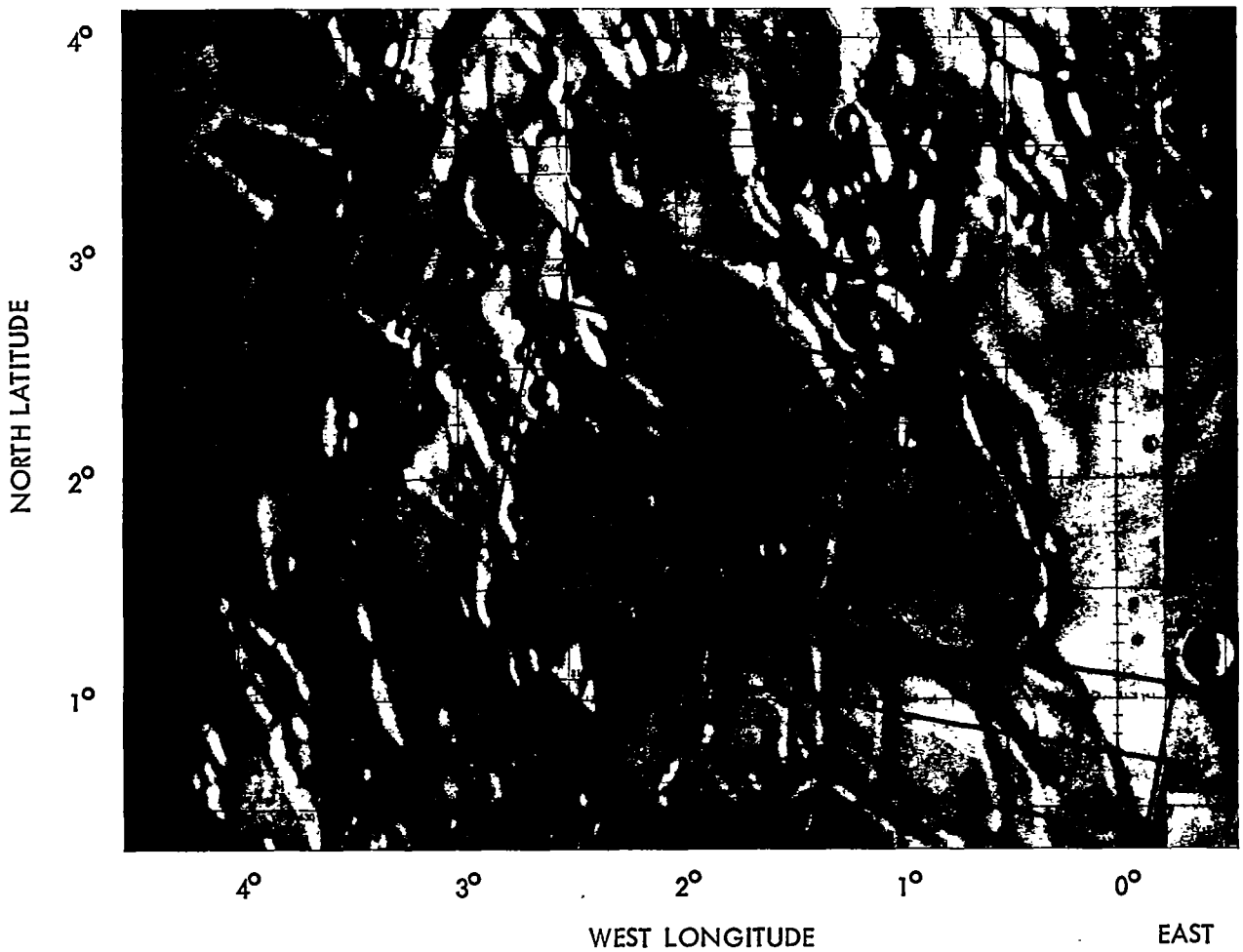

Figure 2.3-20: Sites IIP-7a and IIP-7b Coverage

Exposure of the photographs appeared to be satisfactory considering the lens transmission differential. GRE film densities were normal for the mission.

Resolution estimates indicated that the wide-angle photographs were somewhat better than the telephoto, on the basis of the number of scan lines spanned by the smallest detectable surface features.

2.3.2.7 Site IIP-7

Site IIP-7 is within the north-central part of Sinus Medii. Although mostly mare, the photographed area includes some terra at the western end and surrounding the crater Pallas FA. Most of the area is low relief but covered by small craters. The site was photographed by two eight-frame sequences on successive orbits, providing the coverage shown in Figure 2.3-20.

The exposure appears to be satisfactory and resulted in GRE densities typical of previous sites. Some detail has been lost in the wide-angle photographs in the upland areas where the albedo was higher than the mare area of principal interest as seen in Figure 2.3-21. Although exposure for the site appears acceptable, a slower shutter speed would have resulted in improved telephoto photography, but at the expense of more severe overexposure within areas of higher luminance in the wide-angle photographs.

The photographs of this site have been degraded by processing defects, as noted in Paragraph 2.3.1.2.

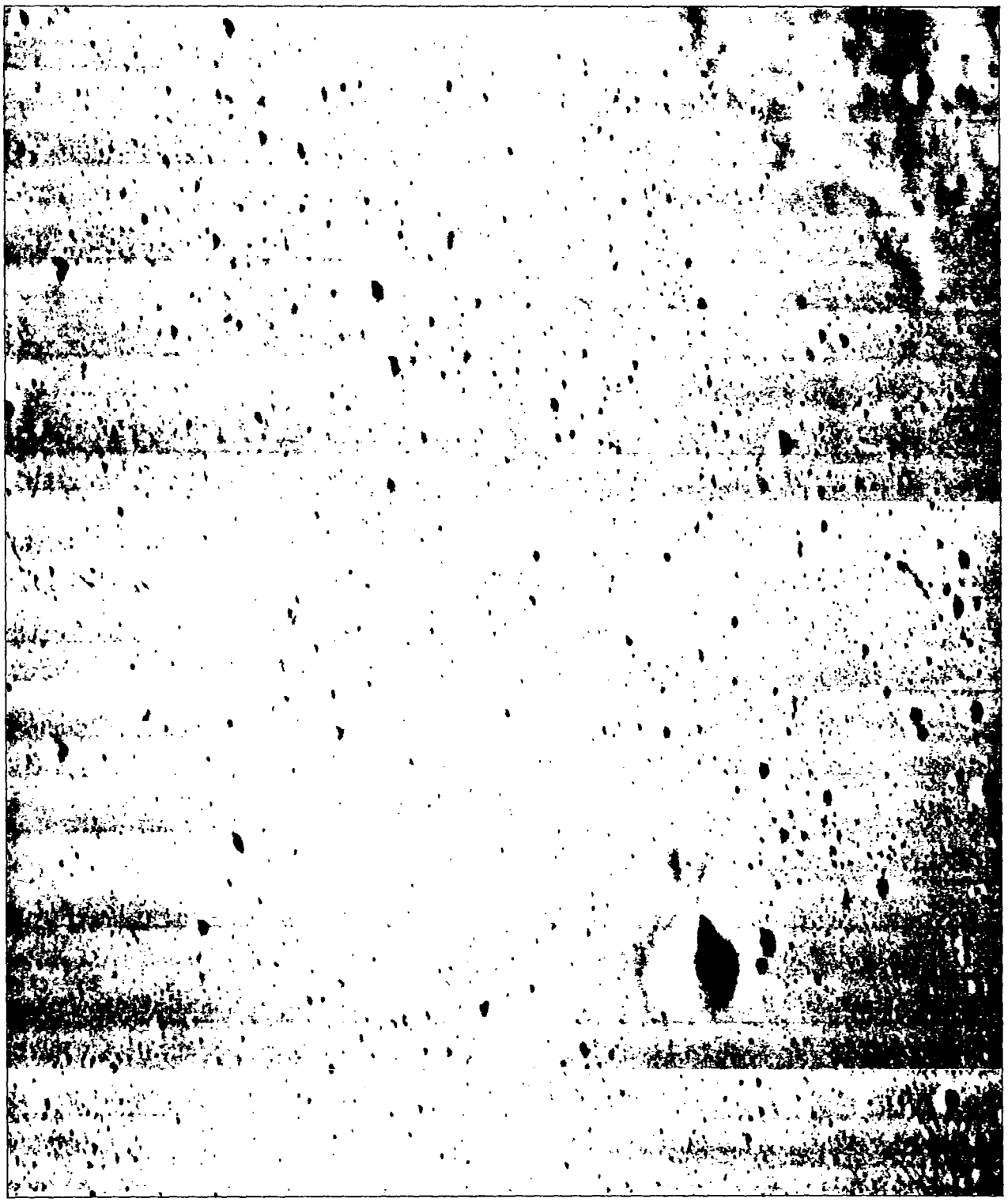

Figure 2.3-21: Wide-Angle Photography of Site IIP-7b

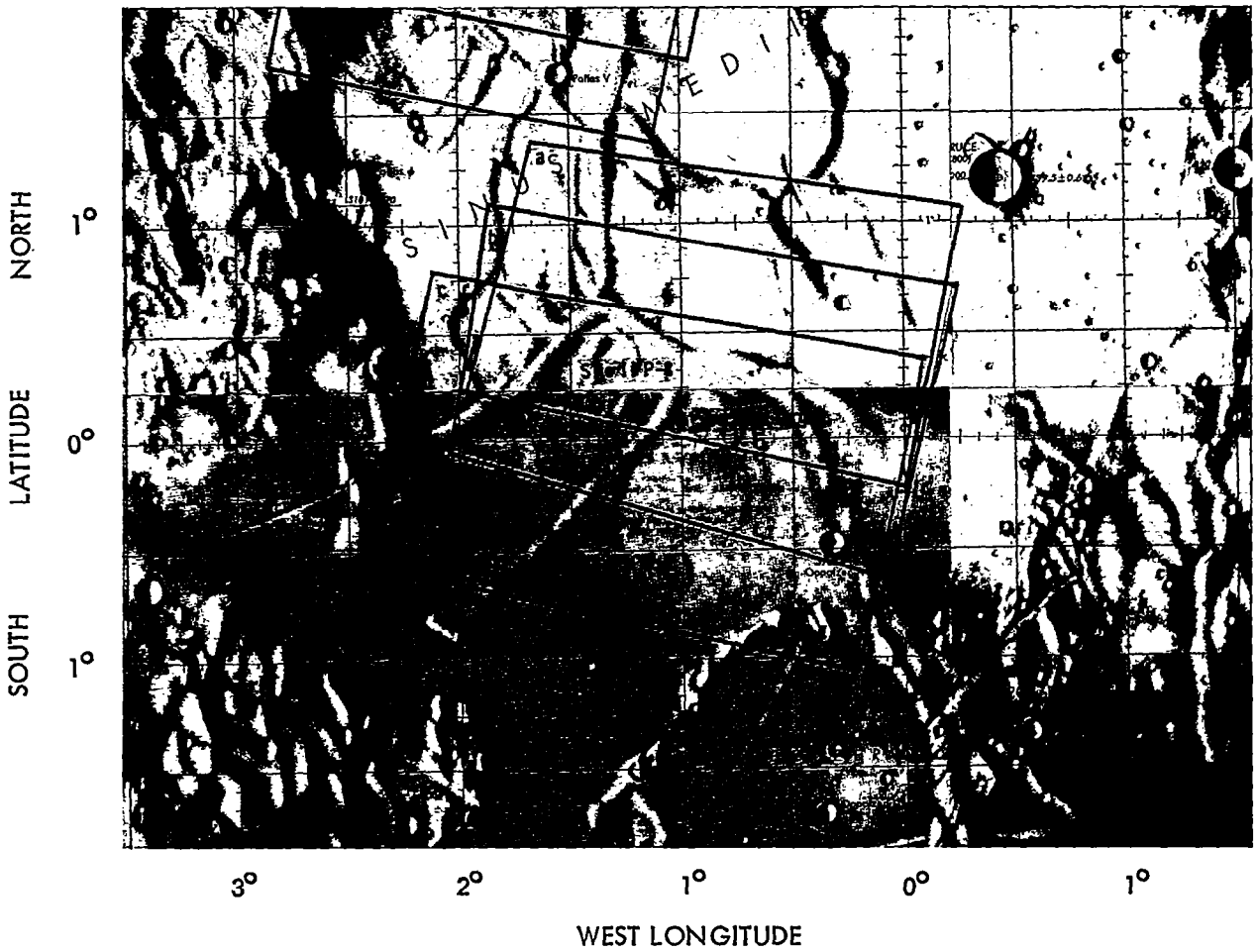

Figure 2.3-22: Sites IIP-8a, IIP-8b, and IIP-8c Coverage

2.3.2.8 Site IIP-8

Site IIP-8 was the only area photographed by three eight-frame sequences on successive orbits. It is located in central Sinus Medii. No prominent topographic features other than low ridges are indicated on lunar charts. The area photographed is shown in Figure 2.3-22.

Site IIP-8 photographs were exposed with a shutter speed of 0.02 second on all three passes, with the phase angles of 63.15, 61.69, and 6.23 degrees for passes a, b, and c, respectively. The small phase angle, together with the moderately high albedo (0.092), resulted in overexposure of the wide-angle photographs sufficient to cause loss of image quality. The small phase angle and flat topography resulted in further lowering image contrast. The telephoto photographs, however, are of very good quality as a result of the increased exposure. Examples of the wide-angle and telephoto photography are shown in Figures 2.3-23 and 2.3-24, respectively.

Surface features spanning approximately four scan lines were detectable near the center portion of the telephoto frames. The more desirable exposure of these frames did not appear to result in significant improvement in resolution by visual estimate. The low contrast and density of the overexposed GRE film made detection of small surface detail difficult in wide-angle photographs, although features spanning four to five scan lines were observed.

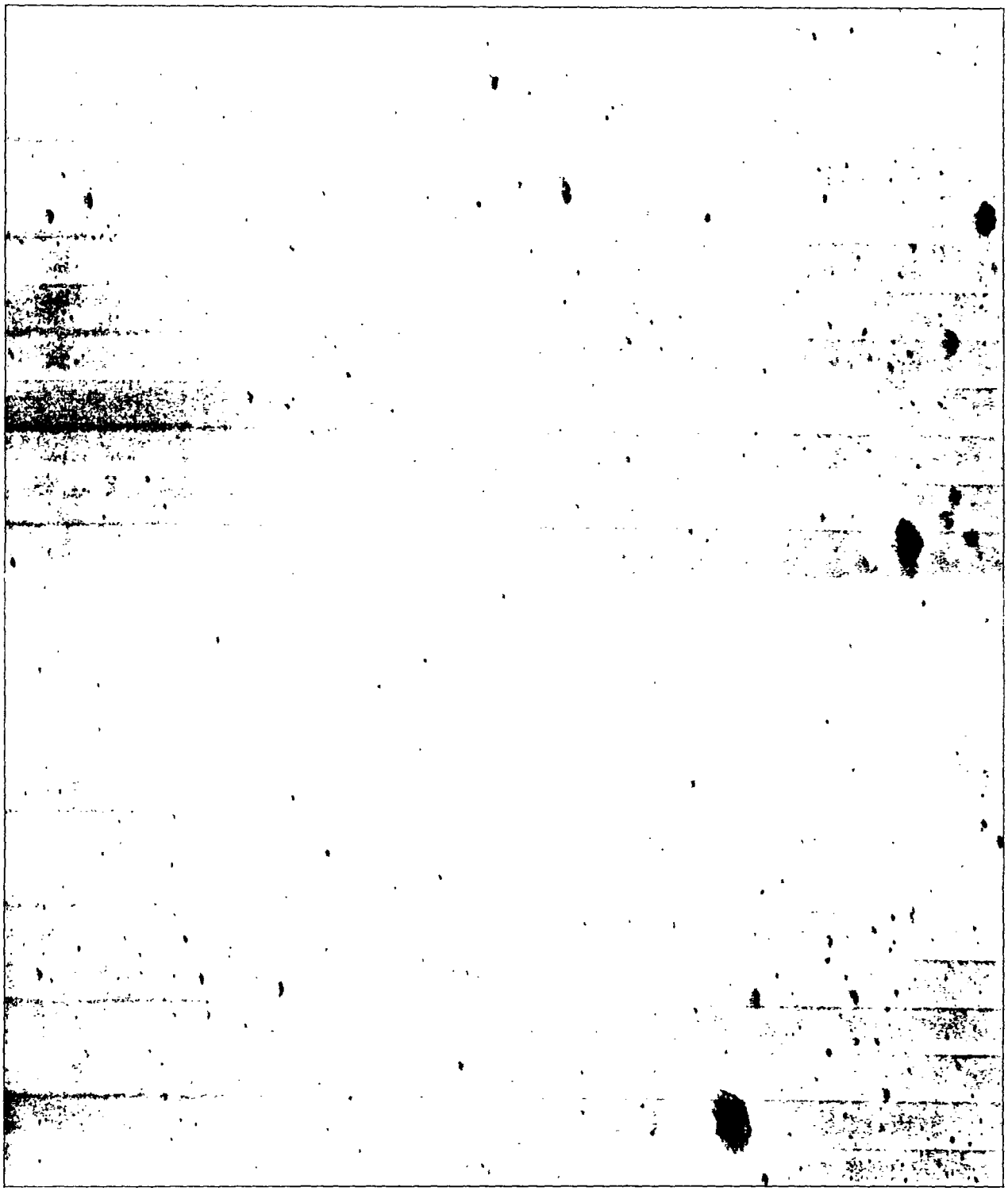

Figure 2.3-23: Wide-Angle Photography of Site IIP-8b

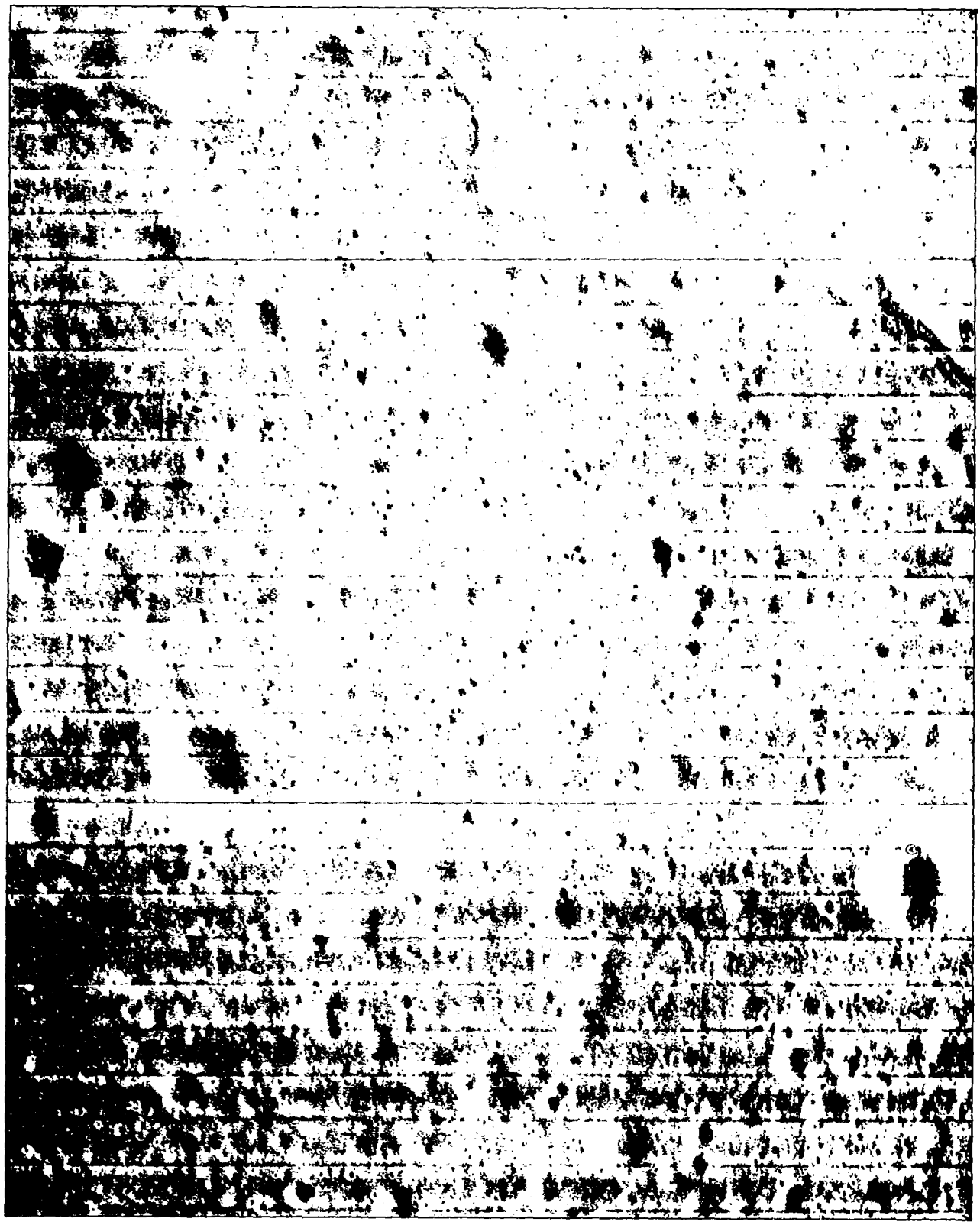

Figure 2.3-24: Telephoto Photography of Site IIP-8b

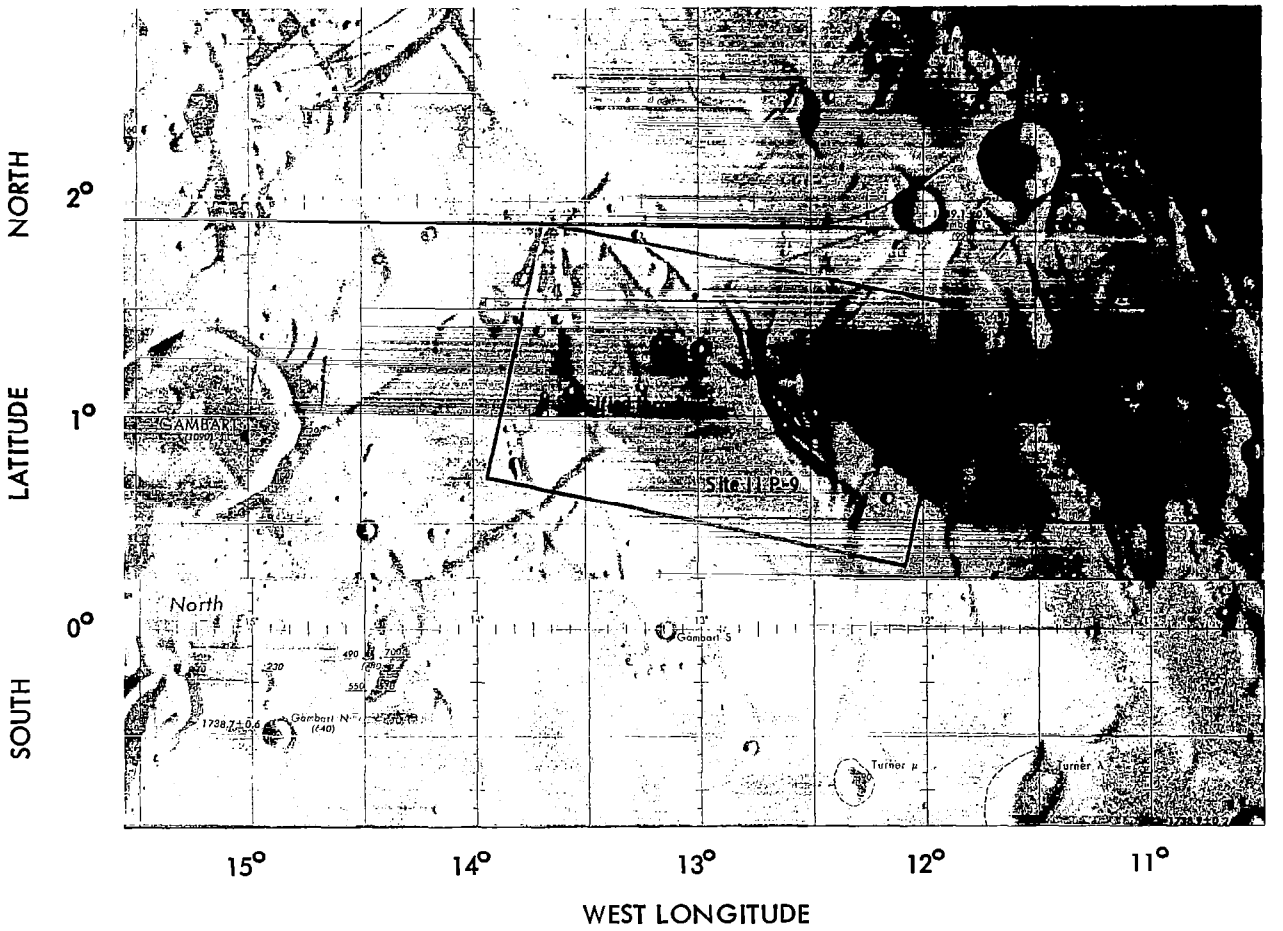

Figure 2.3-25: Site IIP-9 Coverage

2.3.2.9 Site IIP-9

Site IIP-9 is located in mare east of Gambart as shown in Figure 2.3-25. The area includes some low-relief, upland-type of terrain but no major topographic features. The area is within the influence of the Copernican ray system and thus has a relatively high albedo for mare (0.093). Comparison of the wide-angle photographs with the ACIC lunar charts of both the LAC and AIC series (LAC 58, Copernicus, Second Edition, and AIC 58C, Gambart) shows differences in feature positions. These differences introduce uncertainty in location of actual photographic coverage on the above charts.

The shutter speed of 0.02 second resulted in fairly good exposures for the wide-angle photographs, with a tendency towards overexposure (average GRE density 0.6) and loss of detail in the midportion of each frame. Surface features spanning only three to four scan lines were detected near the center of the wide-angle frames, although some detail was lost in highlight areas (Figure 2.3-26).

As expected from the differences in lens transmission characteristics, the telephoto frames tended to be underexposed. Although the average GRE image density was high, lunar features spanning three and one half to four scan lines were observed on the telephoto frames.

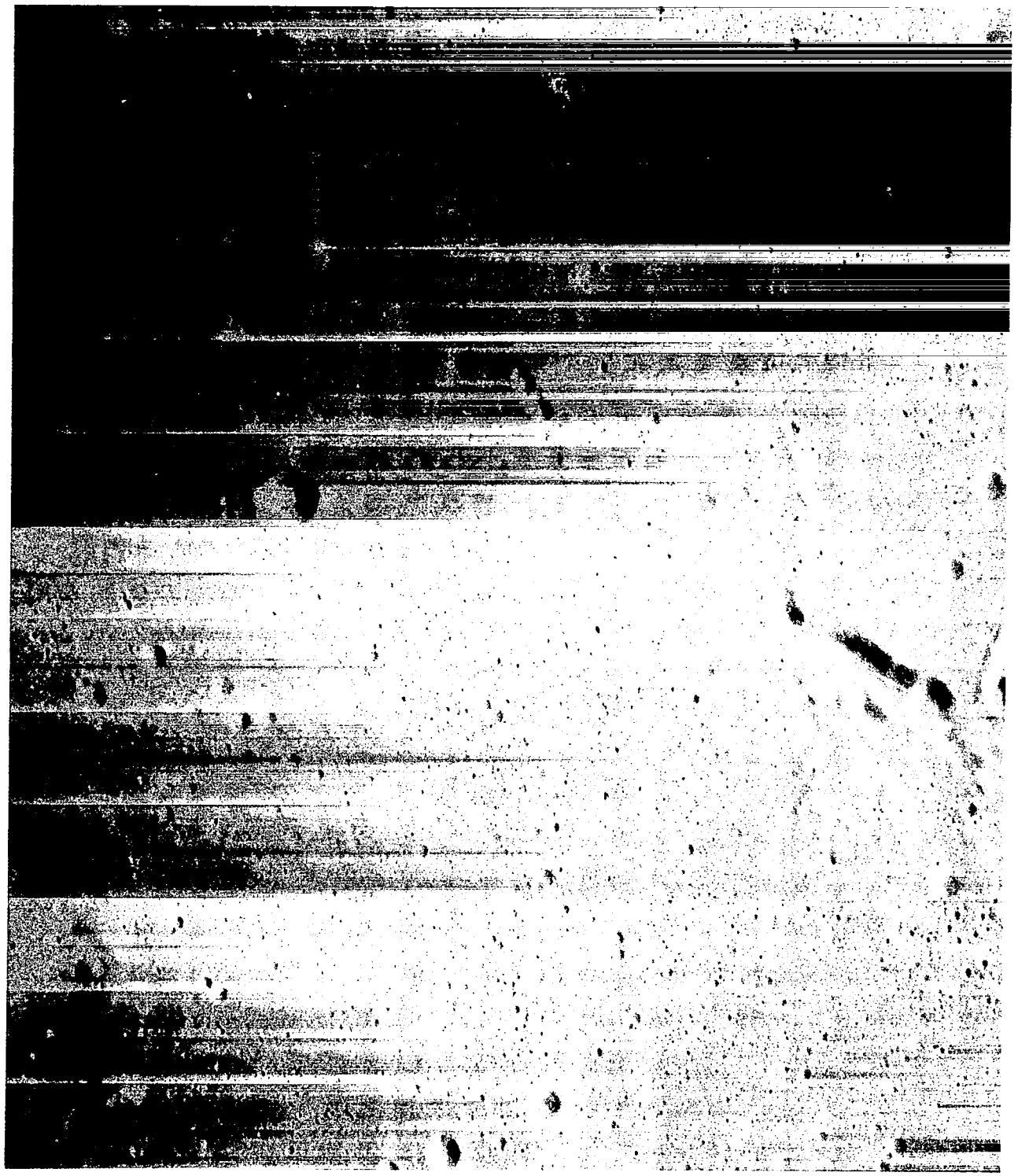

Figure 2.3-26: Wide-Angle Photography of Site IIP-9

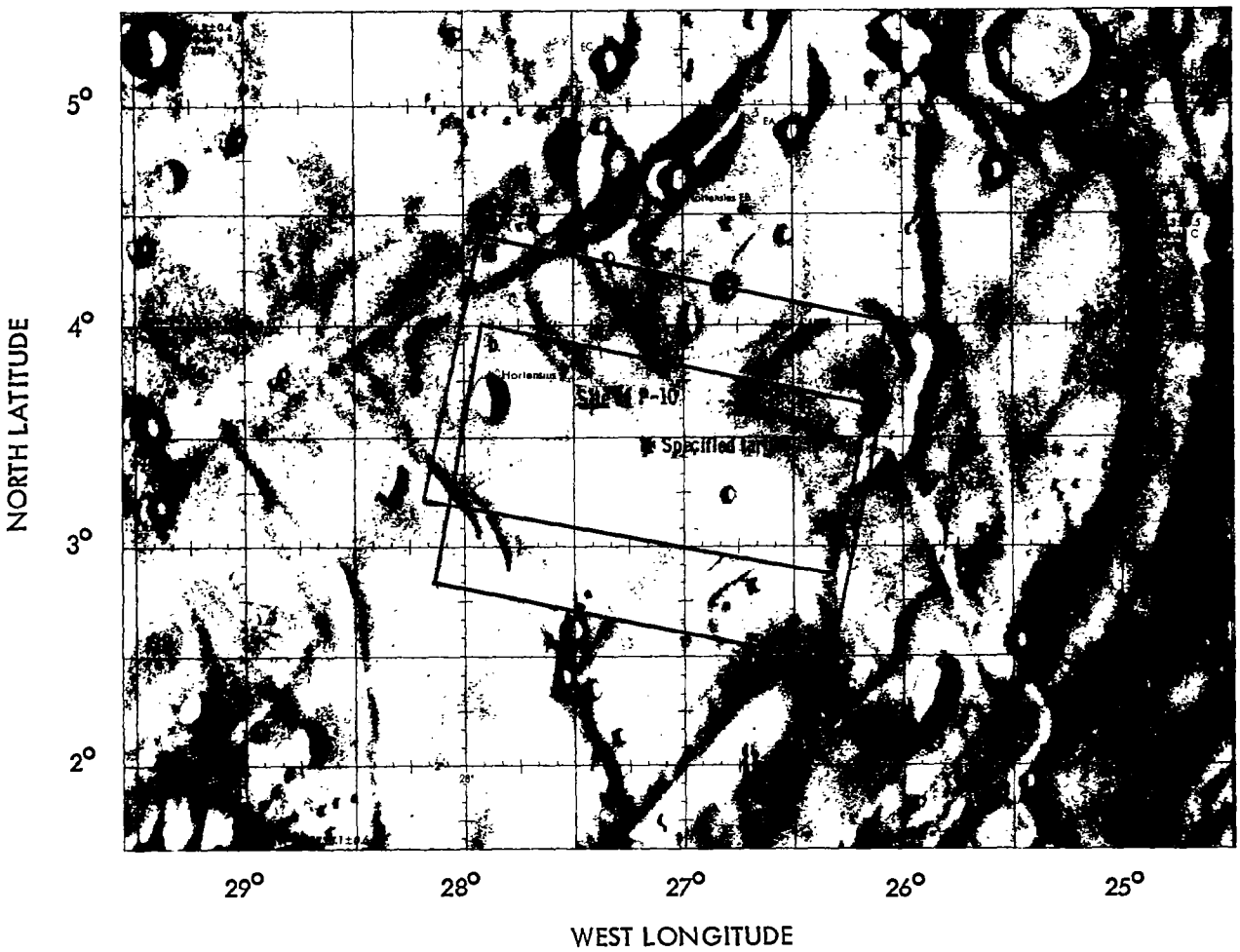

Figure 2.3-27: Sites IIP-10a and IIP-10b Coverage

2.3.2.10 Site IIP-10

Site IIP-10 was photographed with two eight-frame sequences on successive orbits to provide coverage as shown in Figure 2.3-27. The site, west of Reinhold, is depicted on ACIC Chart AIC 58 D, Reinhold, as smooth mare with faint ridges and few craters. Copernican rays occur within the area. The ridges and dome indicated on the charts were not readily apparent in the wide-angle photographs, although the sun angle was 78 degrees. Presence of ray structure was evident more from crater distribution or surface structure than from a difference in luminance, although some indication of the latter is visible. (Figure 2.3-28).

The shutter speed of 0.04 second was correct for this site. Both wide-angle and telephoto frames were of good quality although the latter were exposed less than optimum. Since there are no large areas of steep slopes, information loss from hard shadows or very bright highlighted areas is minimal.

Wide-angle frames of the first sequence appeared to be of higher quality than those of most prior sites. Telephoto frames were also of good quality, although the average GRE film density tended to be greater than for the wide-angle photos. Features identified as craters spanning only three scan lines (0.08 mm on the GRE film) were detected in both wide-angle and telephoto frames of this site.

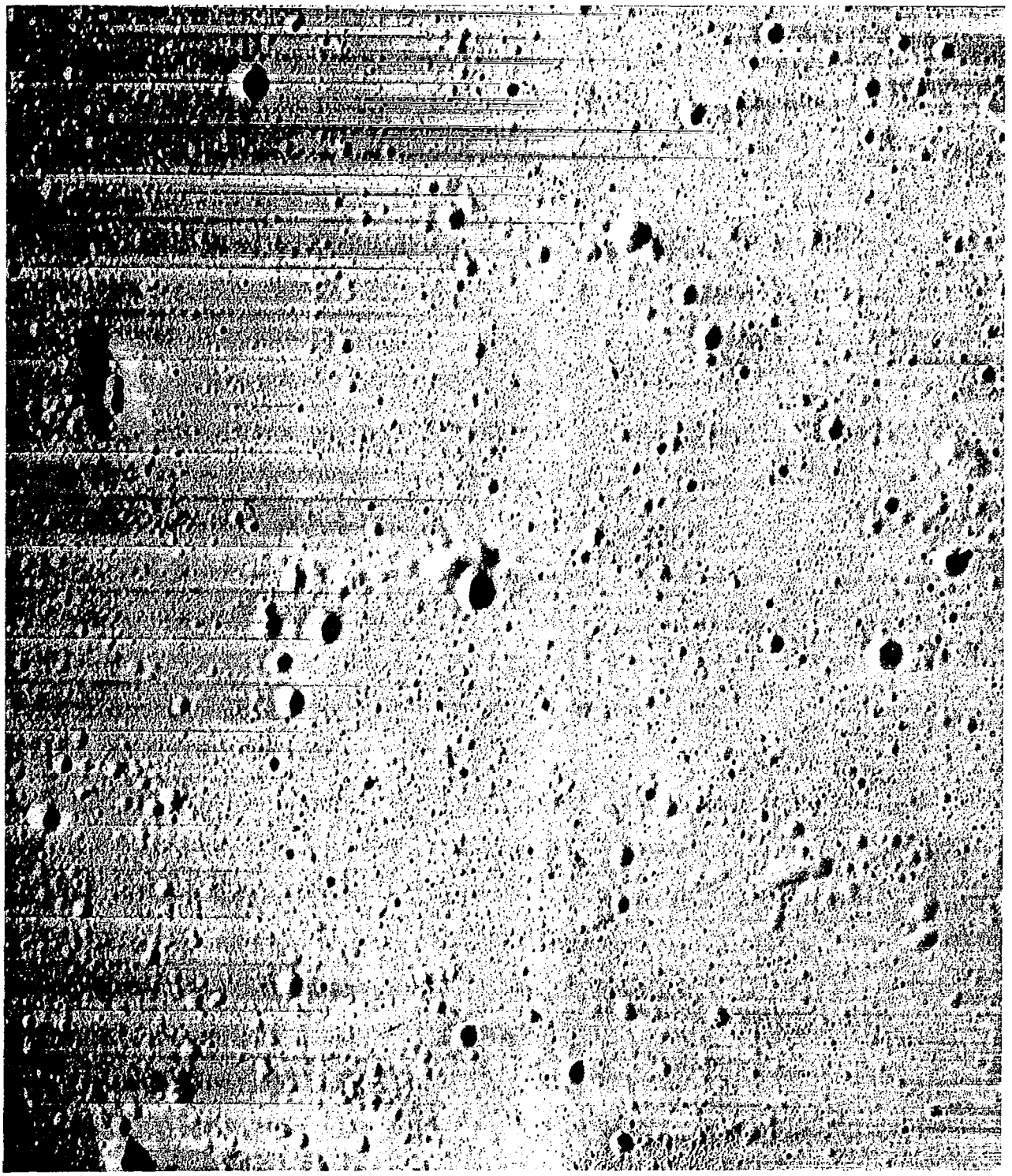

Figure 2.3-28: Wide-Angle Photography of Site IIP-10a

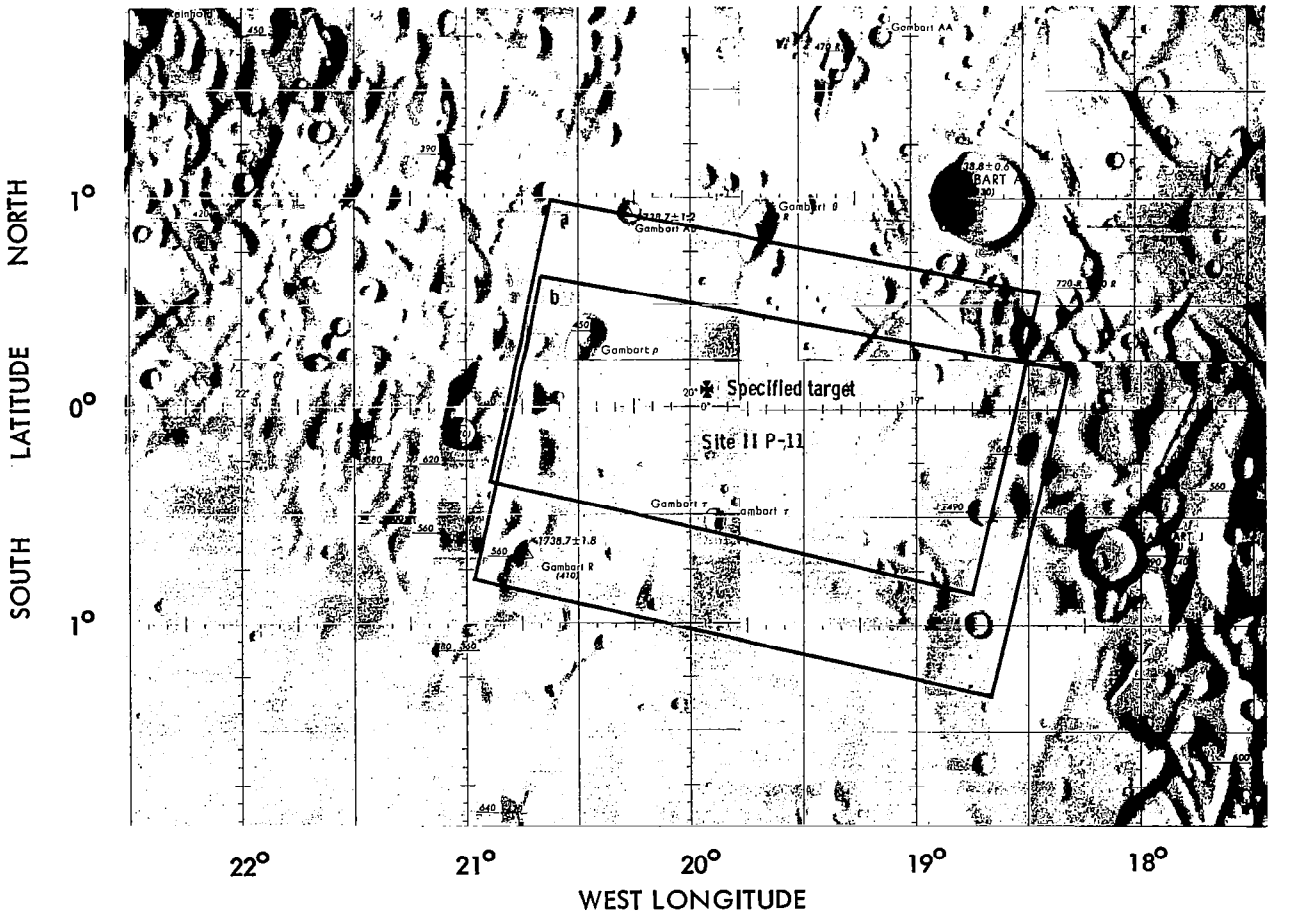

Figure 2.3-29: Sites IIP-11a and IIP-11b Coverage

2.3.2.11 Site IIP-11

Site IIP-11 is located in a mare area about 300 km directly south of Copernicus and between areas of upland character (Figure 2.3-29). This site is within the Copernican ray system, which accounts for its high albedo (0.105). The ACIC charts depict a smooth area almost devoid of topographic features. The photographs of the site show no craters larger than about 3 kilometers in diameter. Numerous smooth, rounded domesor hills, having a surface character typical of upland, are scattered over the site. Only the steeper slopes, exceeding about 27 degrees, produced hard shadows because the incident angle of illumination was between about 62 and 63 degrees. The illumination resulted in low contrasts in smooth areas and the shallow, low-profile craters (Figure 2.3-30).

The shutter speed of 0.02 second resulted in overexposure of the wide-angle photographs sufficient to cause some degradation of image quality. This was anticipated in selection but was accepted to improve exposure of the telephoto frames. The telephoto frames were well exposed in the middle portion and slightly underexposed at each end. An exposure of 0.04 could possibly have been used for the telephoto but at the expense of much detail in wide-angle photography.

In spite of the overexposure of wide-angle photographs and resulting low density of the GRE film, surface features spanning three to four scan lines were detected near the frame centers. Detection of very small craters was difficult because of the low contrast between the lighted interior slope and the surrounding area. Resolution of features spanning three and a half to four scan lines was accomplished near the center of telephoto frames (Figure 2.3-31).

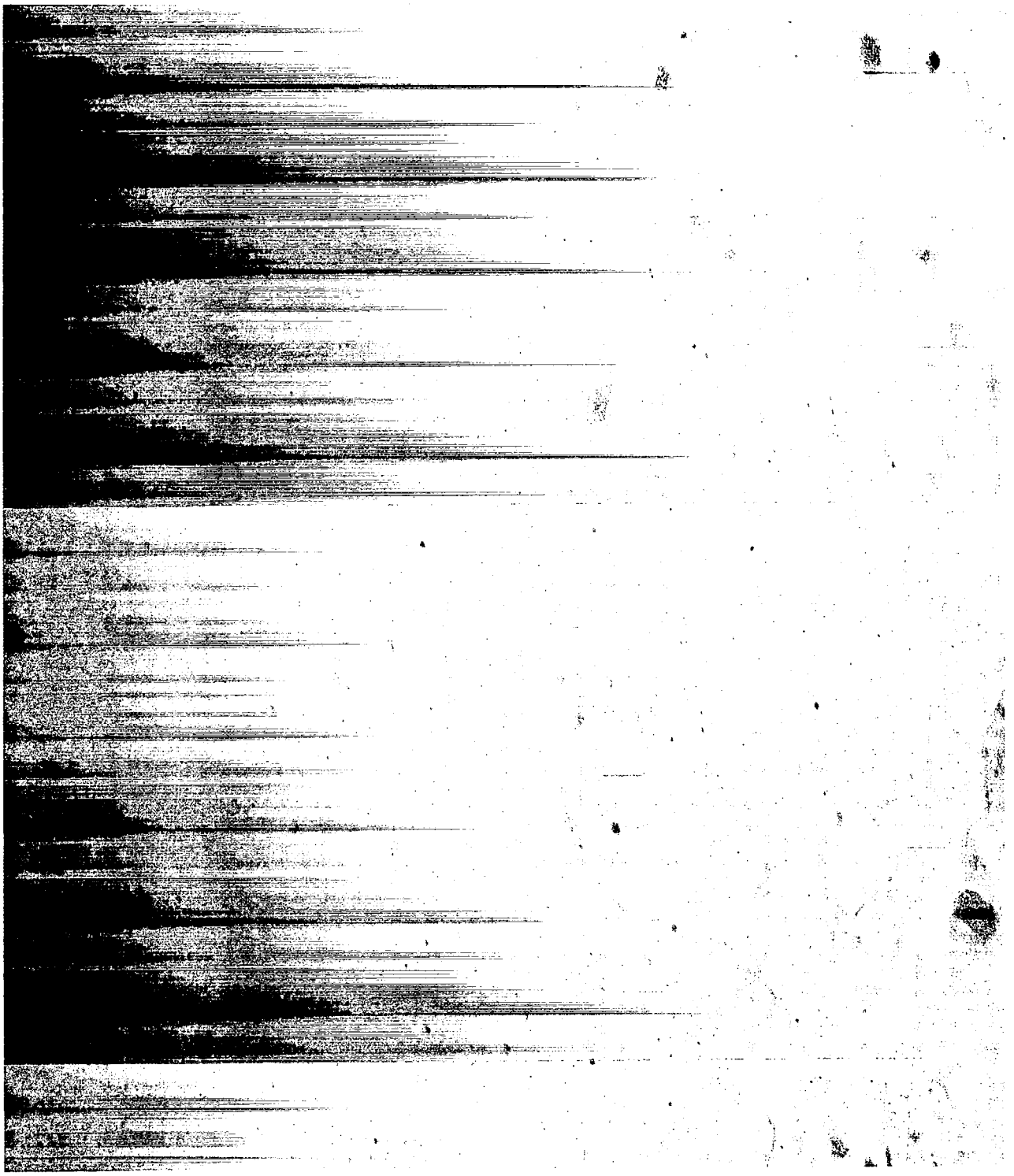

Figure 2.3-30: Wide-Angle Photography of Site IIP-11a

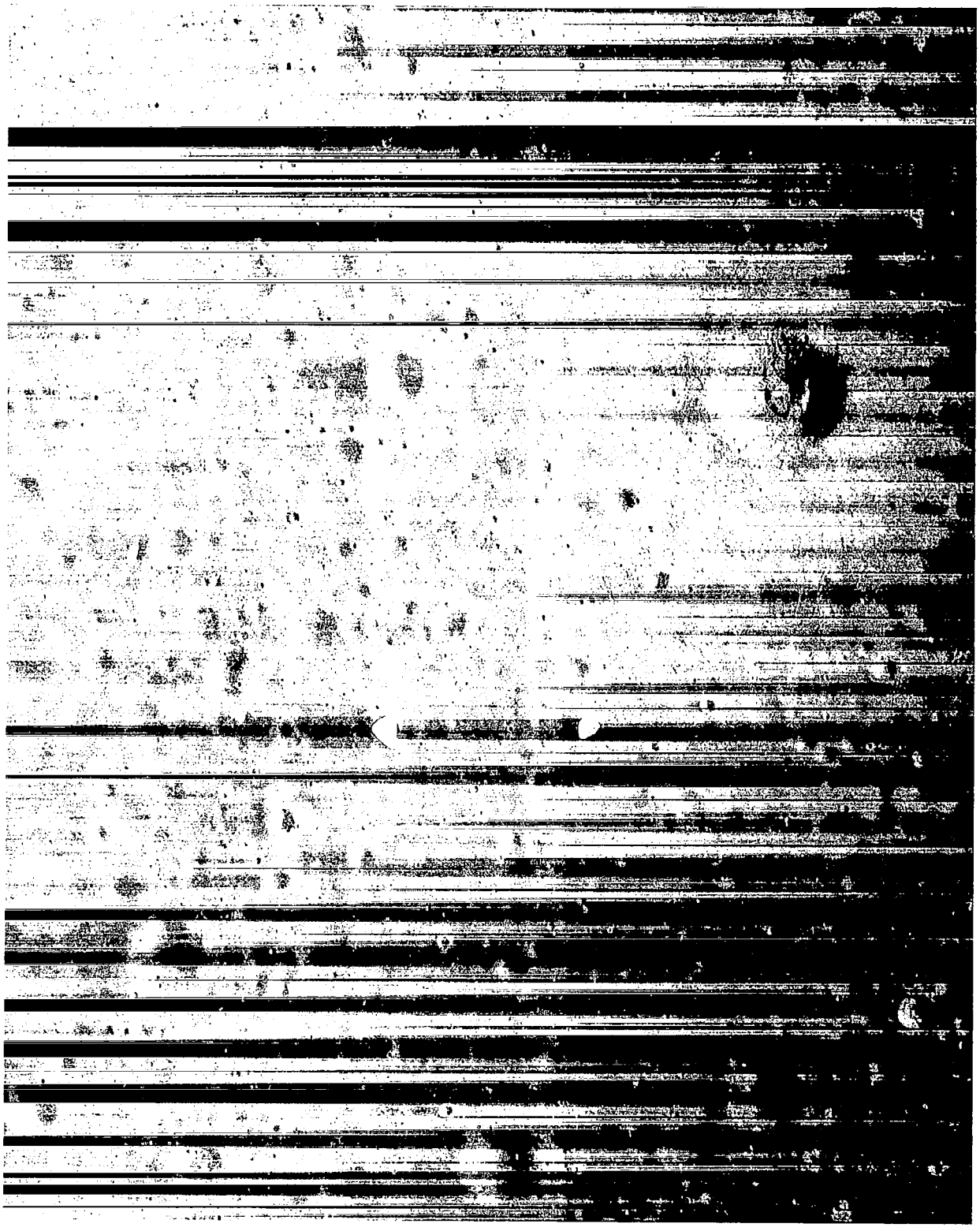

Figure 2.3-31: Telephoto Photography of Site IIP-11b

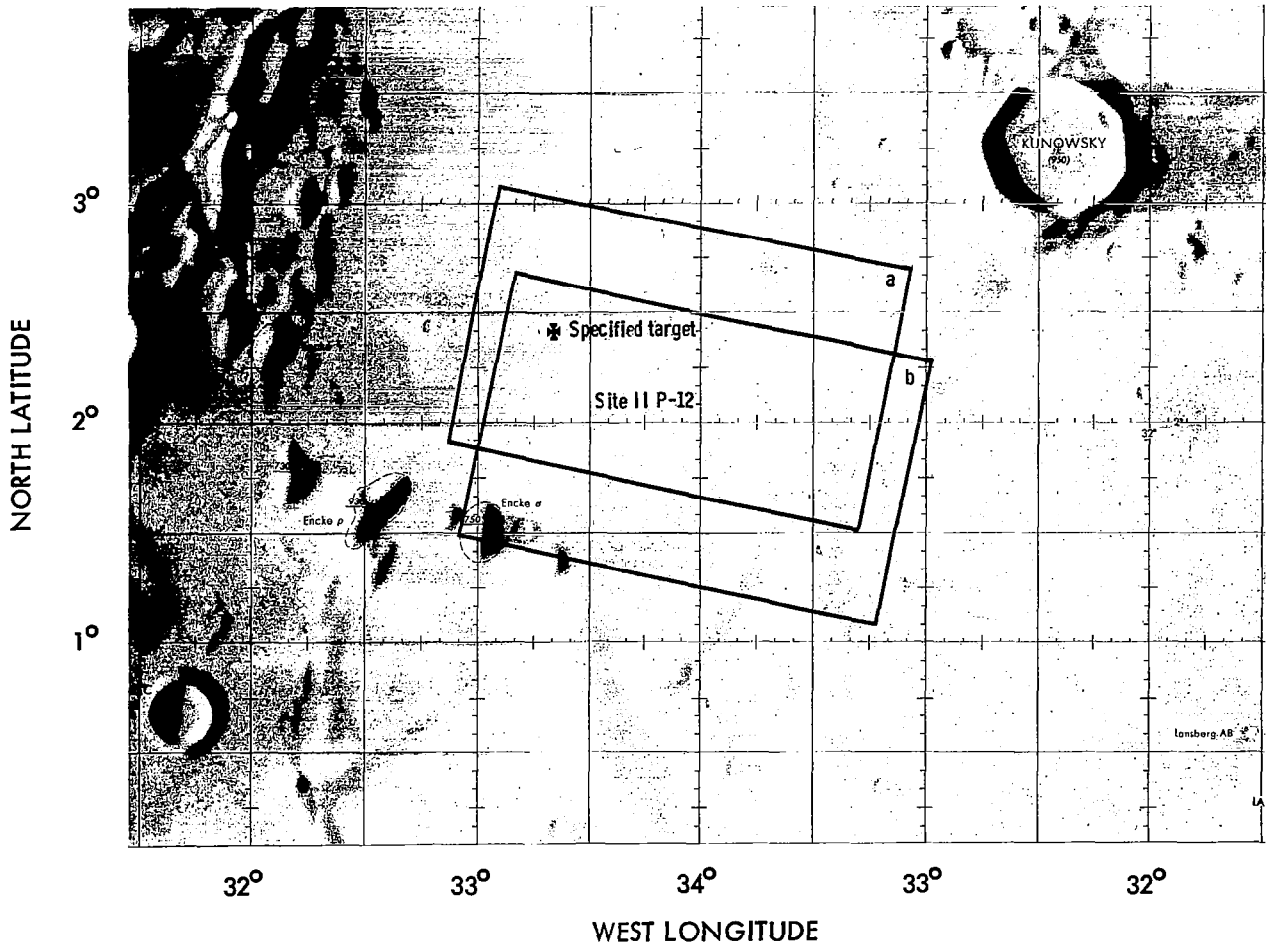

Figure 2.3-32: Sites IIP-12a and IIP-12b Coverage

The relatively small angle of incidence of the illumination (59 to 62 degrees) existing at this site during photography was an important factor in reducing the quality of wide-angle photography by lowering contrasts.

2.3.2.12 Site IIP-12

This site is southeast of Kepler in an area indicated on the ACIC charts as smooth, almost featureless, mare, as shown in Figure 2.3-32. The area does, however, include ray structure originating from both Kepler and Copernicus. The wide-angle photographs show few topographic features, either craters or eminences, larger than 1.5 kilometers in diameter. There is, on the other hand, much evidence of secondary craters and ejecta patterns whose alignment indicates origin from Kepler and Copernicus (Figure 2.3-33).

A shutter speed of 0.04 second was used for the photographs taken on the first of the two eight-frame sequences at this site, and a speed of 0.02 second for the second sequence. The computations for exposure prediction indicated a borderline condition between 0.04 and 0.02 second. Considering the forward and side overlap obtained by the two sequences planned, an exposure of 0.04 second was selected for the first sequence to provide better exposure of the telephoto frames at the expense of overexposure of the wide-angle frames. The 0.02-second shutter speed was used for the second pass for improved exposure of the wide-angle frames.

Telephoto frame exposure of the first pass (IIP-12a) appears to be very good. Since there are no major topographic features, surface detail is lost only within the areas of hard shadows and highlighted slopes within steep-walled craters.

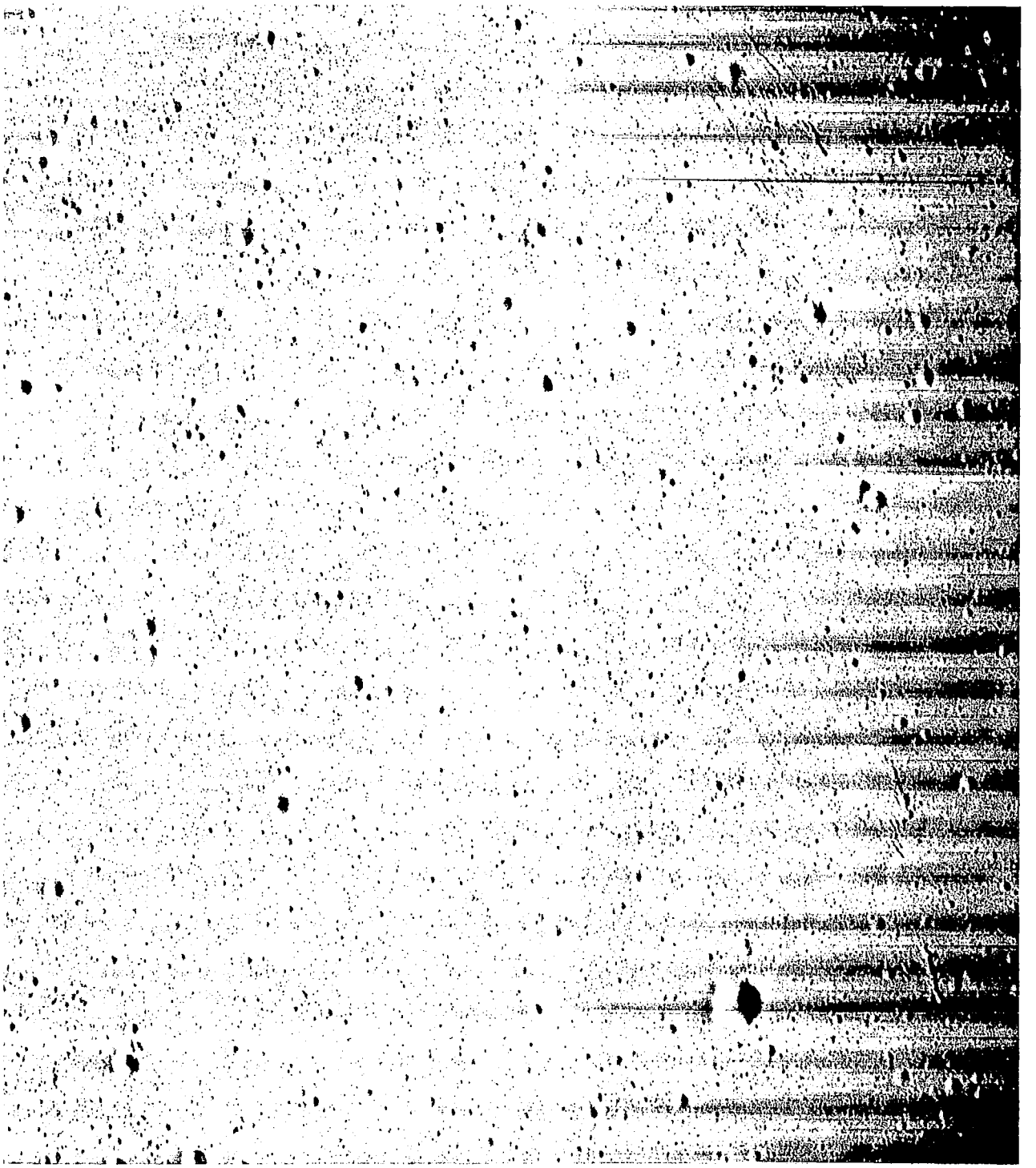

Figure 2.3-33: Wide-Angle Photography of Site IIP-12b

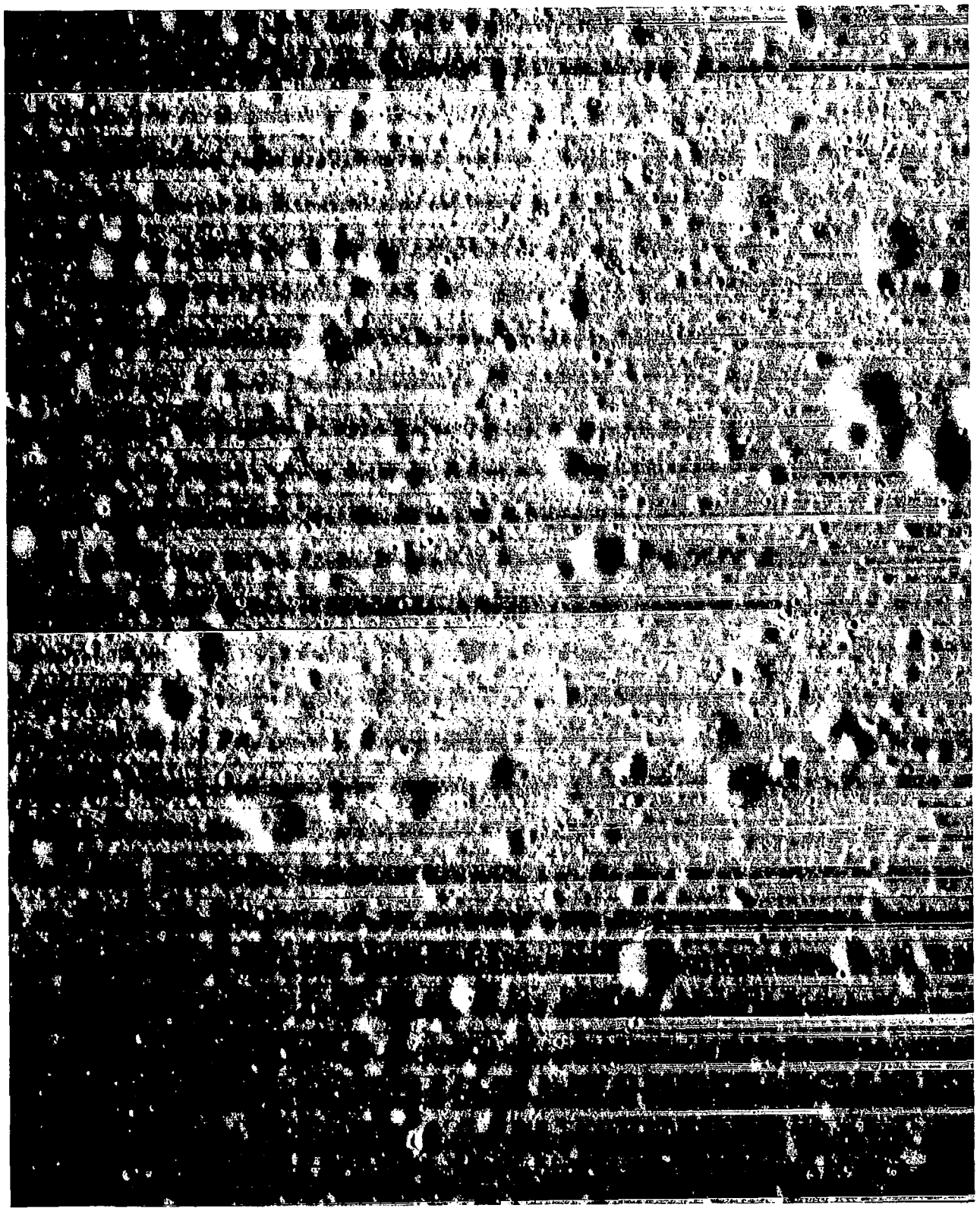

Figure 2.3-34: Telephoto Photography of Site IIP-12b

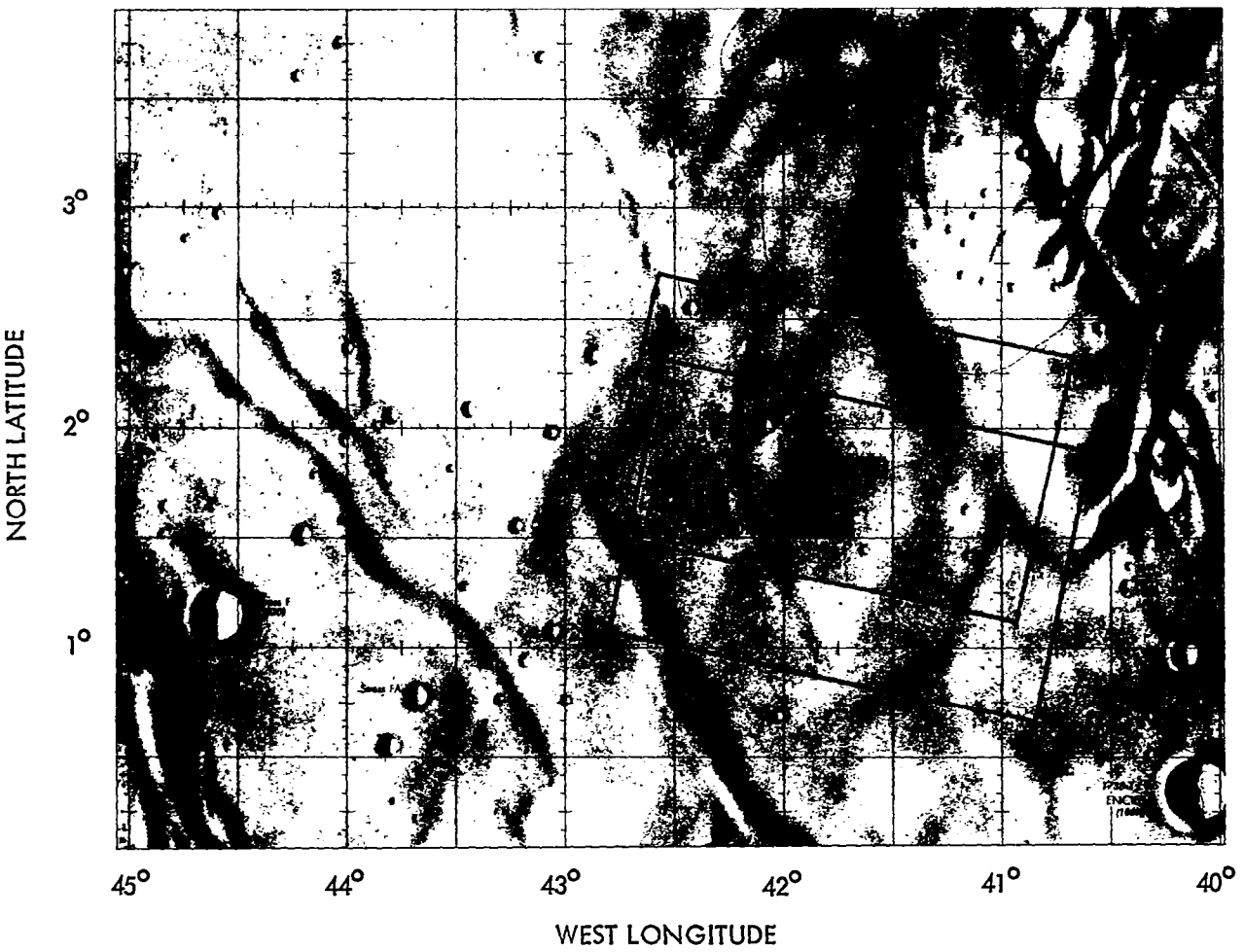

Figure 2.3-35: Sites IIP-13a and IIP-13b Coverage

Albedo variations associated with ray structures are apparent but do not cause a luminance range beyond system capability.

Most wide-angle frames of the first pass are quite overexposed and show little surface detail except hard, or nearly hard, shadows. Small craters can be detected by these shadows, but the crater diameter is uncertain.

The photographs obtained on the second pass (IIP12-b) show the effect of the shorter exposure. The wide-angle frames were appreciably better than those from the first pass. While still exposed more than desirable, surface detail is present and little significant information is lost. The telephoto frames, particularly at the start of the sequence, are underexposed and some information is lost in the areas of slopes away from the Sun. Because this area appears to be rough as a result of a high density of old rounded craters and mounds, the underexposure seems to be accentuated (Figure 2.3-34).

Resolution and feature detection was comparable with previous sites, although degraded at the exposure extremes.

2.3.2.13 Site IIP-13

Site IIP-13 (Figure 2.3-35) is in a mare area about 230 km southwest of Kepler. The largest crater within the area photographed is Maestlin G, about 2 kilometers in diameter. A few 1-km craters are shown on AIC 57 D, Maestlin. The area also is shown on the charts to include several rays from Kepler.

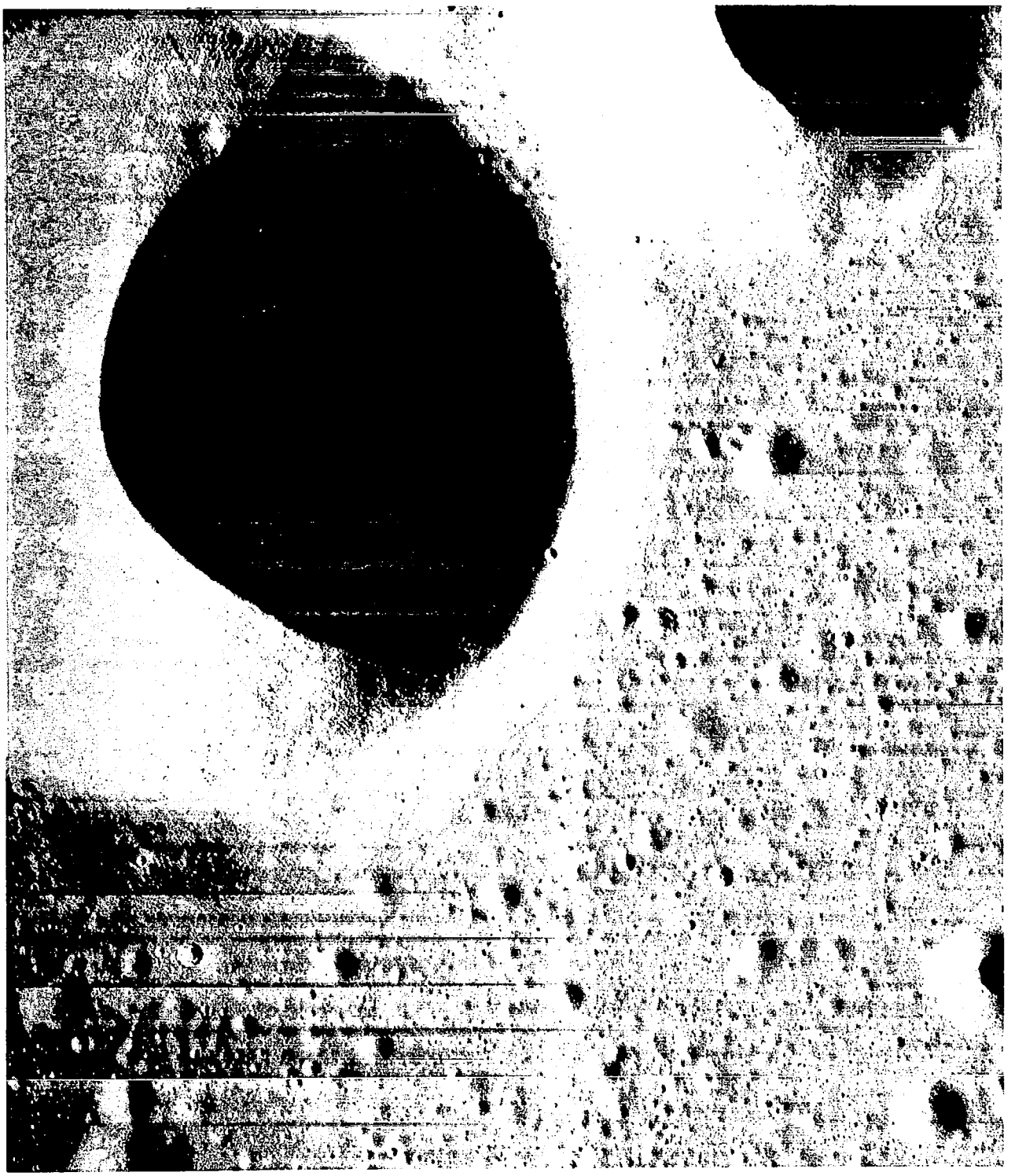

Figure 2.3-36: Telephoto Photography of Site IIP-13a

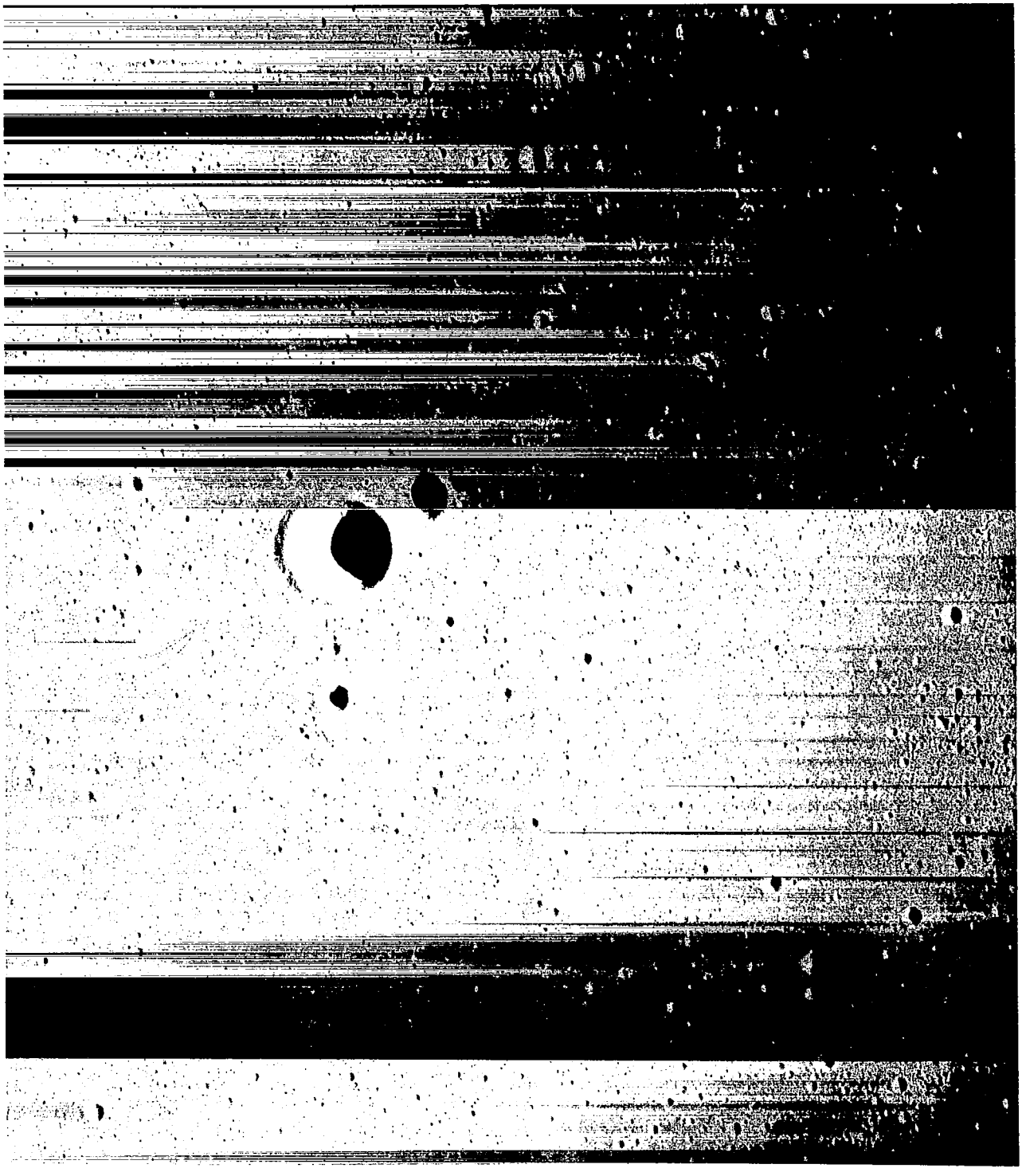

Figure 2.3-37: Wide-Angle Photography of Site IIP-13a

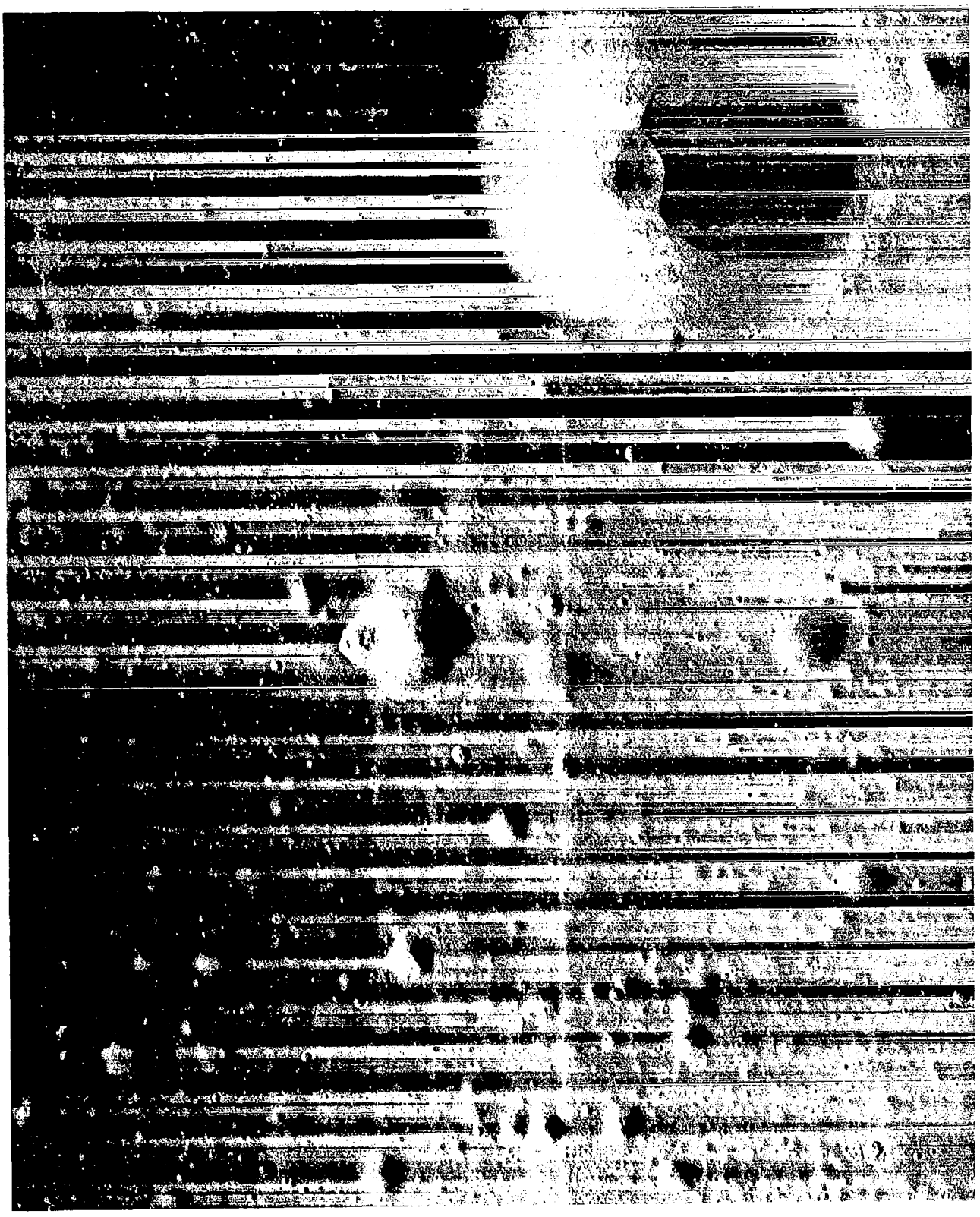

Figure 2.3-38: Telephoto Photography of Site IIP-13b

The site was photographed with eight-frame sequences on two successive orbits. As for the previous site, a shutter speed of 0.04 second was used for IIP13-a and 0.02 second for IIP13-b.

For the first sequence (IIP-13a), the 0.04-second shutter speed resulted in good telephoto exposures and generally overexposed wide-angle photographs. Some surface detail was lost in the wide-angle frames. Craters spanning as few as three scan lines could be discerned occasionally on the GRE film but the actual dimensions were difficult to establish because of the lack of detail. Craters spanning as few as three scan lines could be discerned in the midportions of the telephoto frames (Figure 2.3-36).

The 0.02-second shutter speed used for the second eight-frame sequence (IIP-13b) resulted in good exposures for the wide-angle frames (Figure 2.3-37) and considerable underexposure of the telephoto frames (Figure 2.3-38). Estimated resolutions for the central areas of the wide-angle and telephoto frames were three scan lines and four scan lines, respectively.

2.3.3 SECONDARY-SITE PHOTOGRAPHY

Seventeen secondary sites were selected for photography in mission planning, all of which was accomplished successfully. These sites were chosen to provide information supplementing primary site photography, and to obtain data of special scientific interest concerning features or areas not included in primary sites. Site IIS-1 was photographed by a sequence of four frames, and Site IIS-2 by sequences of four frames on two successive orbits. The remaining 15 sites were each photographed by a single frame. Photographic parameters are included in the photographic supporting data, Table 2.4-4. The secondary sites are summarized in Table 2.3-3.

Although these areas are considered secondary in importance to the primary mission objectives, many of the photographs provide significant scientific information and are of outstanding general interest. This is because of the opportunity to select, within certain limitations, areas or features of special interest or to employ an oblique line of sight.

2.3.3.1 Site IIS-1

This site is, in effect, an extension of Site IIP-1, although the coverage is not contiguous with the primary site. The first frame was exposed 48.3 seconds following the last frame of Site IIP-1. The delay resulted in a separation of 61 kilometers between areas photographed. Photographic parameters were unchanged from those used for the primary site, except for the number of frames exposed.

2.3.3.2 Site IIS-2

Two sequences of four frames were exposed on two successive orbits. In each case, spacecraft attitude was controlled to position the track of the camera axis midway between the nadir of the two orbits. The purpose was to investigate the feasibility of convergent stereo photography by the telephoto lens. The shutter speed was changed from 0.04 second used on the first sequence to 0.02 second for the second pass. This change was necessary because of the change in surface luminance resulting from the different phase angle for each spacecraft attitude.

An analysis of the stereometric potential of the photographs was made by the Aeronautical Chart and Information Center. The results of the study, as reported in Preliminary Geologic Evaluation and Apollo Landing Analysis of Areas Photographed by Lunar Orbiter II, Langley Working Paper LWP-363, NASA Langley Research Center, March 1967, are quoted below.

"a. A spot-heighting test achieved a standard deviation (vertical) of 0.7 meter at random reseau intersections. A standard deviation of 0.46 meter was achieved at well-defined, high-contrast feature points.

b. Two-meter relative contours were drawn over a small area of the model. A repeatability test was made by drawing contours over the same area a number of times.

c. As a result of the test, it is estimated that relative elevations of control points could be computed with a standard deviation of about 1 meter on high-resolution convergent exposures of this type."

2.3.3.3 Farside Photographs

Four secondary sites were located on the lunar farside: Sites IIS-3, -4, -5, and -14. Each was taken from a high altitude (1453, 1450, 1466,

Table 2.3-3: Mission II Secondary Sites

Site	Location		Frame Number(s)	Target
	Latitude	Longitude		
IIS-1	4° 10' N	36° 55' E	21 - 24	Extension of Site IIP-1
IIS-2a IIS-2b	3° 36' N	36° 75' E	25 - 28	Convergent telephoto stereo experiment. Area in south Mare Tranquillitatis. Vicinity of Mission I Frame I-42
IIS-3		176° E	33	Farside
IIS-4		174° E	34	Farside
IIS-5		158° E	75	Farside
IIS-6	4° 15' N	4° 30' E	92	Near Triesnecker. Intersection of Rima Triesnecker I, II, V, and VII
IIS-7	0° 05' N	1° 00' W	93	Sinus Medii southerly oblique
IIS-8	0° 30' N	12° 50' E	94	Sinus Medii. Northern Site I-4
IIS-9	2° 20' N	0° 30' E	95	Sinus Medii S.W. of Triesnecker. N.W. of Site IIP-7a
IIS-10.2	3° 20' N	11° 50' W	112	Gambart C. Thermal anomaly
IIS-11	4° 40' N	27° 04' W	137	S.W. of Copernicus near Hortensius
IIS-12	8° 00' N	20° 00' W	162	Northerly oblique of Copernicus
IIS-13	3° 20' N	43° 50' W	195	Braided ridge. Mare S.W. of Kepler
IIS-14		100° E	196	Farside
IIS-15	11° 00' N	53° 00' W	213	Northerly oblique of Marius
IIS-16	2° 40' N	54° 30' W	214	Smooth mare south of Reiner
IIS-17	7° 25' N	59° 00' W	215	Bright ray structure west of Reiner. Oblique

and 1496 kilometers, respectively). Because of the wide coverage obtained at these altitudes, and the resulting extreme range of surface illumination within the field of view, the median shutter speed of 0.02 second was used. Mission I farside photography also had shown that this exposure produced acceptable results. The farside photographs obtained on Mission II were of good quality. In most wide-angle frames, the exposure ranged from underexposure toward the terminator side to overexposure on the opposite side as expected. The intermediate area was, however, of very good quality. Although the telephoto frames were exposed less than the wide-angle due to the lens characteristics, good quality photographs were obtained. Examples of the wide-angle and telephoto photography from Frame 75 of Site IIS-5 are shown in Figures 2.3-39 and 2.3-40.

Resolution of the farside photographs, in terms of scan lines, was comparable with the general mission photography although some loss occured near the sides of wide-angle frames due to the extreme luminance range.

2.3.3.4 Oblique Photography

Oblique photographs that include the lunar horizon were obtained at four secondary sites: IIS-7, -12, -15, and -17. These photographs, particularly IIS-12 and IIS-15 of Copernicus and Marius, Figures 2.3-41 and 2.3-42, respectively, are of outstanding interest and value.

The principal area of interest in these photographs is shown with very good quality of photography. Because of the extreme range of slant distance to the surface within the field of view, proper image-motion compensation could not be obtained throughout. Unavoidable smear of the image in the near foreground is present, decreasing in amount with increasing distance to the surface. Image smear appeared most pronounced in Frames 213 and 215. Little smear is apparent in the telephoto picture of Copernicus (Frame 162, Figure 2.3-43). The amount of image smear in these photographs is dependent upon the shutter speed used. Frame 162 was exposed with a shutter speed of 0.01 second, Frame 93 at 0.02 second, and Frames 213 and 215 were exposed at 0.04 second.

It should be noted that, in the case of these oblique photographs in which the field of view includes the lunar horizon, the computed coordinates of the corner positions are not valid. Where a corner does not lie on the surface, the computer program beaks down, and none of the four corner positions are correct. Coverage in these cases is most readily obtained by direct comparison of the photographs with the ACIC lunar charts.

2.3.3.5 Miscellaneous Secondary Sites

Photography of the remaining secondary sites not discussed in the previous paragraphs was carried out by nominal operational procedures. Although the subject matter of each of these photographs may be of special interest to the user, detailed analysis of the photographic quality is beyond the scope of this report. In general, the quality was similar to that obtained for primary sites. Photographic parameters are included in the table of supporting data, Table 2.4-4.

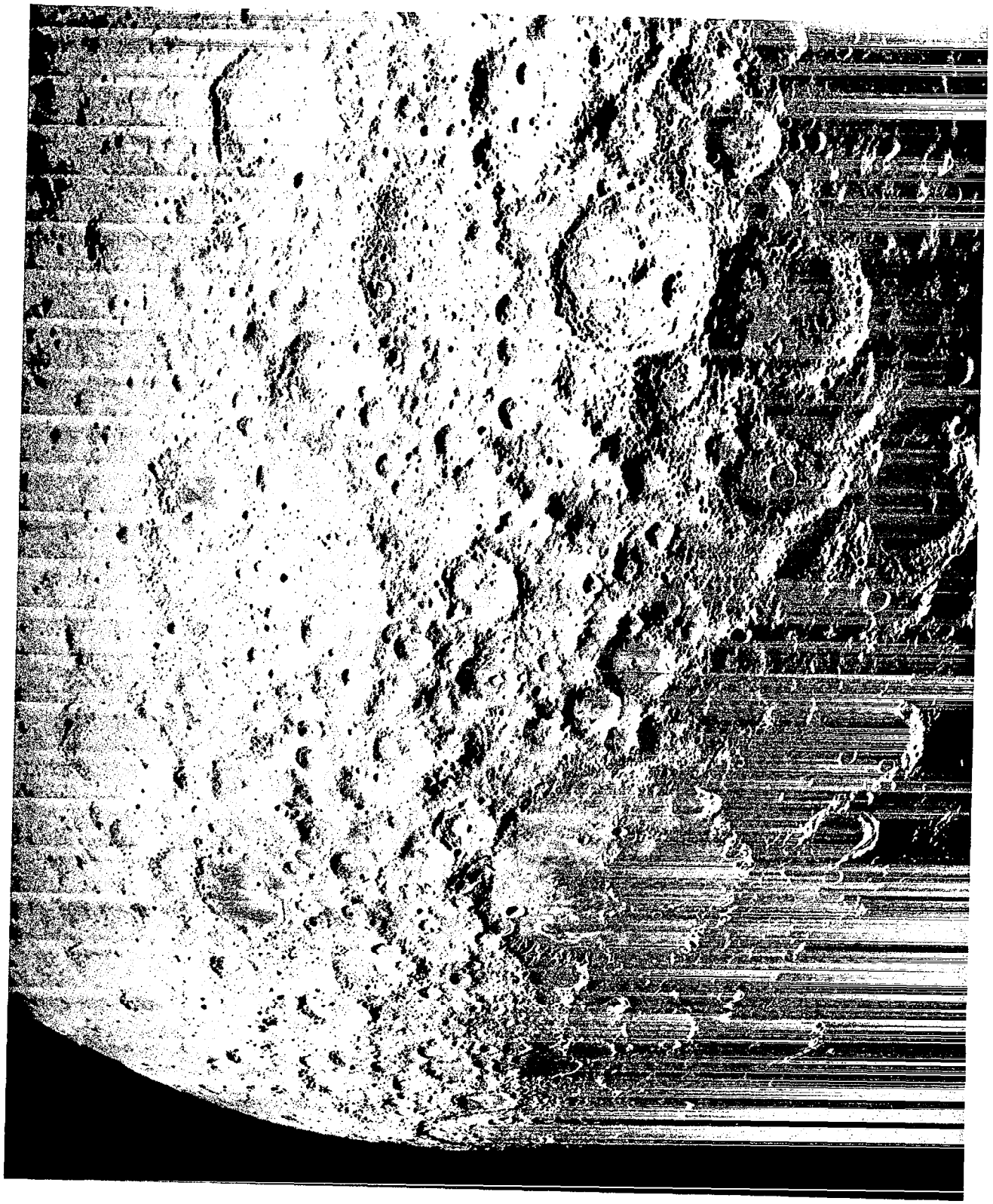

Figure 2.3-39: Wide-Angle Photography of Farside, Site IIS-5

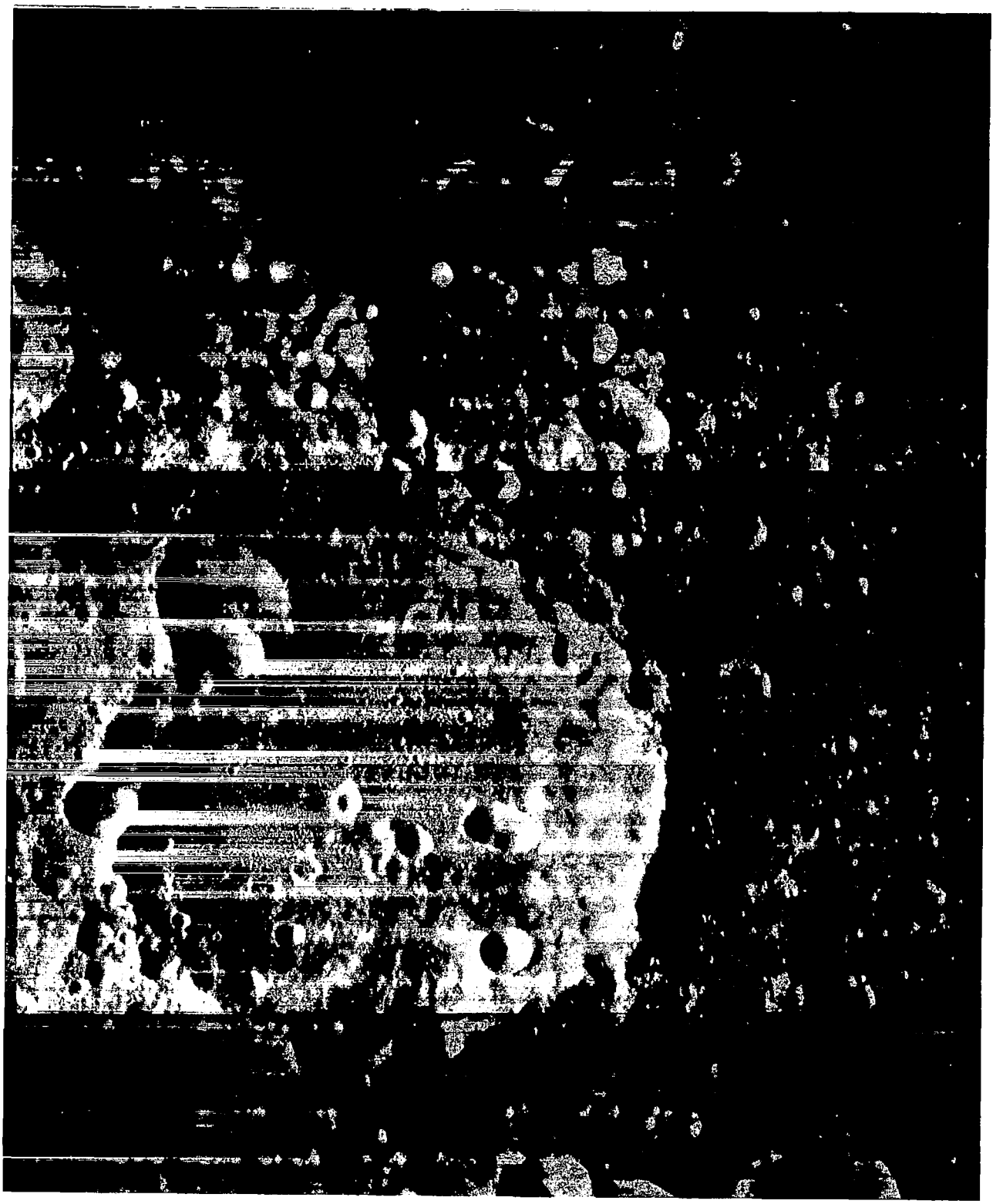

Figure 2.3-40: Telephoto Photography of Farside Site IIS-5

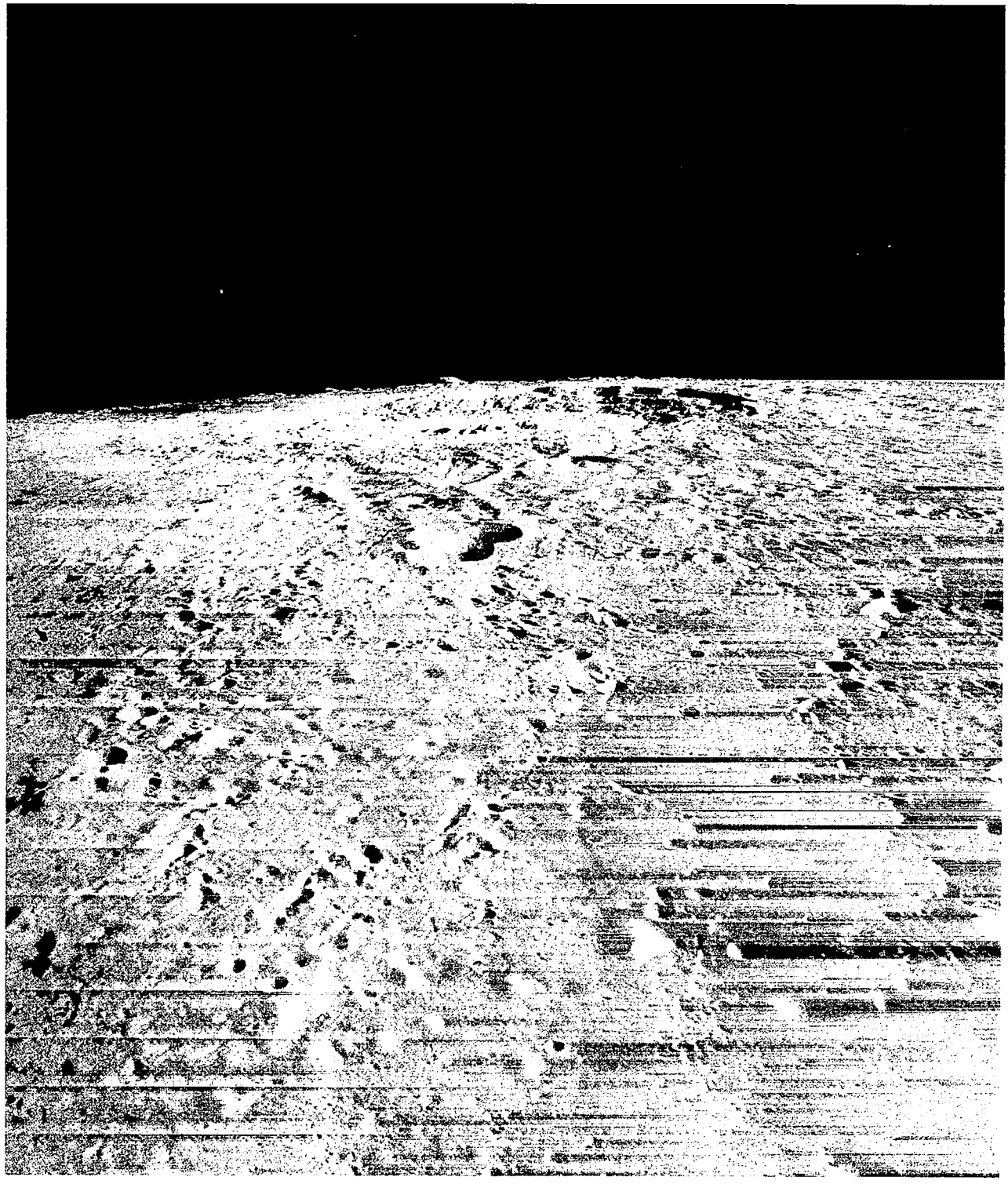

Figure 2.3-41: Oblique Wide-Angle Photography, Copernicus, Site IIS-12

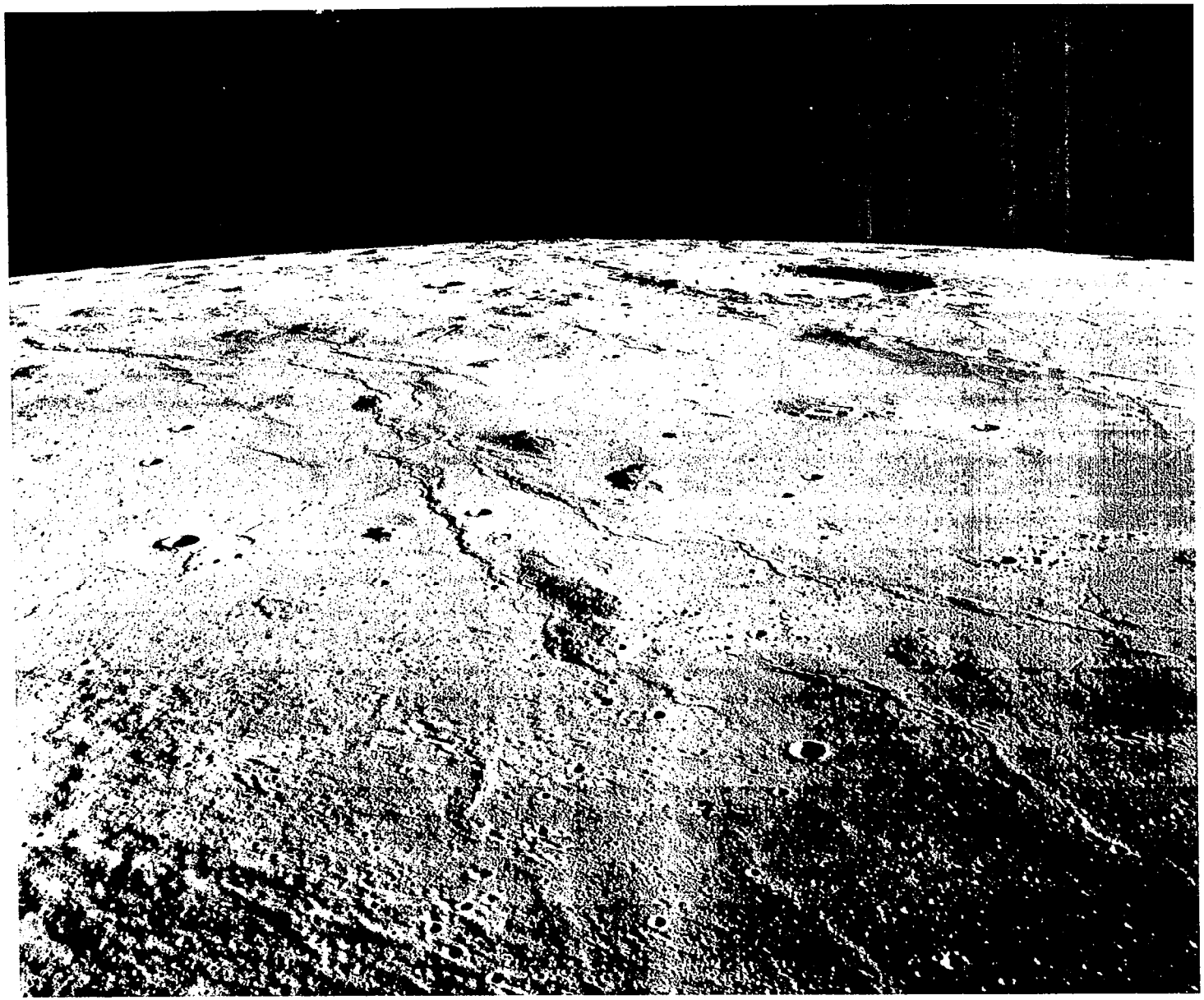

Figure 2.3-42: Oblique Wide-Angle Photography, Marius, Site IIS-15

Figure 2.3-43: Oblique Telephoto Photography, Copernicus, Site IIS-12

2.4 PHOTOGRAPHIC SUPPORTING DATA

Interpretation and evaluation of the lunar photographs requires specific information regarding spacecraft position, attitude, altitude, and velocity at the time each picture was taken. Computer programs (photo and evaluation) were developed that combined prediction requirements for photo mission control, with postmission data requirements. Figure 2.4-1 illustrates the relationship between trajectory and spacecraft performance parameters required to compute the supporting data. Postmission photographic data computations were made at the SFOF shortly after completion of the mission.

2.4.1 INPUT DATA SUMMARY

Input data were obtained primarily from postflight analysis of the doppler tracking data using the SPAC computer program ODPL, postmission evaluation of the spacecraft attitude, and time of exposure as read from the GRE film.

2.4.1.1 Spacecraft Position and Velocity

Postflight orbit determination defined spacecraft position and velocity just prior to the first commanded camera-on time of the sequence for primary site photos. In all cases, data from at least two orbits prior to the site orbit and at least one orbit after the site orbit were used in these calculations.

When a secondary site could be included in a data arc, this was done. Three additional OD solutions were computed for secondary sites. The site determinations were obtained by solving only for the state vector (X, Y, Z, X, Y, Z) and using values of the LRC harmonic coefficients specified in Appendix B of Volume VI.

The postflight orbit determination solutions and their relation to photographic sites are listed in Table 2.4-1. Under "OD Solution" are serial numbers of the programs assigned by the orbit determination (OD) group.

2.4.1.2 Camera-On Times

Camera-on times were obtained by reading the digital time code exposed on the spacecraft film when the 80-mm shutter actuated. A computer routine (TIML) was developed and used to convert the spacecraft time, contained at the start of each telemetry frame, to the correct time and provide a tabulation of significant parameters at 10-minute intervals during any specified period. The digital format was converted to decimal values for entry into the TIML tabulations and the GMT time of exposure determined.

2.4.1.3 Spacecraft Attitude

The roll, pitch, and yaw maneuver angles shown in Table 2.4-2 were used to describe the attitude

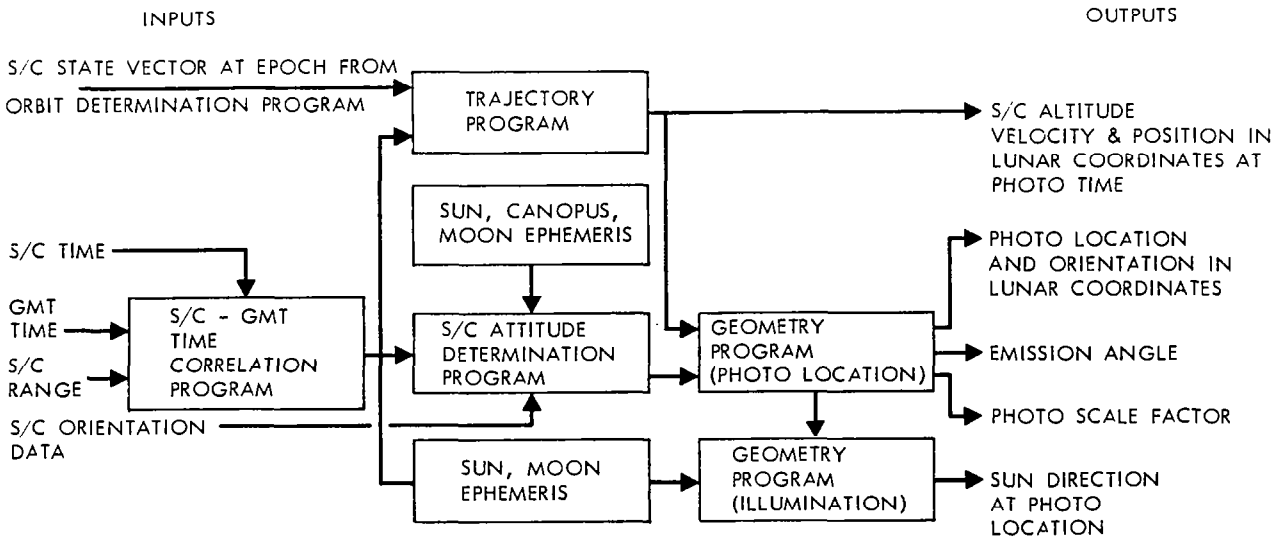

Figure 2.4-1: Photo Supporting Data Flow

Table 2.4-1: Orbit Determination Solutions

Site	Frame Numbers	OD Solution
IIP-1	5-20	9016
IIS-1	21-24	9016
IIS-2a	25-28	9016
IIS-2b	29-32	9016
IIS-3	33	9016
IIS-4	34	9004
IIP-2	35-42	9006
IIP-3a	43-50	9007A
IIP-3b	51-58	9007B
IIP-4	59-66	9008
IIP-5	67-74	9009
IIS-5	75	9005
IIP-6a	76-83	9015A
IIP-6b	84-91	9015B
IIS-7	93	9013
IIS-8	94	9013
IIS-9	95	9013
IIP-7a	96-103	9014A
IIP-7b	104-111	9014B
IIS-10.2	112	9014B
IIP-8a	113-120	9012A
IIP-8b	114-128	9012B
IIP-8c	129-136	9012C
IIS-11	137	9012C
IIP-9	138-145	9010
IIP-10a	146-153	9011A
IIP-10b	154-161	9011B
IIS-12	162	9002
IIP-11a	163-170	9003A
IIP-11b	171-178	9003B
IIP-12a	179-186	9002A
IIP-12b	187-194	9002B
IIS-13	195	9002B
IIS-14	196	9002B
IIP-13a	197-204	9001A
IIP-13b	205-212	9001B
IIS-15	213	9001B
IIS-16	214	9001B
IIS-17	215	9001B

of the spacecraft throughout each photograph sequence. Only the known roll offsets (from postmaneuver drift analysis) were added to the commanded roll angle. No attempt was made to incorporate the variations of pitch and yaw errors within the attitude-control limit cycle in the calculation. Note that all roll maneuvers were executed about the sunline (H roll).

Table 2.4-2: Photographic Maneuver Angles

Site	Maneuver Angles (degrees) Roll	Yaw	Pitch
IIP-1	5.24	9.25	2.81
IIS-1	5.24	9.25	2.81
IIS-2a	-1.47	6.93	11.12
IIS-2b	12.17	11.70	-8.40
IIS-3	-178.00	0.00	0.00
IIS-4	164.00	0.00	0.00
IIP-2	5.30	9.50	-2.40
IIP-3a	5.33	9.50	5.45
IIP-3b	5.33	9.56	4.25
IIP-4	5.33	9.57	7.61
IIP-5	8.66	10.82	-1.25
IIS-5	-165.00	0.00	0.00
IIP-6a	5.38	9.62	-7.74
IIP-6b	5.39	9.65	-9.23
IIS-7	-59.19	-9.72	5.91
IIS-8	5.40	9.82	-8.52
IIS-9	5.42	9.87	-0.63
IIP-7a	5.47	9.79	0.00
IIP-7b	5.47	9.82	-1.50
IIS-10.2	5.42	9.93	4.14
IIP-8a	5.43	9.97	-7.20
IIP-8b	5.44	9.95	-8.69
IIP-8c	5.47	9.91	-10.17
IIS-11	5.50	9.95	11.49
IIP-9	5.50	10.00	-4.20
IIP-10a	5.49	9.98	6.82
IIP-10b	5.50	10.01	5.33
IIS-12	73.09	9.00	25.60
IIP-11a	5.55	10.00	-7.44
IIP-11b	5.57	10.02	-8.92
IIP-12a	5.55	10.08	2.66
IIP-12b	5.57	10.11	1.17
IIS-13	5.52	10.23	6.16
IIS-14	-178.00	0.00	0.00
IIP-13a	5.62	10.16	1.62
IIP-13b	5.60	10.20	0.12
IIS-15	12.60	29.70	60.10
IIS-16	5.52	10.30	7.67
IIS-17	63.40	15.20	25.00

Note:

Maneuver sequence: Roll – yaw – pitch, except for IIS-7 and IIS-17, which was roll – pitch – yaw.

2.4.2 ACCURACY OF CALCULATIONS

The accuracy of data presented in the photo supporting data tabulation was estimated by performing a simplified error analysis using typical photo and orbital parameters, and the best estimates of errors in the flight hardware. The study scope was confined to an investigation of uncertainties in photo location and spacecraft altitude for the prime photo sites. A brief summary of the estimated 1σ errors is given below in Table 2.4-3.

frame times were further manually rounded off to the nearest tenth, introducing an additional 0.05 second of error, and yielding an RSS total of 0.119 second of error. Distribution of the error tends to be uniform; therefore one standard deviation – that number which encompasses 68% of the possible cases – becomes 0.68 X 0.119 or 0.081 second. A typical value for horizontal velocity at the time of photography is 1.917 kilometers per second; hence, the distance traveled downrange is:

$$1.917 \text{ km/s} \times 0.081 = 0.155$$

Table 2.4-3: Summary of Data Standard Deviations

	Standard Deviations		
	Longitude	Latitude	Altitude
Photo Centers	0.0100 deg.	0.0117 deg.	0.160 km
Arc Distance	0.303 km	0.355 km	
Photo Corners			
Telephoto	0.0102 deg.	0.0131 deg.	---
Arc Distance	0.309 km	0.397 km	
Wide Angle	0.0167 deg.	0.0164 deg.	---
Arc Distance	0.507 km	0.498 km	

2.4.2.1 Error Sources

For each primary input to the photo evaluation program (attitude maneuvers, time of photos, and state vector), there is some uncertainty of the exact value; each contributes something to the total uncertainty or error in the photo parameters. The following discussion identifies the various factors and their relationship to the uncertainty in longitude and latitude of photo centers and corners, and in photo altitude.

Timing Errors

After the time-code data is corrected for spacecraft clock errors, a timing uncertainty of 0.1 second still exists relative to GMT. An additional 0.04 second of error exists for telephoto frames since the only corrected frame times are those for the wide-angle frames. In some cases,

Using an altitude of 50 kilometers as representative of those for the prime sites and an inclination figure of 12 degrees, the distance traveled downrange can be converted into degrees of longitude and latitude on the lunar surface:

$\Delta\lambda = 0.0049$ degree (longitude)
$\Delta\mu = 0.0010$ degree (latitude)

Uncertainty of exact photo time also contributes a small uncertainty of photo altitude. A typical value of mean altitude rate is 0.050 km/s, thus,

$$\Delta h = 0.050 \text{ km/s} \times 0.081 \text{ sec} = 0.004 \text{ km}$$

Attitude Maneuver Errors

A per-axis analysis of attitude errors of a nominal assumed photo maneuver of 20-degree roll, 20-degree pitch, and 20-degree yaw is shown in Tables 2.4-4 and -5.

Table 2.4-4: Nominal Assumed Attitude Errors – Initial Conditions			
	3 σ Error (degrees)		
	Roll	Pitch	Yaw
Alignment of Canopus tracker null to reference prism	0.075		
Alignment of sun sensor null to mirror		0.017	0.017
Alignment of sun sensor mirror to reference prism		0.017	0.017
IRU alignment to reference prism	0.020	0.020	0.020
Sun sensor null shift		0.006	0.006
Limit cycle error (= $\sqrt{2}$ (0.22°))	0.311	0.311	0.311
RSS subtotal	0.320	0.313	0.313

Table 2.4-5: Photo Maneuver Errors			
	3 σ Error (degrees)		
	Roll	Pitch	Yaw
Initial condition error	0.32	0.313	0.313
Gyro drift (RIM)	0.08	0.08	0.08
Gyro error (RM)	0.03	0.03	0.03
Resolution error	0.025	0.025	0.025
V/H converter error	0.06	0.06	0.06
Cross-axis drift	0.02	0.02	0.02
Gyro nonorthogonality	0.09	0.06	0.01
Camera – S/C misalign	0.30	0.30	0.30
3σ	0.461	0.451	0.447
1σ *	0.240	0.238	0.237

*For 1σ, sources having uniform distributions (resolution and limit cycle) are taken as 0.68 x 3σ; all others, 0.33-⅓ x 3σ.

A value of 0.24 can be used as the 1σ error for each axis within the accuracy of the analysis. Since these errors are assumed normal and independent, the same value applies to errors described in camera roll, pitch, and crab coordinates, or

$\sigma r = 0.24$ degree
$\sigma p = 0.24$ degree
$\sigma c = 0.24$ degree

The σr error results in a cross-frame positioning error and the σp results in an along-frame positioning error. These cross- and along-frame errors are rotated through the 12-degree inclination angle into latitude-longitude errors. Since again the roll and pitch errors are normal and independent, the error in the latitude and longitude directions are also 0.24 degree.

$\sigma_\mu = 0.24$ camera degree at 55 km alt = 0.0076 degree latitude
$\sigma_\lambda = 0.24$ camera degree at 55 km alt = 0.0076 degree longitude

Uncertainty in State Vectors

Accuracy of the state vectors must be considered with the uncertainties in actual photo location. Typical uncertainties for a state vector at a photo site are:

$\sigma x = 76$ m	$\dot{\sigma} x = 0.14$ m/s
$\sigma y = 130$ m	$\dot{\sigma} y = 0.33$ m/s
$\sigma z = 275$ m	$\dot{\sigma} z = 0.50$ m/s

Assuming a spacecraft altitude of 50 km, these errors transform to the following:

$\sigma_\lambda = 0.0042$ degree
$\sigma_\mu = 0.0088$ degree
$\sigma_h = 0.16$ km

2.4.2.2 Uncertainty In Site Elevation

The elevation of prime photo sites above or below the mean radius of the Moon is known (1σ basis) only to within about 1 km. Since the camera axis intersect is only very slightly different from the nadir (prime sites only), site-elevation uncertainty has no noticeable effect on location of the photo centers. However, location of the photo corners is directly dependent on site elevation and this relationship is investigated. Also, because the telephoto and wide-angle lenses have different fields of view, the effects must be studied separately.

Telephoto

The telephoto field of view is 20.36 degrees in the crossrange direction and 5.17 degrees in the downrange direction. An orbit inclination of 12 degrees and spacecraft altitude of 50 km are assumed. The longitude and latitude components in the crossrange direction were determined,

$\Delta\lambda c = 0.0012$ degree
$\Delta\mu c = 0.0058$ degree

Uncertainty due to the 5.17-degree field of view downrange is similarly calculated:

$\Delta\lambda d = 0.00147$ degree
$\Delta\mu d = 0.0031$ degree

Having found the downrange and crossrange components of uncertainty, it is necessary to sum these to complete the estimate of uncertainty in photo corner location due to site elevation,

$\Delta\lambda = (\Delta\lambda\, c^2 + \Delta\lambda\, d^2)^{1/2} = 0.0019$ degree (high-resolution longitude)

$\Delta\mu = (\Delta\mu\, c^2 + \Delta\mu\, d^2)^{1/2} = 0.0058$ degree (high-resolution latitude)

Wide Angle

The wide-angle-lens field of view is 44.24 degrees crossrange by 37.92 degrees downrange. Proceeding in identically the same manner,

$\Delta\lambda c = 0.0027$ degree
$\Delta\mu c = 0.0131$ degree
$\Delta\mu d = 0.0112$ degree
$\Delta\lambda d = 0.0023$ degree

Summing the downrange and crossrange components,

$\Delta\lambda = 0.0133$ degree
$\Delta\mu = 0.0115$ degree

2.4.2.3 SUMMATION OF ERRORS

Sources that are known to contribute uncertainty to photo locations and altitude and that have been investigated here are considered independent, and are lumped together by the root-sum-square method (See Table 2.4-6).

Table 2.4-6: Summation of Errors

PHOTO CENTERS

Source	$\sigma\lambda$	$\sigma\mu$	$\sigma\gamma$
Photo Timing	0.0049 degree	0.0010 degree	0.004 km
Camera Pointing	0.0076 degree	0.0076 degree	----------
Position	0.0042 degree	0.0088 degree	0.16 km
RSS Total	0.0100 degree	0.0117 degree	0.160 km
Arc distance on lunar surface	0.303 km	0.355 km	

PHOTO CORNERS

Telephoto

Source	$\sigma\lambda$	$\sigma\mu$
Site Elevation	0.0019 degree	0.0058 degree
Total of others above	0.0100 degree	0.0117 degree
RSS Total	0.0102 degree	0.0131 degree
Arc Distance	0.309 km	0.397 km
Wide Angle		

Source	$\sigma\lambda$	$\sigma\mu$
Site Elevation	0.0133 degree	0.0115 degree
Total of others above	0.0100 degree	0.0117 degree
RSS Total	0.0167 degree	0.0164 degree
Arc Distance	0.507 km	0.498 km

For the photo corner locations, effects due to uncertainty in site elevation must be added to the below figures for uncertainty in photo center location. This is done for both the telephoto and wide-angle cases below.

It is repeated that the frames evaluated by use of in-flight orbit determination are not as accurate as those for which postflight OD was done using improved data. Where conflict with actual photos is observed to exist, the EVAL data must be adjusted to obtain meaningful values. For instance, an error in longitude of frame locations requires approximately a one-to-one correction to the incidence angle printed (+ if away from Sun, - if toward Sun).

2.4.3 PHOTOGRAPH LOCATION FRAME COORDINATION

Preliminary attempts were made to correlate the lunar topographic features in the Mission II photographs with existing 1:500,000 and 1:1,000,000 scale lunar Mercator projection charts. It was immediately apparent that such a correlation could only be approximate. In some cases, features larger than several kilometers could be identified on both charts and photographs. However, discrepancies amounting to several kilometers were frequently found between relative positions of these features. In other cases, features over 2 or 3 kilometers, seen in the photographs, could not be identified on the charts. The limitations that have been im-

posed by Earth-based observation in preparing current lunar charts in some instances make their use for precisely locating the position of Lunar Orbiter photographs difficult. In plotting locations of photograph corners on the charts by the above method, deviations of as much as an order of magnitude greater than the errors shown in Paragraph 2.4.2.3 from the computed positions were noted. This effort confirmed that an extensive study will be required to transfer the topographic information from the unrectified, nonorthographic projection photographs to lunar chart form. Furthermore, the currently available "actual" postmission EVAL data for frame coordinates have limited value in this application because of the assumptions made in the EVAL computer program. In this program the Moon was assumed to be a sphere, with a mean radius of 1738.09 km. Consequently, elevation differences over a given site were not considered. Also, spacecraft dynamics were simplified and did not include pitch and yaw errors in the postmission EVAL computation of frame corner coordinates. Further complications were introduced by uncertainties in timing, as well as by the different fields of view of the telephoto and wide-angle cameras. To establish corner coordinates, and to properly correlate them to existing lunar charts, a full photogrammetric space resection should be performed. Each usable frame must be analyzed with respect to spacecraft position, altitude, velocity, and attitude prevailing at the moment a given target area was photographed. In turn, these factors must be related to camera geometry and the lunar surface. Further uncertainties in positional accuracy are inherent in the Lunar Orbiter photographic system.

- The Schneider Xenotar lens used for the wide-angle photographs is not a photogrammetric lens and as such introduces some distortion. This lens was calibrated prior to flight to reduce the effect of distortion error in final analysis.
- Processing of the film aboard the spacecraft and the subsequent reconstructed record introduces distortion of the film image. These distortions are sensitive to temperature and relative humidity of each film or copy generation.
- A random error in the mechanical scan direction of the optical-mechanical scanner introduces one of the major errors in the spacecraft camera system. To permit at least partial correction of this distortion, reseau marks in the form of small crosses were pre-exposed on the spacecraft film in conjunction with pre-exposure of the edge data. These marks are described in Figure 2.3-1.
- The optical-mechanical scanner may also introduce a small error in the film-advance direction.
- Slight errors in both the longitudinal and transverse direction with respect to the spacecraft film may be introduced by the reassembly process.

Although the primary objective of the Lunar Orbiter mission was to secure topographic data regarding the lunar surface, there was no specific plan in the original concept to produce accurate maps of specified topographic detail. A comprehensive error analysis, as discussed above and necessary for such photograph utilization, was not made and has not been incorporated into the photodata reduction.

2.4.3.1 Photographic Image Distortion

The final photo image in the spacecraft camera is distorted by an aggregate of internal camera phenomena. These can be conveniently lumped into two areas: (1) uncalibrated lens distortion; and (2) thermal-chemical emulsion distortions.

Lens Distortions

The Lunar Orbiter II mission was predominately reconnaissance rather than cartographic. The 80-mm Xenotar lens used was chosen for its excellent resolution rather than metric fidelity. A typical 80-mm-focal-length Xenotar can have as much as 340 μ maximum distortion and still qualify as a suitable reconnaissance lens. This can be contracted with a selected, 76-mm focal-length mapping Biogon that has a maximum distortion of 30 μ radially and 10 μ tangentially.

Thermal-Chemical Emulsion Changes

The Lunar Orbiter II mission used Type SO-243 film for the photography because of its high-resolution characteristics. Since SO-243 uses a triacetate base, it does not have the extreme dimensional stability characteristic of estar (mylar) base films used for cartographic photography.

Photographic film changes under the following primary influences:

1) Changes of temperature and humidity;
2) Aging, long term and short term;
3) Processing.

Second-order parameters influencing dimension changes do not contribute significantly. The unpredicted image distortion expected in Lunar Orbiter II photography from the cited internal camera influences is summarized in Table 2.4-7. It is emphasized that this table is by no means exhaustive, and is presented to show orders of magnitude of the problem rather than to determine a cartographic error budget for the film. Although the photographic image is subject to the above distortions and to additional distortions during readout, reconstruction, and reassembly, the reseau pattern provides a means of correction for all but the lens distortions. Correction for the latter in the wide-angle photographs is provided by the lens calibration.

2.4.4 PHOTOGRAPHIC SUPPORTING DATA TABLES

The information presented in the supporting data tables has been extracted from the computer program EVAL tabulated output. Figure 2.4-2 is a sample of EVAL program tabulations. The EVAL program was developed to satisfy the operational requirement of predicting photo coverage and determining spacecraft maneuvers required to obtain the desired coverage for each photo sequence.

The following is a definition of terms used in the EVAL program and, with one exception, are the same terms and definitions used in the supporting-data tables. The single difference is that the term "camera axis magnitude" in the EVAL tabulation is identified as "slant distance" in the supporting-data table. Figure 2.4-3 is a diagram of the geometry of these parameters.

Information required to support the photo analysis function was coordinated with NASA and the user agencies during the program design period. These requirements were implemented in the form of the double-page tables of supporting data, Table 2.4-8.

All of the spacecraft position and attitude data is listed on the left-hand page. The data tabulations on the right-hand page are grouped to support the high- and moderate-resolution photographs. The predicted corner positions are based on normal operation of each camera. Each line in the table presents all of the supporting data for that dual exposure.

The supporting data in Table 2.4-8 has been arranged by order of exposure for each primary site. This is then followed by the secondary-site photographs arranged by order of exposure.

The convention for presenting the coordinates of the four corners is illustrated in Figure 2.4-4.

It should be pointed out that the solution for the photograph corners by the EVAL program breaks down where the lunar horizon is included in the field of view. For this reason, corner coordinates for the oblique photographs of Sites IIS-7, -12, -15, and -17 are not included in the tabulation.

Table 2.4-7: Sources of Image Distortion

PARAMETER	RANGE	ILLUSTRATIVE VALUE	PARAMETRIC CHANGE	% FILM DIMENSION
% DIMENSION PER % RELATIVE HUMIDITY	0.008 - 0.010	0.009	10% RH	0.09
% DIMENSION PER DEGREE FAHRENHEIT	0.003 - 0.004	0.004	10°F	0.04
PROCESSING DIMENSION CHANGE	0.08 - 0.10	0.09	---	0.09
FILM AGING PAST PROCESSING	0.15 - 0.25	0.15	---	0.15
				RSS = 0.20%

```
**********************************
*   PHOTO FRAME NUMBER  2 OF  4  *
**********************************

                    YEAR    MONTH    DAY    HOUR   MINUTE   SECOND
                GMT  66      11      18      22      23     14.709

LONGITUDE OF NADIR POINT      =    36.8437486 DEG     LATITUDE OF NADIR POINT       =     3.2883279 DEG
LONG OF CAMERA AXIS INTERSECT =    36.6312671 DEG     LATI OF CAMERA AXIS INTERSECT =     3.5237039 DEG
SPACECRAFT RADIUS             =  1783.6529083 KM      SPACECRAFT ALTITUDE           =    45.5629120 KM
MEAN ALTITUDE RATE            =    -0.0085107 KM/SEC  TIME FROM PERIAPSIS           =   -16.3998415 SEC
HORIZONTAL VELOCITY           =     1.9166221 KM/SEC  TRUE ANOMALY                  =   358.9901314 DEG
SCALE FACTOR (HIGH)           =     0.0133881 M/KM    TILT DISTANCE (HIGH)        =   126.6060276 MM
SCALE FACTOR (LOW)            =     0.0017558 M/KM    TILT DISTANCE (LOW)         =    16.8663642 MM
IMAGE MOTION COMPENSATION (V/H)=    0.0420698 RAD/SEC  SWING ANGLE                 =   127.2153053 DEG
EMISSION ANGLE                =    12.2221454 DEG     INCIDENCE ANGLE             =    70.2803831 DEG
PHASE ANGLE                   =    62.1474490 DEG     NORTH DEVIATION ANGLE       =   349.8523178 DEG
TILT ANGLE                    =    11.9052939 DEG     RESOLUTION CONSTANT         =     0.9887152 MTR
TILT AZIMUTH                  =   317.9831886 DEG     SUN AZIMUTH AT PRINCIPAL GND PT=   91.4987173 DEG
SUN ANGLE AT NADIR            =    70.0620518 DEG     SUN ARC AT NADIR            =  2125.3598938 KM
LONGITUDE DISTANCE TO TARGET  =     0.4267488 DEG     LATITUDE DISTANCE TO TARGET   =    -0.3056721 DEG
LONGITUDE ARC LENGTH TO TARGET =   12.9455912 KM      LATITUDE ARC LENGTH TO TARGET =    -9.2726828 KM
FORWARD OVERLAP RATIO         =    14.8351394 PCT     SIDE OVERLAP RATIO          =     0.         PCT
TIME BETWEEN PHOTOS           =     1.9002914 SEC

                                    X              Y              Z          MAGNITUDE (KM)
DIRECTION COSINES TO TARGET      -0.60295258    -0.78584789     0.13744549     48.32780266
        CAMERA AXIS              -0.70600680    -0.70154638     0.09688699     46.59169006
            C1                   -0.73921973    -0.62203047     0.25813232     48.12425232
            C2                   -0.71169133    -0.69723281    -0.08580130     45.99111938
            C3                   -0.64919493    -0.75761244    -0.06759687     46.70896437
            C4                   -0.67672332    -0.68241011     0.27633674     48.91184998

                    X              Y              Z          X DOT          Y DOT          Z DOT
STATE VECTOR    1425.0603333   1067.7794342    102.3114796  -1.1158330      1.5114329     -0.3804824


LONG  37.2762 DEG          LONG  36.9903 DEG
LATI   4.0216 DEG          LATI   2.8619 DEG
                                                                  LONG  36.7570 DEG          LONG  36.6445 DEG
       *          36.22762 KM      *                              LATI   3.7649 DEG          LATI   3.2443 DEG
      (1)                        (2)
                                                                         *          16.74976 KM      *
                                                                        (1)                        (2)
            LOW RESOLUTION

                                                                              HIGH RESOLUTION
  34.73519 KM                31.15055 KM          DIRECTION        4.37898 KM                 4.17724 KM
                                                  OF MOTION

                                                                        (4)                        (3)
      (4)                        (3)                                    *          17.02214 KM      *
       *          41.03630 KM      *                              LONG  36.6170 DEG          LONG  36.5090 DEG
LONG  36.1781 DEG          LONG  35.9741 DEG                      LATI   3.8211 DEG          LATI   3.2704 DEG
LATI   4.3560 DEG          LATI   3.0186 DEG
```

Figure 2.4-2: Sample EVAL Program Tabulation

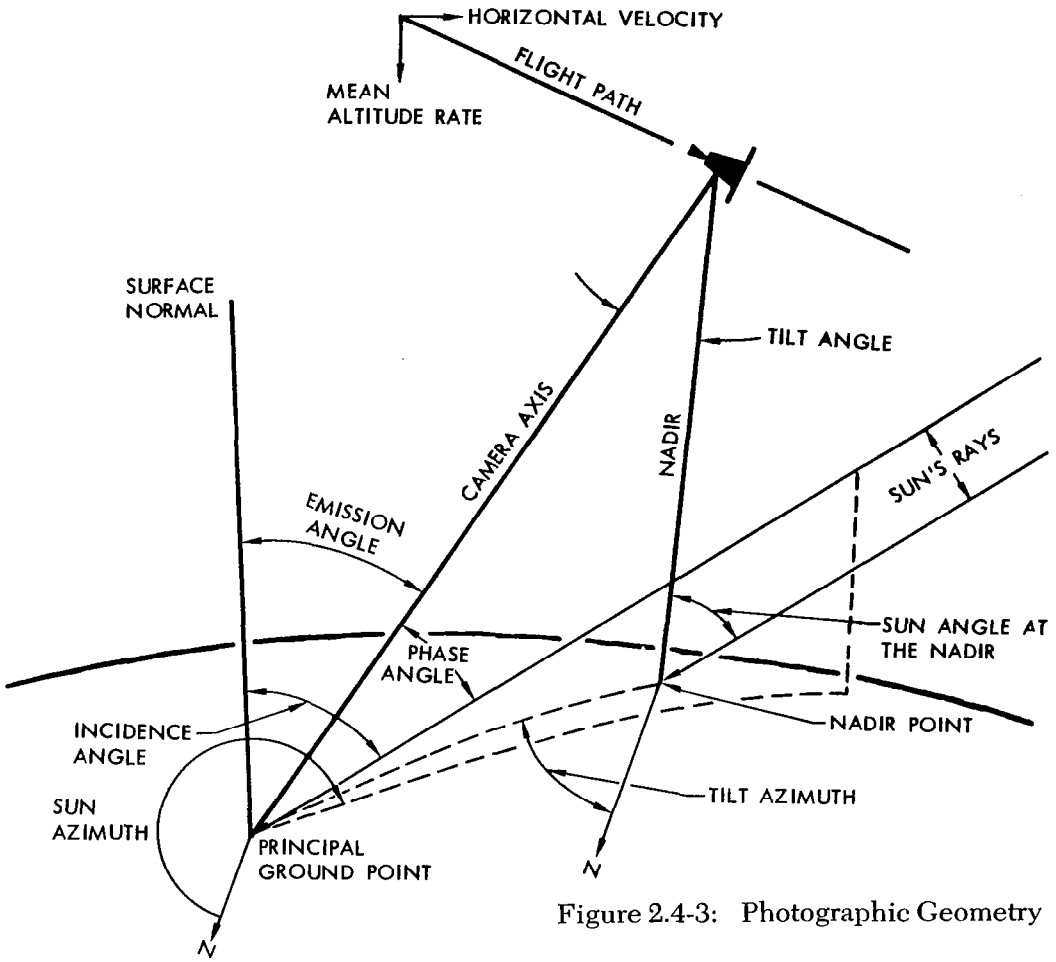

Figure 2.4-3: Photographic Geometry

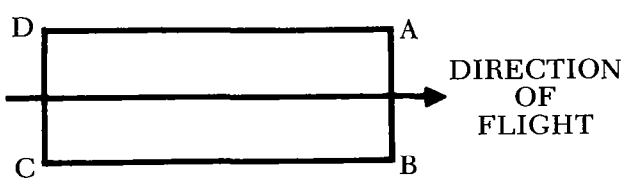

Figure 2.4-4: Corner Coordinate Designation Convention

The Theoretical on-axis ground resolution of the photographs is given by:

$$\text{Telephoto:} \quad R = \frac{H}{46}$$

$$\text{Wide angle:} \quad R = \frac{H}{5.75}$$

Where R is the resolution in meters, and H is spacecraft altitude in kilometers. For oblique photographs, R is approximate when H is the slant distance from spacecraft to ground principal point.

DEFINITION OF TERMS

Camera Axis (Slant Distance): Direction cosines and magnitude (selenographic of date) of camera axis at time of photo.

C1, C2, C3, C4: Direction cosines and magnitude (selenographic of date) of the vectors from spacecraft to photo corners.

Direction Cosines to Target: The direction cosines and magnitude (selenographic of date) of the vector from the spacecraft to the point targets.

Emission Angle: Angle between surface normal and camera axis. Also, the angle between the photo image plane and the subject plane.

Forward Overlap Ratio: Ratio of amount of overlap to telephoto frame dimension along the direction of the flight path.

Horizontal Velocity: That component of spacecraft velocity perpendicular to a radial line

through the spacecraft and in the direction of the flight path.

Image Motion Compensation (V/H): The IMC rate is the instantaneous rate of movement of the image across the focal plane and is a function of spacecraft velocity and its height above the surface (V/H ratio), and the lens focal length.

Incidence Angle: The angle between surface normal and the Sun's rays.

Longitude (latitude) Arc Length to Target: Arc distance measured on lunar surface between the meridian (parallel) through the spacecraft nadir and the meridian (parallel) through the target. (+ is east longitude or north latitude).

Longitude (latitude) of Camera Axis Intersect: The selenographic longitude (latitude) of the point on Moon surface intersected by the camera axis. (+ is east longitude or north latitude).

Longitude (latitude) Distance to Target: Angular distance in longitude (latitude) between camera axis intersect and point target.

Longitude (latitude) of Nadir Point: The selenographic longitude (latitude) of the point on the Moon's surface directly below the spacecraft.

Mean Altitude Rate: Rate of change of altitude with respect to time.

North Deviation Angle: Deviation of north from the cross frame (cross) film axis (Y-axis) measured clockwise.

Phase Angle: The angle between the camera axis and the Sun's rays.

Principal Ground Point: Intersection of camera axis with the lunar surface.

Resolution Constant: The theoretical ground resolution of the high-resolution photographs. Moderate-resolution is larger by a factor of 8. The constant is equal to actual altitude in km, divided by 46 (the nominal altitude giving 1-meter resolution on the high-resolution photographs).

Scale Factor: The proportionality constant to relate dimensions on the spacecraft film to dimensions on the lunar surface. Given for both 80- and 610-mm camera systems.

Side Overlap Ratio: Ratio of amount of overlap to frame dimension perpendicular to flight path (e.g. on adjacent orbits).

Spacecraft Altitude: Altitude of spacecraft above Moon surface.

Spacecraft Radius: Distance from spacecraft to Moon center.

State Vector: Spacecraft position and velocity components in selenographic (of date) coordinates at the time of photo.

Sun Angle at Nadir: Angle between the spacecraft/nadir line and the Sun's rays.

Sun Arc at Nadir: Arc length from the nadir point to the intersection on lunar surface of Moon center to Sun centerline.

Sun Azimuth at Principal Ground Point: Azimuth of Sun's rays at the camera axis intersection, measured clockwise from north.

Surface Normal: A line normal to the Moon surface at the point of camera axis intersection.

Swing Angle: Angle between cross-axis of film frame (the Y' axis) and a line from center of the frame to the image of the nadir point. Measured positive clockwise from the positive Y' axis.

Tilt Angle: Angle between the camera axis and the spacecraft/nadir line.

Tilt Azimuth: Azimuth of principle ground point from spacecraft nadir.

Tilt Distance: Distance from the image of the camera axis intersect to the image of the nadir point measured on the spacecraft film. Given for both high- and low-resolution frames.

Time between Photos: Predicted time between exposure of current frame and succeeding frame taken in a film sequence based on the V/H at the time of current frame.

Time from Pariapsis: Time in seconds before (minus) or after (plus) periapsis passage.

True Anomaly: The angle in the orbital plane measured from pariapsis to the spacecraft in the direction of motion.

Direction of Motion: The arrow that appears on the printout illustrates the general direction of spacecraft motion for determination of the photo footprint orientation.

Photo Footprint: Numbered asterisks that appear on the printout which represent the four corners of the photo frames as projected on the lunar surfaces. Adjacent to each of the asterisks are the longitude and latitude of that corner of the footprint; between the asterisks is the surface distance in kilometers between those corners.

Table 2.4-8: Photo Supporting Data

PHOTO		TIME OF EXPOSURE		SPACECRAFT				PRINCIPAL GROUND POINT		SLANT DIST	SUN AZIM	EMISSION ANGLE	PHASE ANGLE	INCIDENCE ANGLE	TILT ANGLE	TILT AZIM	SWING ANGLE	NORTH DEVIATION
SITE NO.	EXP NO.	S/C	GMT	ALT	ALT RT	LAT	LONG	LAT	LONG									
		SECONDS	HR:MIN:SEC	KM	KM/SEC	DEG	DEG	DEG	DEG	KM	DEG	DEG	DEG	DEG	DEG	DEG	DEG	DEG
		ESTIMATED ERROR ±	.03	1.1	.001	.01	.006	.01	.006	1.1	.01	.12	.12	.01	.12	.01	.10	.10
			DAY 310															
P-1	5		15:24:53.1	48	-0.048	4.25	35.98	4.26	35.94	48	91.47	1.6	73.0	74.52	1.6	280.41	89.4	348.9
	7		15:24:57.2	48	-0.046	4.20	36.23	4.21	36.20	48	91.48	1.3	73.0	74.26	1.3	280.29	89.2	348.9
	9		15:25:01.5	48	-0.043	4.15	36.49	4.16	36.46	48	91.49	1.1	73.0	73.99	1.0	280.09	89.0	348.9
	12		15:25:07.8	47	-0.040	4.08	36.87	4.08	36.86	47	91.50	0.7	73.0	73.60	0.6	279.45	88.3	348.9
	13		15:25:09.9	47	-0.039	4.05	37.00	4.05	36.99	47	91.50	0.5	73.0	73.47	0.5	279.01	87.9	348.9
	14		15:25:12.0	47	-0.038	4.03	37.13	4.03	37.12	47	91.50	0.4	73.0	73.34	0.4	278.28	87.1	348.9
	15		15:25:14.1	47	-0.037	4.00	37.25	4.00	37.25	47	91.50	0.3	73.0	73.20	0.3	276.78	85.6	348.9
	16		15:25:16.2	47	-0.036	3.98	37.38	3.98	37.38	47	91.51	0.1	73.0	73.07	0.1	272.11	80.9	348.8
	17		15:25:18.3	47	-0.035	3.95	37.51	3.95	37.51	47	91.51	0.0	73.0	72.94	0.0	169.31	338.2	348.8
	18		15:25:20.4	47	-0.034	3.93	37.63	3.92	37.64	47	91.51	0.1	73.0	72.81	0.1	109.34	278.2	348.8
	19		15:25:22.5	47	-0.033	3.90	37.76	3.90	37.77	47	91.51	0.3	73.0	72.68	0.3	105.45	274.3	348.8
	20		15:25:24.6	47	-0.031	3.88	37.89	3.87	37.90	47	91.51	0.4	73.0	72.55	0.4	104.09	272.9	348.8
			DAY 311															
P-2	35		8:49:41.0	44	0.012	2.78	33.57	2.78	33.56	44	91.44	0.2	67.8	68.04	0.2	295.40	103.8	348.4
	36		8:49:43.1	45	0.013	2.76	33.69	2.76	33.69	45	91.44	0.1	67.8	67.91	0.1	311.67	120.0	348.3
	37		8:49:45.1	45	0.014	2.73	33.81	2.73	33.81	45	91.43	0.1	67.8	67.79	0.1	43.46	211.8	348.3
	38		8:49:47.1	45	0.015	2.71	33.93	2.71	33.93	45	91.43	0.2	67.8	67.66	0.2	83.03	251.4	348.3
	39		8:49:49.1	45	0.016	2.68	34.05	2.68	34.06	45	91.43	0.3	67.8	67.54	0.3	91.00	259.3	348.3
	40		8:49:51.0	45	0.017	2.66	34.17	2.66	34.18	45	91.43	0.4	67.8	67.42	0.4	94.11	262.4	348.3
	41		8:49:53.0	45	0.018	2.63	34.29	2.63	34.30	45	91.42	0.5	67.8	67.30	0.5	95.89	264.2	348.3
	42		8:49:55.0	45	0.019	2.61	34.41	2.61	34.42	45	91.42	0.7	67.8	67.17	0.6	96.99	265.3	348.3
P-3a	43		15:44:22.3	48	-0.065	4.54	20.89	4.55	20.84	48	91.34	1.7	75.6	77.28	1.7	282.67	91.6	349.0
	44		15:44:24.4	48	-0.064	4.51	21.01	4.52	20.97	48	91.35	1.6	75.6	77.15	1.6	282.81	91.8	349.0
	45		15:44:26.6	48	-0.063	4.49	21.15	4.50	21.11	48	91.35	1.5	75.6	77.01	1.4	282.99	91.9	348.9
	46		15:44:28.7	47	-0.062	4.46	21.27	4.47	21.24	47	91.36	1.3	75.6	76.88	1.3	283.18	92.1	348.9
	47		15:44:30.8	47	-0.061	4.44	21.40	4.45	21.37	47	91.36	1.2	75.6	76.77	1.2	283.42	92.3	348.9
	48		15:44:33.0	47	-0.060	4.41	21.53	4.42	21.51	47	91.36	1.1	75.6	76.61	1.0	283.72	92.6	348.9
	49		15:44:35.1	47	-0.059	4.39	21.66	4.39	21.64	47	91.37	0.9	75.6	76.48	0.9	284.10	93.0	348.9
	50		15:44:37.2	47	-0.058	4.36	21.79	4.37	21.77	47	91.37	0.8	75.6	76.35	0.8	284.59	93.5	348.9
P-3b	51		19:13:24.7	46	-0.051	4.19	20.69	4.20	20.66	46	91.39	1.3	74.4	75.69	1.3	283.27	92.0	348.8
	52		19:13:26.7	46	-0.050	4.17	20.81	4.17	20.78	46	91.39	1.2	74.4	75.57	1.2	283.48	92.3	348.8
	53		19:13:28.8	46	-0.049	4.14	20.94	4.15	20.91	46	91.39	1.1	74.4	75.44	1.1	283.77	92.5	348.8
	54		19:13:30.8	46	-0.048	4.12	21.06	4.12	21.04	46	91.40	1.0	74.4	75.31	0.9	284.11	92.9	348.8
	55		19:13:32.9	46	-0.047	4.09	21.19	4.10	21.17	46	91.40	0.8	74.4	75.18	0.8	284.58	93.3	348.7
	56		19:13:35.0	45	-0.046	4.07	21.31	4.07	21.30	45	91.40	0.7	74.4	75.05	0.7	285.23	94.0	348.7
	57		19:13:37.0	45	-0.045	4.04	21.43	4.05	21.42	45	91.41	0.6	74.4	74.92	0.5	286.12	94.8	348.7
	58		19:13:39.1	45	-0.044	4.02	21.56	4.02	21.55	45	91.41	0.4	74.4	74.80	0.4	287.62	96.3	348.7
P-4	59		22:40:59.4	50	-0.082	4.88	15.20	4.89	15.15	50	91.23	1.8	77.7	79.45	1.7	282.17	91.2	349.1
	60		22:41:01.6	50	-0.081	4.86	15.33	4.87	15.28	50	91.24	1.7	77.7	79.31	1.6	282.28	91.3	349.1
	61		22:41:03.8	49	-0.080	4.83	15.46	4.84	15.42	49	91.24	1.5	77.7	79.18	1.5	282.41	91.5	349.0
	62		22:41:05.9	49	-0.079	4.81	15.59	4.82	15.55	49	91.25	1.4	77.7	79.04	1.3	282.55	91.5	349.0
	63		22:41:08.1	49	-0.078	4.78	15.72	4.79	15.69	49	91.26	1.2	77.7	78.91	1.2	282.74	91.8	349.0
	64		22:41:10.2	49	-0.077	4.76	15.85	4.76	15.82	49	91.25	1.1	77.7	78.78	1.1	282.95	92.0	349.0
	65		22:41:12.3	49	-0.075	4.73	15.97	4.74	15.95	49	91.27	1.0	77.7	78.65	0.9	283.22	92.2	349.0
	66		22:41:14.5	49	-0.075	4.71	16.11	4.71	16.08	49	91.27	0.8	77.7	78.51	0.8	283.60	92.6	349.0
			DAY 312															
P-5	67		02:12:35.7	43	0.012	2.76	24.32	2.85	24.34	43	91.42	3.7	69.1	68.45	3.6	10.12	178.5	348.4
	68		02:12:37.8	43	0.013	2.74	24.45	2.82	24.47	43	91.42	3.7	69.1	68.32	3.6	12.15	180.5	348.4
	69		02:12:39.7	43	0.014	2.71	24.56	2.80	24.59	43	91.42	3.7	69.1	68.20	3.6	14.00	182.4	348.4
	70		02:12:41.7	43	0.015	2.69	24.69	2.77	24.71	43	91.42	3.7	69.1	68.08	3.6	15.95	184.3	348.4
	71		02:12:43.7	43	0.016	2.66	24.81	2.75	24.83	43	91.41	3.7	69.1	67.95	3.6	17.89	186.3	348.4
	72		02:12:45.7	43	0.017	2.64	24.93	2.72	24.96	43	91.41	3.7	69.1	67.83	3.7	19.82	188.2	348.4
	73		02:12:47.7	43	0.018	2.61	25.05	2.70	25.08	43	91.41	3.8	69.1	67.70	3.7	21.72	190.1	348.3
	74		02:12:49.6	43	0.019	2.59	25.16	2.67	25.20	43	91.40	3.8	69.1	67.58	3.7	23.51	191.9	348.3

Table 2.4-8: Photo Supporting Data (Continued)

EXP NO.	TELEPHOTO										WIDE ANGLE									
	TILT DIST	SCALE FACTOR	PHOTO CORNER COORDINATES								TILT DIST	SCALE FACTOR	PHOTO CORNER COORDINATES							
			A		B		C		D				A		B		C		D	
			LAT	LONG	LAT	LONG	LAT	LONG	LAT	LONG			LAT	LONG	LAT	LONG	LAT	LONG	LAT	LONG
	MM	$X10^{-3}$	DEG	DEG	DEG	DEG	DEG	DEG	DEG	DEG	MM	$X10^{-3}$	DEG	DEG	DEG	DEG	DEG	DEG	DEG	DEG
	2%	2%									2%	2%								
5	16.5	0.013	4.53	36.06	3.97	35.95	3.99	35.81	4.55	35.92	2.2	0.002	4.78	36.60	3.53	36.35	3.73	35.27	5.01	35.52
7	13.7	0.013	4.47	36.32	3.92	36.21	3.94	36.07	4.50	36.18	1.8	0.002	4.73	36.85	3.48	36.60	3.68	35.53	4.95	35.78
9	10.9	0.013	4.42	36.59	3.87	36.48	3.89	36.34	4.45	36.45	1.4	0.002	4.68	37.12	3.43	36.87	3.63	35.80	4.90	36.05
12	6.8	0.013	4.34	36.98	3.79	36.87	3.82	36.73	4.37	36.84	0.9	0.002	4.60	37.51	3.35	37.26	3.56	36.20	4.81	36.45
13	5.4	0.013	4.31	37.11	3.76	37.00	3.79	36.86	4.34	36.97	0.7	0.002	4.57	37.64	3.33	37.39	3.53	36.33	4.79	36.58
14	4.0	0.013	4.29	37.24	3.74	37.13	3.77	36.99	4.32	37.10	0.5	0.002	4.55	37.77	3.30	37.52	3.51	36.46	4.76	36.71
15	2.7	0.013	4.26	37.37	3.71	37.26	3.74	37.12	4.29	37.23	0.4	0.002	4.52	37.90	3.28	37.65	3.48	36.59	4.73	36.84
16	1.3	0.013	4.24	37.50	3.69	37.39	3.72	37.25	4.26	37.36	0.2	0.002	4.29	38.03	3.25	37.78	3.46	36.73	4.70	36.97
17	0.3	0.013	4.21	37.63	3.66	37.52	3.69	37.38	4.24	37.49	0.04	0.002	4.47	38.16	3.23	37.99	3.43	36.86	4.68	37.10
18	1.5	0.013	4.18	37.76	3.64	37.65	3.67	37.51	4.21	37.62	0.2	0.002	4.44	38.29	3.20	38.04	3.41	36.99	4.65	37.24
19	2.8	0.013	4.16	37.89	3.61	37.78	3.64	37.64	4.18	37.75	0.4	0.002	4.41	38.42	3.17	38.17	3.38	37.12	4.62	37.37
20	4.2	0.013	4.13	38.02	3.59	37.91	3.61	37.77	4.16	37.88	0.6	0.002	4.39	38.55	3.15	38.30	3.36	37.25	4.59	37.50
35	2.3	0.014	3.03	33.68	2.51	33.58	2.54	33.45	3.05	33.55	0.3	0.002	3.27	34.18	2.10	33.94	2.30	32.95	3.47	33.19
36	1.1	0.014	3.00	33.81	2.49	33.70	2.51	33.57	3.03	33.68	0.1	0.002	3.24	34.30	2.07	34.06	2.27	33.07	3.45	33.31
37	0.7	0.014	2.98	33.93	2.46	33.82	2.49	33.69	3.00	33.80	0.09	0.002	3.22	34.43	2.04	34.19	2.25	33.19	3.42	33.44
38	1.8	0.014	2.95	34.05	2.43	33.95	2.46	33.82	2.98	33.92	0.2	0.002	3.19	34.55	2.02	34.31	2.22	33.32	3.40	33.56
39	3.0	0.014	2.93	34.18	2.41	34.07	2.44	33.94	2.95	34.05	0.4	0.002	3.17	34.68	1.99	34.43	2.20	33.44	3.37	33.68
40	4.2	0.014	2.90	34.29	2.38	34.19	2.41	34.06	2.93	34.16	0.6	0.002	3.14	34.80	1.97	34.55	2.17	33.56	3.35	33.80
41	5.6	0.014	2.88	34.42	2.36	34.31	2.39	34.18	2.90	34.29	0.7	0.002	3.12	34.92	1.94	34.68	2.15	33.68	3.32	33.92
42	6.9	0.014	2.85	34.54	2.33	34.44	2.36	34.30	2.88	34.41	0.9	0.002	3.09	35.05	1.91	34.80	2.12	33.81	3.29	34.05
43	18.1	0.013	4.81	20.97	4.26	20.86	4.28	20.72	4.84	20.83	2.4	0.002	5.07	21.50	3.82	21.25	4.02	20.17	5.29	20.42
44	16.8	0.013	4.79	21.10	4.23	20.99	4.26	20.85	4.82	20.96	2.2	0.002	5.04	21.62	3.80	21.38	3.99	20.31	5.27	20.56
45	15.3	0.013	4.76	21.23	4.21	21.12	4.23	20.98	4.79	21.09	2.01	0.002	5.02	21.76	3.77	21.51	3.97	20.45	5.24	20.69
46	13.9	0.013	4.73	21.36	4.18	21.25	4.21	21.11	4.76	21.22	1.8	0.002	4.99	21.89	3.75	21.64	3.94	20.58	5.21	20.83
47	12.6	0.013	4.71	21.49	4.16	21.38	4.18	21.24	4.73	21.35	1.6	0.002	4.96	22.02	3.72	21.77	3.92	20.71	5.18	20.96
48	11.1	0.013	4.68	21.63	4.13	21.52	4.16	21.38	4.71	21.49	1.5	0.002	4.93	22.15	3.70	21.91	3.90	20.85	5.15	21.10
49	9.8	0.013	4.65	21.76	4.11	21.65	4.13	21.51	4.68	21.62	1.3	0.002	4.91	22.28	3.67	22.04	3.87	20.98	5.12	21.23
50	8.4	0.013	4.63	21.89	4.08	21.78	4.11	21.64	4.65	21.75	1.1	0.002	4.88	22.41	3.65	22.17	3.85	21.12	5.09	21.63
51	13.9	0.013	4.45	20.78	3.92	20.67	3.94	20.54	4.48	20.64	1.8	0.002	4.70	21.29	3.50	21.05	3.69	20.02	4.91	20.26
52	12.6	0.013	4.23	20.90	3.89	20.80	3.92	20.66	4.45	20.77	1.6	0.002	4.67	21.41	3.47	21.17	3.67	20.14	4.89	20.39
53	11.2	0.013	4.40	21.03	3.87	20.93	3.90	20.79	4.43	20.90	1.5	0.002	4.65	21.54	3.45	21.30	3.64	20.28	4.86	20.52
54	9.9	0.013	4.38	21.16	3.85	21.05	3.87	20.92	4.40	21.02	1.3	0.002	4.62	21.66	3.42	21.42	3.62	20.40	4.83	20.64
55	8.5	0.013	4.35	21.29	3.82	21.18	3.85	21.05	4.38	21.15	1.1	0.002	4.59	21.79	3.40	21.55	3.60	20.53	4.80	20.77
56	7.1	0.013	4.32	21.42	3.79	21.31	3.82	21.18	4.35	21.28	0.9	0.002	4.57	21.92	3.37	21.68	3.57	20.67	4.78	20.91
57	5.8	0.013	4.30	21.54	3.77	21.43	3.80	21.30	4.32	21.41	0.8	0.002	4.54	22.05	3.35	21.81	3.55	20.79	4.75	21.03
58	4.5	0.013	4.27	21.67	3.74	21.56	3.77	21.43	4.30	21.54	0.6	0.002	4.52	22.17	3.32	21.94	3.52	20.92	4.72	21.16
59	18.5	0.012	5.17	15.28	4.59	15.16	4.62	15.02	5.20	15.13	2.4	0.002	5.44	15.83	4.14	15.57	4.34	14.45	5.67	14.71
60	17.1	0.012	5.14	15.41	4.57	15.30	4.59	15.16	5.17	15.27	2.2	0.002	5.41	15.96	4.11	15.71	4.31	14.59	5.64	14.85
61	15.6	0.012	5.11	15.55	4.54	15.44	4.57	15.29	5.14	15.40	2.1	0.002	5.38	16.10	4.09	15.84	4.29	14.79	5.61	14.99
62	14.3	0.012	5.09	15.68	4.52	15.57	4.54	15.42	5.12	15.53	1.9	0.002	5.35	16.22	4.07	15.97	4.27	14.87	5.58	15.12
63	12.8	0.012	5.06	15.81	4.49	15.70	4.52	15.56	5.09	15.67	1.7	0.002	5.33	16.36	4.04	16.11	4.24	15.01	5.55	15.26
64	11.5	0.012	5.03	15.94	4.47	15.83	4.49	15.69	5.06	15.80	1.5	0.002	5.30	16.49	4.02	16.24	4.22	15.14	5.52	15.39
65	10.1	0.013	5.01	16.07	4.44	15.96	4.47	15.82	5.04	15.93	1.3	0.002	5.27	16.62	3.99	16.36	4.20	15.27	5.49	15.52
66	8.7	0.013	4.98	16.21	4.42	16.10	4.44	15.96	5.01	16.07	1.1	0.002	5.24	16.75	3.97	16.50	4.17	15.41	5.46	15.66
67	38.6	0.014	3.09	24.46	2.59	24.35	2.61	24.23	3.11	24.33	5.1	0.002	3.33	24.95	2.20	24.69	2.39	22.76	3.53	23.97
68	38.6	0.014	3.06	24.58	2.56	24.48	2.59	24.36	3.09	24.46	5.1	0.002	3.31	25.08	2.18	24.82	2.37	23.89	3.51	24.10
69	38.6	0.014	3.04	24.70	2.54	24.60	2.56	24.47	3.06	24.57	5.1	0.002	3.28	25.20	2.15	24.94	2.34	24.01	3.48	24.21
70	38.7	0.014	3.01	24.83	2.51	24.72	2.54	24.60	3.04	24.70	5.1	0.002	3.26	25.32	2.12	25.06	2.32	24.13	3.46	24.34
71	38.8	0.014	2.99	24.95	2.49	24.85	2.51	24.72	3.01	24.82	5.1	0.002	3.23	25.45	2.10	25.19	2.29	24.25	3.43	24.46
72	39.0	0.014	2.96	25.07	2.46	24.97	2.49	24.84	2.99	24.95	5.1	0.002	3.21	25.57	2.07	25.31	2.27	24.38	3.41	24.58
73	39.2	0.014	2.94	25.20	2.44	25.09	2.46	24.97	2.96	25.07	5.1	0.002	3.18	25.70	2.05	25.44	2.24	24.50	3.38	24.71
74	39.5	0.014	2.91	25.31	2.41	25.21	2.44	25.09	2.94	25.19	5.2	0.002	3.16	25.82	2.02	25.56	2.22	24.62	3.36	24.82

Table 2.4-8: Photo Supporting Data (Continued)

PHOTO		TIME OF EXPOSURE		SPACECRAFT				PRINCIPAL GROUND POINT		SLANT DIST	SUN AZIM	EMIS-SION ANGLE	PHASE ANGLE	INCI-DENCE ANGLE	TILT ANGLE	TILT AZIM	SWING ANGLE	NORTH DEVIA TION
SITE NO.	EXP NO.	S/C	GMT	ALT	ALT RT	LAT	LONG	LAT	LONG	DIST	AZIM	ANGLE	ANGLE	ANGLE	ANGLE	AZIM	ANGLE	TION
		SECONDS	HR:MIN:SEC	KM	KM/SEC	DEG	DEG	DEG	DEG	KM	DEG	DEG	DEG	DEG	DEG	DEG	DEG	DEG
		ESTIMATED ERROR ±		1.1	.001	.01	.006	.01	.006	1.1	.01	.12	.12	.01	.12	.01	.10	.10
			DAY 312 (continued)															
P-6a	76		16:08:27.5	47	0.070	1.20	23.66	1.20	23.68	47	91.00	0.6	62.6	62.01	0.6	93.59	264.7	348.1
	77		16:08:49.6	47	0.071	1.17	23.79	1.17	23.81	47	91.00	0.7	62.6	61.88	0.69	97.58	265.7	348.1
	78		16:08:51.7	47	0.072	1.15	23.92	1.14	23.94	47	90.93	0.8	62.6	61.75	0.8	98.26	266.4	348.1
	79		16:08:53.7	47	0.073	1.12	24.04	1.12	24.06	47	90.97	1.0	62.6	61.63	0.9	98.74	266.9	348.1
	80		16:08:56.0	47	0.074	1.09	24.17	0.09	24.20	47	90.96	1.1	62.6	61.49	1.1	99.15	267.3	348.1
	81		16:08:58.2	47	0.076	1.07	24.31	1.06	24.34	47	90.95	1.3	62.6	61.35	1.2	99.46	267.6	348.1
	82		16:09:00.3	47	0.077	1.04	24.43	1.03	24.47	47	90.94	1.4	62.6	61.22	1.3	99.69	267.8	348.1
	83		16:09:02.5	48	0.078	1.01	24.57	1.00	24.61	48	90.92	1.5	62.6	61.08	1.5	99.90	268.0	348.1
P-6b	84		19:37:51.1	49	0.085	0.81	23.53	0.81	23.55	49	90.84	0.8	61.1	60.37	0.7	97.74	265.9	348.1
	85		19:37:53.3	49	0.086	0.78	23.66	0.78	23.69	49	90.82	0.9	61.1	60.23	0.9	98.38	266.5	348.1
	86		19:37:55.5	49	0.087	0.76	23.80	0.75	23.82	49	90.81	1.0	61.1	60.09	1.0	98.85	267.0	348.1
	87		19:37:57.7	49	0.088	0.73	23.93	0.72	23.96	49	90.80	1.2	61.1	59.96	1.2	99.22	267.3	348.1
	88		19:38:00.0	49	0.089	0.70	24.07	0.69	24.10	49	90.78	1.3	61.1	59.82	1.3	99.51	267.6	348.1
	89		19:38:02.2	50	0.090	0.67	24.20	0.67	24.24	50	90.77	1.5	61.1	59.68	1.4	99.74	267.8	348.1
	90		19:38:04.5	50	0.092	0.64	24.33	0.64	24.38	50	90.75	1.6	61.1	59.54	1.6	99.94	268.0	348.1
	91		19:38:06.8	50	0.093	0.61	24.47	0.61	24.52	50	90.74	1.8	61.1	59.40	1.7	100.11	268.2	348.1
			DAY 314															
P-7a	96		02:52:34.8	41	0.007	2.53	-2.10	2.53	-2.10	41	91.29	0.1	70.2	70.21	0.1	356.70	165.1	348.4
	97		02:52:36.5	41	0.007	2.51	-1.99	2.51	-1.99	41	91.28	0.1	70.2	70.11	0.1	57.05	225.4	348.4
	98		02:52:38.3	41	0.008	2.49	-1.88	2.49	-1.88	41	91.28	0.2	70.2	69.99	0.2	78.08	246.4	348.4
	99		02:52:40.1	41	0.009	2.46	-1.77	2.46	-1.77	41	91.28	0.3	70.2	69.88	0.3	86.00	254.3	348.3
	100		02:52:41.9	41	0.010	2.44	-1.66	2.44	-1.65	41	91.28	0.4	70.2	69.77	0.4	89.98	258.3	348.3
	101		02:52:43.7	41	0.011	2.42	-1.56	2.42	-1.54	41	91.27	0.6	70.2	69.66	0.5	92.36	260.7	348.3
	102		02:52:45.5	41	0.012	2.40	-1.45	2.38	-1.43	41	91.27	0.7	70.2	69.57	0.7	93.94	262.3	348.3
	103		02:52:47.4	41	0.013	2.37	-1.33	2.37	-1.31	41	91.27	0.8	70.2	69.43	0.8	95.12	263.4	348.3
P-7b	104		06:21:36.7	41	0.021	2.17	-2.28	2.17	-2.28	41	91.23	0.1	68.7	68.62	0.1	57.26	225.5	348.3
	105		06:21:38.6	41	0.022	2.15	-2.17	2.15	-2.17	41	91.23	0.2	68.7	68.51	0.2	78.22	246.5	348.3
	106		06:21:40.4	42	0.023	2.12	-2.06	2.12	-2.05	42	91.22	0.3	68.7	68.40	0.3	85.93	254.2	348.3
	107		06:21:42.2	42	0.024	2.10	-1.95	2.10	-1.94	42	91.22	0.4	68.7	68.29	0.4	89.88	258.1	348.3
	108		06:21:44.1	42	0.025	2.08	-1.84	2.08	-1.83	42	91.22	0.6	68.7	68.17	0.6	92.37	260.6	348.3
	109		06:21:45.9	42	0.026	2.05	-1.73	2.05	-1.71	42	91.21	0.7	68.7	68.06	0.7	93.96	262.2	348.3
	110		06:21:47.7	42	0.027	2.03	-1.62	2.03	-1.60	42	91.21	0.8	68.7	67.94	0.8	95.06	263.3	348.3
	111		06:21:49.6	42	0.028	2.01	-1.50	2.01	-1.48	42	91.20	0.9	68.7	67.83	0.9	95.93	264.2	348.3
P-8a	113		16:49:09.2	47	0.077	0.73	-1.32	0.73	-1.30	47	90.80	0.8	63.1	62.33	0.8	96.90	264.9	348.0
	114		16:49:11.3	47	0.078	0.71	-1.20	0.70	-1.17	47	90.78	1.0	63.1	62.20	0.9	97.59	265.6	348.0
	115		16:49:13.3	47	0.079	0.68	-1.08	0.68	-1.05	47	90.77	1.1	63.1	62.08	1.1	98.09	266.1	348.0
	116		16:49:15.4	47	0.080	0.65	-0.95	0.65	-0.92	47	90.76	1.2	63.1	61.94	1.2	98.51	266.4	348.0
	117		16:49:17.5	47	0.081	0.63	-0.83	0.62	-0.79	47	90.75	1.3	63.1	61.82	1.3	98.84	266.8	348.0
	118		16:49:19.6	47	0.082	0.60	-0.70	0.59	-0.66	47	90.74	1.5	63.1	61.69	1.4	99.11	267.1	348.0
	119		16:49:21.7	48	0.083	0.57	-0.57	0.57	-0.53	48	90.73	1.6	63.1	61.56	1.6	99.34	267.3	348.0
	120		16:49:23.8	48	0.084	0.55	-0.45	0.54	-0.40	48	90.71	1.7	63.1	61.43	1.7	99.54	267.5	348.0
P-8b	121		20:18:12.0	49	0.091	0.35	-1.48	0.35	-1.46	49	90.62	1.0	61.7	60.72	1.0	98.45	266.5	348.0
	122		20:18:14.1	49	0.092	0.33	-1.35	0.32	-1.32	49	90.61	1.1	61.7	60.58	1.1	98.88	266.9	348.0
	123		20:18:16.3	49	0.093	0.30	-1.22	0.29	-1.19	49	90.59	1.3	61.7	60.44	1.2	99.22	267.2	348.0
	124		20:18:18.5	50	0.095	0.27	-1.09	0.26	-1.05	50	90.58	1.4	61.7	60.30	1.4	99.49	267.5	348.0
	125		20:18:20.8	50	0.096	0.24	-0.96	0.24	-0.92	50	90.56	1.5	61.7	60.17	1.5	99.71	267.7	348.0
	126		20:18:22.9	50	0.097	0.22	-0.83	0.21	-0.78	50	90.55	1.7	61.7	60.04	1.6	99.89	267.9	348.0
	127		20:18:25.2	50	0.098	0.19	-0.69	0.18	-0.64	50	90.53	1.8	61.7	59.90	1.8	100.05	268.1	348.0
	128		20:18:27.4	50	0.099	0.16	-0.56	0.15	-0.51	51	90.52	2.0	61.7	59.78	1.9	100.18	268.2	348.0

Table 2.4-8: Photo Supporting Data (Continued)

EXP NO.	TELEPHOTO										WIDE ANGLE									
	TILT DIST	SCALE FACTOR	PHOTO CORNER COORDINATES								TILT DIST	SCALE FACTOR	PHOTO CORNER COORDINATES							
			A		B		C		D				A		B		C		D	
			LAT	LONG	LAT	LONG	LAT	LONG	LAT	LONG			LAT	LONG	LAT	LONG	LAT	LONG	LAT	LONG
	MM	$X10^{-3}$	DEG	DEG	DEG	DEG	DEG	DEG	DEG	DEG	MM	$X10^{-3}$	DEG	DEG	DEG	DEG	DEG	DEG	DEG	DEG
	2%	2%									2%	2%								
76	6.0	0.013	1.45	23.80	0.92	23.69	0.94	23.55	1.48	23.67	0.8	0.002	1.70	24.33	0.48	24.07	0.70	23.03	1.92	23.29
77	7.4	0.013	1.43	23.93	0.89	23.82	0.92	23.68	1.46	23.80	1.0	0.002	1.68	24.46	0.45	24.20	0.67	23.16	1.89	23.42
78	8.7	0.013	1.40	24.06	0.86	23.95	0.89	23.81	1.43	23.93	1.1	0.002	1.65	24.59	0.42	24.33	0.64	23.29	1.87	23.55
79	10.0	0.013	1.38	24.19	0.83	24.07	0.68	23.93	1.41	24.05	1.3	0.002	1.63	24.72	0.39	24.46	0.61	23.41	0.84	23.67
80	11.5	0.013	1.35	24.33	0.80	24.21	0.83	24.08	1.38	24.19	1.5	0.002	1.60	24.86	0.35	24.60	0.58	23.55	1.82	23.81
81	13.0	0.013	1.32	24.46	0.77	24.35	0.80	24.21	1.35	24.33	1.7	0.002	1.58	25.00	0.32	24.74	0.55	33.69	1.79	23.95
82	14.4	0.013	1.29	24.59	0.74	24.48	0.77	24.34	1.32	24.46	1.9	0.002	1.55	25.13	0.29	24.87	0.52	23.81	1.76	24.07
83	15.8	0.013	1.27	24.73	0.71	24.62	0.74	24.48	1.29	24.59	2.1	0.002	1.52	25.27	0.26	25.01	0.49	23.95	1.74	24.21
84	7.9	0.013	1.08	23.68	0.51	23.56	0.54	23.42	1.11	23.54	1.0	0.002	1.34	24.23	0.09	23.96	0.29	22.88	1.56	23.15
85	9.4	0.013	1.05	23.82	0.48	23.70	0.51	23.56	1.08	23.68	1.2	0.002	1.31	24.37	0.06	24.10	0.26	23.01	1.53	23.28
86	10.8	0.012	1.02	23.96	0.45	23.84	0.48	23.69	1.05	23.81	1.4	0.002	1.29	24.51	-0.01	24.24	0.23	23.15	1.51	23.42
87	12.2	0.012	0.99	24.09	0.42	23.97	0.45	23.83	1.02	23.95	1.6	0.002	1.26	24.65	-0.04	24.37	0.20	23.28	1.48	23.55
88	13.7	0.012	0.96	24.23	0.39	24.11	0.42	23.97	0.99	24.09	1.8	0.002	1.23	24.79	-0.08	24.52	0.16	23.42	1.45	23.69
89	15.2	0.012	0.94	24.36	0.36	24.25	0.39	24.10	0.97	24.23	2.0	0.002	1.21	24.93	-0.11	24.65	0.13	23.55	1.43	23.83
90	16.7	0.012	0.91	24.51	0.33	24.39	0.36	24.25	0.94	24.37	2.2	0.002	1.18	25.08	-0.14	24.80	0.10	23.69	1.40	23.97
91	18.2	0.012	0.88	24.65	0.30	24.53	0.33	24.39	0.91	24.51	2.4	0.002	1.15	25.22	-0.18	24.94	0.07	23.83	1.37	24.11
96	0.9	0.015	2.76	- 1.99	2.28	-2.09	2.31	-2.21	2.78	-2.11	0.1	0.002	2.98	-1.53	1.90	-1.75	2.09	-2.67	3.17	-2.45
97	1.3	0.015	2.73	- 1.88	2.26	-1.98	2.28	-2.10	2.76	-2.00	0.2	0.002	2.96	-1.42	1.88	-1.64	2.06	-2.56	3.14	-2.33
98	2.3	0.015	2.71	- 1.77	2.24	-1.87	2.26	-1.99	2.74	-1.89	0.3	0.002	2.93	-1.31	1.85	-1.53	2.04	-2.44	3.12	-2.22
99	3.4	0.015	2.69	- 1.66	2.21	-1.75	2.24	-1.87	2.71	-1.78	0.5	0.002	2.91	-1.20	1.83	-1.42	2.02	-2.33	3.10	-2.11
100	4.6	0.015	2.67	- 1.55	2.19	-1.64	2.22	-1.76	2.69	-1.67	0.6	0.002	2.89	-1.08	1.81	-1.31	2.00	-2.22	3.07	-2.00
101	5.7	0.005	2.64	- 1.43	2.17	-1.53	2.19	-1.65	2.67	-1.55	0.8	0.002	2.87	-0.97	1.78	-1.20	1.97	-2.11	3.05	-1.89
102	6.9	0.015	2.62	- 1.32	2.14	-1.42	2.17	-1.54	2.65	-1.44	0.9	0.002	2.84	-0.86	1.76	-1.08	1.95	-2.00	3.03	-1.78
103	8.2	0.015	2.60	- 1.20	2.12	-1.30	2.14	-1.42	2.62	-1.32	1.1	0.002	2.82	-0.74	1.73	-0.97	1.93	-1.88	3.00	-1.66
104	1.4	0.015	2.40	- 2.17	1.92	-2.27	1.94	-2.39	2.42	-2.29	0.2	0.002	2.62	-1.71	1.53	-1.93	1.72	-2.85	2.81	-2.63
105	2.4	0.015	2.38	- 2.06	1.89	-2.16	1.92	-2.28	2.40	-2.18	0.3	0.002	2.60	-1.59	1.51	-1.82	1.70	-2.74	2.79	-2.52
106	3.5	0.015	2.35	- 1.94	1.87	-2.04	1.90	-2.17	2.38	-2.07	0.5	0.002	2.58	-1.48	1.48	-1.70	1.67	-2.63	2.77	-2.40
107	4.7	0.015	2.33	- 1.83	1.85	-1.93	1.87	-2.05	2.36	-1.95	0.6	0.002	2.55	-1.37	1.46	-1.59	1.65	-2.52	2.74	-2.29
108	5.9	0.015	2.31	- 1.72	1.82	-1.82	1.85	-1.94	2.33	-1.84	0.8	0.002	2.53	-1.25	1.43	-1.47	1.63	-2.40	2.72	-2.18
109	7.1	0.015	2.28	- 1.60	1.80	-1.70	1.82	-1.82	2.31	-1.72	0.9	0.002	2.51	-1.13	1.41	-1.36	1.60	-2.29	2.70	-2.06
110	8.3	0.015	2.26	- 1.49	1.78	-1.59	1.80	-1.71	2.29	-1.61	1.1	0.002	2.49	-1.02	1.38	-1.25	1.58	-2.18	2.67	-1.95
111	9.5	0.015	2.24	- 1.37	1.75	-1.47	1.78	-1.59	2.26	-1.49	1.2	0.002	2.46	-0.90	1.36	-1.13	1.56	-2.06	2.65	-1.83
113	8.6	0.013	0.99	- 1.18	0.45	-1.29	0.47	-1.43	1.01	-1.31	1.1	0.002	1.24	-0.65	0.00	-0.91	0.23	-1.95	1.45	-1.69
114	9.9	0.013	0.96	- 1.05	0.42	-1.16	0.44	-1.30	0.99	-1.18	1.3	0.002	1.21	-0.52	-0.03	-0.78	0.20	-1.82	1.42	-1.56
115	11.2	0.013	0.93	- 0.92	0.39	-1.04	0.42	-1.17	0.96	-1.06	1.5	0.002	1.19	-0.39	-0.05	-0.66	0.17	-1.70	1.40	-1.44
116	12.6	0.013	0.91	- 0.79	0.36	-0.91	0.39	-1.05	0.94	-0.93	1.7	0.002	1.16	-0.26	-0.09	-0.52	0.14	-1.57	1.37	-1.31
117	14.0	0.013	0.88	- 0.66	0.33	-0.78	0.36	-0.92	0.91	-0.80	1.9	0.002	1.14	-0.13	-0.12	-0.39	0.11	-1.44	1.35	-1.18
118	15.3	0.013	0.85	- 0.53	0.30	-0.65	0.33	-0.79	0.88	-0.67	2.0	0.002	1.11	0.00	-0.15	-0.26	0.09	-1.31	1.32	-1.05
119	16.7	0.013	0.83	- 0.40	0.28	-0.52	0.31	-0.66	0.86	-0.54	2.2	0.002	1.09	0.14	-0.18	-0.13	0.06	-1.19	1.30	-0.93
120	18.1	0.013	0.80	- 0.27	0.25	-0.39	0.28	-0.53	0.83	-0.41	2.4	0.002	1.06	0.27	-0.21	0.00	0.03	-1.06	1.27	-0.80
121	10.1	0.012	0.62	- 1.33	0.05	-1.45	0.08	-1.59	0.65	-1.47	1.3	0.002	0.88	-0.77	-0.41	-1.05	-0.18	-2.13	1.11	-1.86
122	11.6	0.012	0.59	- 1.19	0.02	-1.31	0.05	-1.45	0.62	-1.33	1.5	0.002	0.86	-0.63	-0.45	-0.91	-0.21	-2.00	1.08	-1.73
123	13.0	0.012	0.56	- 1.05	-0.00	-1.17	0.02	-1.32	0.59	-1.20	1.7	0.002	0.83	-0.49	-0.48	-0.77	-0.24	-1.87	1.05	-1.60
124	14.4	0.012	0.54	- 0.92	-0.04	-1.04	-0.01	-1.18	0.57	-1.06	1.9	0.002	0.81	-0.35	-0.51	-0.63	-0.27	-1.74	1.03	-1.46
125	15.9	0.012	0.51	- 0.78	-0.07	-0.90	-0.04	-1.05	0.54	-0.93	2.0	0.002	0.78	-0.22	-0.54	-0.50	-0.30	-1.60	1.00	-1.33
126	17.3	0.012	0.48	- 0.65	-0.10	-0.77	-0.07	-0.92	0.51	-0.79	2.2	0.002	0.75	-0.08	-0.58	-0.36	-0.33	-1.47	0.98	-1.20
127	18.6	0.012	0.45	- 0.51	-0.13	-0.63	-0.10	-0.78	0.48	-0.66	2.5	0.002	0.73	0.06	-0.61	-0.22	-0.36	-1.34	0.95	-1.06
128	20.2	0.012	0.43	- 0.37	-0.16	-0.49	-0.13	-0.64	0.46	-0.52	2.7	0.002	0.70	0.21	-0.64	-0.08	-0.39	-1.20	0.92	-0.92

Table 2.4-8: Photo Supporting Data (Continued)

PHOTO		TIME OF EXPOSURE		SPACECRAFT				PRINCIPAL GROUND POINT		SLANT	SUN	EMIS-	PHASE	INCI-	TILT	TILT	SWING	NORTH
SITE NO.	EXP NO.	S/C	GMT	ALT	ALT RT	LAT	LONG	LAT	LONG	DIST	AZIM	SION ANGLE	ANGLE	DENCE ANGLE	ANGLE	AZIM	ANGLE	DEVIATION
		SECONDS	HR:MIN:SEC	KM	KM/SEC	DEG	DEG	DEG	DEG	KM	DEG	DEG	DEG	DEG	DEG	DEG	DEG	DEG
		ESTIMATED ERROR ±	.03	1.1	.001	.01	.006	.01	.006	1.1	.01	.12	.12	.01	.12	.01	.10	.10
			DAY 314 (Continued)															
P-8c	129		23:47:13.7	52	0.105	-0.01	-1.71	-0.01	-1.68	52	90.43	1.1	60.2	59.18	1.0	99.18	267.3	348.1
	130		23:47:16.0	52	0.106	-0.04	-1.58	-0.04	-1.54	52	90.41	1.2	60.3	59.03	1.2	99.51	267.6	348.1
	131		23:47:18.3	52	0.107	-0.07	-1.44	-0.07	-1.40	52	90.39	1.4	60.2	58.89	1.3	99.77	267.8	348.1
	132		23:47:20.6	53	0.108	-0.10	-1.30	-0.10	-1.26	53	90.38	1.5	60.2	58.75	1.5	99.97	268.0	348.1
	133		23:47:22.4	53	0.109	-0.12	-1.20	-0.13	-1.15	53	90.36	1.6	60.2	58.64	1.6	100.11	268.2	348.1
	134		23:47:25.3	53	0.111	-0.16	-1.02	-0.17	-0.97	53	90.34	1.8	60.2	58.46	1.7	100.29	268.4	348.1
	135		23:47:27.7	53	0.112	-0.19	-0.88	-0.20	-0.82	53	90.32	2.0	60.2	58.31	1.9	100.42	268.5	348.1
	136		23:47:30.1	54	0.113	-0.22	-0.73	-0.23	-0.67	54	90.30	2.1	60.2	58.16	2.0	100.53	268.6	348.1
			DAY 315															
P-9	138		10:11:15.1	44	0.053	1.20	-13.34	1.20	-13.33	44	90.97	0.5	66.1	65.57	0.5	94.16	262.3	348.1
	139		10:11:17.1	45	0.054	1.18	-13.22	1.18	-13.21	45	90.96	0.7	66.1	65.45	0.6	95.63	263.7	348.1
	140		10:11:19.1	45	0.055	1.15	-13.10	1.15	-13.08	45	90.95	0.8	66.1	65.32	0.8	96.62	264.7	348.1
	141		10:11:21.1	45	0.056	1.13	-12.98	1.13	-12.96	45	90.94	0.0	66.1	65.20	0.9	97.34	265.4	348.1
	142		10:11:23.0	45	0.057	1.10	-12.87	1.10	-12.84	45	90.93	1.0	66.1	65.08	1.0	97.86	266.0	348.1
	143		10:11:25.1	45	0.058	1.08	-12.74	1.07	-12.71	45	90.92	1.2	66.1	64.95	1.1	98.31	266.4	348.1
	144		10:11:27.1	45	0.059	1.05	-12.62	1.05	-12.59	45	90.92	1.3	66.1	64.83	1.3	98.65	266.7	348.1
	145		10:11:29.1	45	0.060	1.03	-12.50	1.02	-12.46	45	90.91	1.4	66.1	64.70	1.4	98.94	267.0	348.1
P-10a	146		13:36:25.1	45	-0.053	3.71	-27.53	3.71	-27.55	45	91.18	1.2	76.9	78.10	1.2	282.18	90.8	348.7
	147		13:36:27.1	45	-0.052	3.68	-27.40	3.69	-27.43	45	91.18	1.1	76.9	77.98	1.0	282.29	90.9	348.6
	148		13:36:29.1	45	-0.051	3.66	-27.28	3.66	-27.31	45	91.18	0.9	76.9	77.85	0.9	282.44	91.1	348.6
	149		13:36:31.0	44	-0.050	3.63	-27.17	3.64	-27.19	44	91.19	0.8	76.9	77.73	0.8	282.62	91.2	348.6
	150		13:36:33.0	44	-0.049	3.61	-27.05	3.61	-27.06	44	91.19	0.7	76.9	77.61	0.7	282.87	91.5	348.6
	151		13:36:35.0	44	-0.048	3.59	-26.93	3.59	-26.94	44	91.19	0.6	76.9	77.48	0.6	283.23	91.8	348.6
	152		13:36:37.0	44	-0.047	3.56	-26.81	3.56	-26.82	44	91.20	0.4	76.9	77.36	0.4	283.79	92.4	348.6
	153		13:36:38.9	44	-0.046	3.59	-26.69	3.54	-26.70	44	91.20	0.3	76.9	77.24	0.3	284.73	93.3	348.6
P-10b	154		17:05:29.9	44	-0.037	3.31	-27.52	3.32	-27.54	44	91.21	0.9	75.5	76.32	0.8	283.22	91.7	348.5
	155		17:05:31.8	44	-0.037	3.29	-27.41	3.29	-27.42	44	91.21	0.8	75.5	76.20	0.7	283.51	92.0	348.5
	156		17:05:33.7	43	-0.086	3.27	-27.29	3.27	-27.31	43	91.21	0.6	75.5	76.08	0.6	283.92	92.4	348.5
	157		17:05:35.6	43	-0.035	3.24	-27.18	3.25	-27.19	43	91.21	0.5	75.5	75.97	0.5	284.52	93.0	348.5
	158		17:05:37.6	43	-0.033	3.22	-27.06	3.22	-27.06	43	91.21	0.4	75.5	75.84	0.4	285.54	94.0	348.5
	159		17:05:39.5	43	-0.033	3.20	-26.94	3.20	-26.95	43	91.22	0.3	75.5	75.72	0.3	287.40	95.9	348.5
	160		17:05:41.5	43	-0.031	3.17	-26.82	3.17	-26.82	43	91.22	0.1	75.5	75.60	0.1	292.73	101.2	348.5
	161		17:05:43.4	43	-0.030	3.15	-26.70	3.15	-26.70	43	91.22	0.0	75.5	75.48	0.0	340.57	149.1	348.5
			DAY 316															
P-11a	163		07:03:50.2	51	0.089	0.20	-20.22	0.20	-20.19	51	90.56	1.1	62.9	61.85	1.0	99.18	267.3	348.1
	164		07:03:52.4	52	0.090	0.17	-20.09	0.17	-20.05	52	90.55	1.2	62.9	61.71	1.2	99.49	267.6	348.1
	165		07:03:54.7	52	0.092	0.14	-19.95	0.14	-19.91	52	90.54	1.4	62.9	61.57	1.3	99.74	267.9	348.1
	166		07:03:57.0	52	0.093	0.11	-19.81	0.11	-19.77	52	90.52	1.5	62.9	61.43	1.5	99.95	268.1	348.1
	167		07:03:59.3	52	0.094	0.09	-19.67	0.08	-19.63	52	90.51	1.7	62.9	61.29	1.6	100.12	268.3	348.1
	168		07:04:01.6	52	0.095	0.06	-19.54	0.05	-19.49	52	90.49	1.8	62.9	61.15	1.7	100.26	268.4	348.1
	169		07:04:04.0	53	0.096	0.03	-19.39	0.02	-19.34	53	90.47	1.9	62.9	61.00	1.9	100.39	268.5	348.1
	170		07:04:06.2	53	0.098	-0.00	-19.26	-0.01	-19.20	53	90.46	2.1	62.9	60.86	2.0	100.49	268.6	348.1
P-11b	171		10:32:54.5	55	0.105	-0.21	-20.25	-0.21	-20.20	55	90.38	1.4	61.5	60.08	1.4	98.79	266.9	348.1
	172		10:32:56.8	55	0.106	-0.24	-20.11	-0.24	-20.06	55	90.36	1.5	61.5	59.94	1.5	99.18	267.3	348.1
	173		10:32:59.4	55	0.107	-0.27	-19.96	-0.28	-19.90	55	90.29	1.7	61.5	59.81	1.6	100.08	268.2	348.2
	174		10:33:01.8	55	0.109	-0.30	-19.81	-0.31	-19.76	55	90.27	1.8	61.5	59.65	1.8	100.26	268.4	348.2
	175		10:33:04.3	56	0.110	-0.33	-19.66	-0.34	-19.60	56	90.27	2.0	61.5	59.50	1.9	100.17	268.3	348.1
	176		10:33:06.8	56	0.111	-0.36	-19.52	-0.37	-19.45	56	90.27	2.2	61.5	59.33	2.1	100.14	268.3	348.1
	177		10:33:09.3	56	0.112	-0.39	-19.37	-0.41	-19.29	56	90.24	2.3	61.5	59.17	2.3	100.29	268.4	348.1
	178		10:33:11.8	57	0.114	-0.42	-19.22	-0.44	-19.14	57	90.21	2.5	61.5	59.03	2.4	100.53	268.7	348.2

Table 2.4-8: Photo Supporting Data (Continued)

EXP NO.	TELEPHOTO TILT DIST MM 2%	TELEPHOTO SCALE FACTOR $\times 10^{-3}$ 2%	TELEPHOTO PHOTO CORNER COORDINATES A LAT DEG	A LONG DEG	B LAT DEG	B LONG DEG	C LAT DEG	C LONG DEG	D LAT DEG	D LONG DEG
129	11.0	0.012	0.27	-1.54	-0.33	-1.67	-0.30	-1.82	0.30	-1.70
130	12.5	0.012	0.24	-1.40	-0.36	-1.53	-0.33	-1.68	0.27	-1.55
131	14.0	0.012	0.21	-1.26	-0.39	-1.39	-0.36	-1.54	0.24	-1.41
132	15.5	0.012	0.18	-1.12	-0.43	-1.25	-0.39	-0.40	0.22	-1.27
133	16.7	0.012	0.16	-1.01	-0.45	-1.14	-0.42	-1.29	0.19	-1.16
134	18.6	0.011	0.13	-0.83	-0.49	-0.96	-0.46	-1.11	0.16	-0.98
135	20.2	0.011	0.10	-0.68	-0.52	-0.81	-0.49	-0.96	0.13	-0.83
136	21.7	0.011	0.07	-0.53	-0.56	-0.66	-0.52	-0.82	0.10	-0.69
138	5.5	0.014	1.45	-13.21	0.93	-13.32	0.96	-13.45	1.47	-13.34
139	6.8	0.014	1.42	-13.09	0.91	-13.19	0.93	-13.32	1.45	-13.22
140	8.1	0.014	1.40	-12.96	0.88	-13.07	0.91	-13.20	1.42	-13.09
141	9.4	0.014	1.37	-12.84	0.85	-12.95	0.88	-13.08	1.40	-12.97
142	10.6	0.014	1.35	-12.72	0.83	-12.83	0.85	-12.96	1.37	-12.85
143	12.1	0.014	1.32	-12.59	0.80	-12.70	0.83	-12.83	1.35	-12.72
144	13.3	0.014	1.30	-12.46	0.77	-12.58	0.80	-12.71	1.32	-12.60
145	14.6	0.013	1.27	-12.34	0.75	-12.45	0.77	-12.59	1.30	-12.48
146	12.4	0.014	3.96	-27.44	3.44	-27.54	3.46	-27.67	3.98	-27.57
147	11.1	0.014	3.93	-27.31	3.41	-27.42	3.44	-27.55	3.96	-27.44
148	9.8	0.014	3.91	-27.19	3.39	-27.29	3.42	-27.42	3.93	-27.32
149	8.5	0.014	3.88	-27.07	3.37	-27.18	3.39	-27.31	3.91	-27.20
150	7.2	0.014	3.86	-26.95	3.34	-27.05	3.37	-27.18	3.88	-27.08
151	5.9	0.014	3.83	-26.82	3.32	-26.93	3.35	-27.06	3.86	-26.95
152	4.6	0.014	3.81	-26.70	3.30	-26.80	3.32	-26.93	3.83	-26.83
153	3.3	0.014	3.78	-26.58	3.27	-26.69	3.30	-26.81	3.81	-26.71
154	9.0	0.014	3.56	-27.42	3.05	-27.53	3.08	-27.65	3.58	-27.55
155	7.8	0.014	3.53	-27.31	3.03	-27.41	3.05	-27.54	3.56	-27.44
156	6.6	0.014	3.51	-27.19	3.01	-27.29	3.03	-27.42	3.54	-27.32
157	5.3	0.014	3.49	-27.07	2.98	-27.18	3.01	-27.30	3.51	-27.20
158	4.0	0.014	3.46	-26.95	2.96	-27.05	2.98	-27.18	3.49	-27.08
159	2.8	0.014	3.44	-26.83	2.93	-26.93	2.96	-27.06	3.46	-26.96
160	1.5	0.014	3.41	-26.71	2.91	-26.81	2.94	-26.94	3.44	-26.84
161	0.4	0.014	3.39	-26.59	2.89	-26.69	2.91	-26.82	3.41	-26.72
163	11.2	0.012	0.48	-20.05	-0.12	-20.17	-0.09	-20.32	0.51	-20.20
164	12.6	0.012	0.45	-19.91	-0.15	-20.04	-0.12	-20.19	0.48	-20.06
165	14.1	0.012	0.42	-19.77	-0.18	-19.90	-0.15	-20.05	0.45	-19.92
166	15.6	0.012	0.39	-19.63	-0.21	-19.76	-0.18	-19.91	0.42	-19.78
167	17.1	0.012	0.36	-19.49	-0.24	-19.61	-0.21	-19.77	0.40	-19.64
168	18.6	0.012	0.34	-19.34	-0.27	-19.47	-0.24	-19.63	0.37	-19.50
169	20.1	0.012	0.31	-19.20	-0.31	-19.33	-0.27	-19.48	0.34	-19.35
170	21.6	0.012	0.28	-19.06	-0.34	-19.19	-0.30	-19.34	0.31	-19.21
171	14.5	0.011	0.09	-20.06	-0.55	-20.19	-0.51	-20.35	0.12	-20.22
172	15.9	0.011	0.06	-19.91	-0.58	-20.05	-0.55	-20.21	0.09	-20.07
173	17.4	0.011	0.03	-19.76	-0.62	-19.89	-0.58	-20.05	0.06	-19.92
174	19.0	0.011	0.00	-19.61	-0.65	-19.74	-0.61	-19.91	0.03	-19.77
175	20.7	0.011	-0.04	-19.45	-0.68	-19.59	-0.65	-19.75	-0.00	-19.62
176	22.4	0.011	-0.07	-19.30	-0.72	-19.44	-0.68	-19.60	-0.03	-19.46
177	24.1	0.011	-0.10	-19.14	-0.75	-19.28	-0.71	-19.45	-0.06	-19.31
178	25.5	0.011	-0.13	-18.99	-0.78	-19.13	-0.75	-19.29	-0.09	-19.16

EXP NO.	WIDE ANGLE TILT DIST MM 2%	WIDE ANGLE SCALE FACTOR $\times 10^{-3}$ 2%	WIDE ANGLE PHOTO CORNER COORDINATES A LAT DEG	A LONG DEG	B LAT DEG	B LONG DEG	C LAT DEG	C LONG DEG	D LAT DEG	D LONG DEG
129	1.4	0.002	0.55	-0.96	-0.82	-1.25	-0.57	-2.40	0.78	-2.11
130	1.6	0.002	0.52	-0.81	-0.86	-1.10	-0.60	-2.26	0.76	-1.97
131	1.8	0.002	0.50	-0.67	-0.89	-0.96	-0.64	-2.12	0.73	-1.83
132	2.0	0.002	0.47	-0.52	-0.93	-0.82	-0.67	-1.98	0.70	-1.69
133	2.2	0.002	0.45	-0.41	-0.95	-0.70	-0.69	-1.88	0.68	-1.59
134	2.4	0.002	0.41	-0.22	-1.00	-0.52	-0.73	-1.70	0.65	-1.41
135	2.6	0.001	0.39	-0.07	-1.04	-0.37	-0.77	-1.55	0.62	-1.26
136	2.9	0.001	0.36	0.08	-1.07	-0.22	-0.80	-1.41	0.59	-1.12
138	0.7	0.002	1.69	-12.71	0.51	-12.96	0.72	-13.94	1.89	-13.70
139	0.9	0.002	1.66	-12.59	0.49	-12.83	0.70	-13.82	1.86	-13.58
140	1.1	0.002	1.64	-12.46	0.46	-12.71	0.67	-13.70	1.84	-13.46
141	1.2	0.002	1.61	-12.33	0.43	-12.58	0.64	-13.58	1.82	-13.33
142	1.4	0.002	1.59	-12.21	0.40	-12.46	0.62	-13.46	1.79	-13.22
143	1.6	0.002	1.57	-12.08	0.37	-12.33	0.59	-13.33	1.77	-13.09
144	1.7	0.002	1.54	-11.96	0.34	-12.21	0.56	-13.21	1.74	-12.96
145	1.9	0.002	1.52	-11.83	0.32	-12.08	0.54	-13.09	1.72	-12.84
146	1.6	0.002	4.20	-26.94	3.03	-27.18	3.22	-28.18	4.41	-27.94
147	1.5	0.002	4.17	-26.82	3.00	-27.05	3.19	-28.05	4.38	-27.81
148	1.3	0.002	4.15	-26.69	2.98	-26.93	3.17	-27.92	4.35	-27.69
149	1.1	0.002	4.12	-26.58	2.96	-26.81	3.15	-27.80	4.33	-27.57
150	0.9	0.002	4.10	-26.45	2.93	-26.69	3.13	-27.68	4.30	-27.44
151	0.8	0.002	4.07	-26.33	2.91	-26.57	3.10	-27.55	4.27	-27.32
152	0.6	0.002	4.05	-26.21	2.89	-26.44	3.08	-27.43	4.25	-27.19
153	0.5	0.002	4.02	-26.09	2.86	-26.32	3.06	-27.31	4.22	-27.08
154	1.2	0.002	3.79	-26.94	2.65	-27.17	2.84	-28.14	3.99	-27.91
155	1.0	0.002	3.77	-26.82	2.63	-27.06	2.82	-28.03	3.97	-27.80
156	0.8	0.002	3.74	-26.71	2.60	-26.94	2.79	-27.91	3.94	-27.68
157	0.7	0.002	3.72	-26.59	2.58	-26.82	2.77	-27.79	3.92	-27.56
158	0.5	0.002	3.69	-26.47	2.56	-26.70	2.75	-27.66	3.89	-27.43
159	0.4	0.002	3.67	-26.35	2.53	-26.58	2.72	-27.55	3.87	-27.32
160	0.2	0.002	3.64	-26.23	2.51	-26.46	2.70	-27.42	3.84	-27.19
161	0.0	0.002	3.62	-26.11	2.48	-26.34	2.68	-27.39	3.81	-27.07
163	1.5	0.002	0.76	-19.47	-0.61	-19.76	-0.36	-20.90	0.99	-20.61
164	1.7	0.002	0.73	-19.33	-0.64	-19.62	-0.39	-20.76	0.96	-20.48
165	1.8	0.002	0.70	-19.18	-0.67	-19.47	-0.42	-20.62	0.93	-20.34
166	2.0	0.002	0.68	-19.04	-0.71	-19.33	-0.45	-20.48	0.91	-20.20
167	2.2	0.002	0.65	-18.89	-0.74	-19.19	-0.48	-20.35	0.88	-20.06
168	2.4	0.002	0.62	-18.75	-0.77	-19.04	-0.51	-20.21	0.85	-19.92
169	2.6	0.002	0.59	-18.60	-0.81	-18.89	-0.55	-20.06	0.82	-19.77
170	2.8	0.002	0.57	-18.45	-0.84	-18.75	-0.58	-19.92	0.80	-19.63
171	1.9	0.001	0.38	-19.44	-1.07	-19.74	-0.80	-20.96	0.63	-20.66
172	2.1	0.001	0.36	-19.29	-1.10	-19.60	-0.83	-20.82	0.60	-20.51
173	2.3	0.001	0.33	-19.13	-1.14	-19.44	-0.87	-20.66	0.57	-20.36
174	2.5	0.001	0.30	-18.98	-1.18	-19.29	-0.90	-20.52	0.54	-20.22
175	2.7	0.001	0.27	-18.82	-1.22	-19.13	-0.94	-20.37	0.51	-20.06
176	2.9	0.001	0.24	-18.66	-1.25	-18.97	-0.97	-20.21	0.48	-19.91
177	3.2	0.001	0.21	-18.50	-1.29	-18.82	-1.01	-20.07	0.46	-19.76
178	3.3	0.001	0.18	-18.34	-1.33	-18.66	-1.04	-19.92	0.43	-19.61

Table 2.4-8: Photo Supporting Data (Continued)

PHOTO		TIME OF EXPOSURE		SPACECRAFT				PRINCIPAL GROUND POINT		SLANT DIST	SUN AZIM	EMIS-SION ANGLE	PHASE ANGLE	INCI-DENCE ANGLE	TILT ANGLE	TILT AZIM	SWING ANGLE	NORTH DEVIA TION
SITE NO.	EXP NO.	S/C	GMT	ALT	ALT RT	LAT	LONG	LAT	LONG									
		SECONDS	HR:MIN:SEC	KM	KM/SEC	DEG	DEG	DEG	DEG	KM	DEG	DEG	DEG	DEG	DEG	DEG	DEG	DEG
		ESTIMATED ERROR ±		1.1	.001	.01	.006	.01	.006	1.1	.01	.12	.12	.01	.12	.01	.10	.10
			DAY 316 (continued)															
P-12a	179		13:58:00.8	44	-0.001	2.39	-34.55	2.39	-34.54	44	91.17	0.1	72.8	72.74	0.1	66.67	235.0	348.3
	180		13:58:02.7	44	-0.000	2.36	-34.43	2.36	-34.42	44	91.17	0.2	72.8	72.62	0.2	85.31	253.6	348.3
	181		13:58:04.6	44	0.001	2.34	-34.31	2.34	-34.30	44	91.17	0.3	72.8	72.50	0.3	91.07	259.4	348.3
	182		13:58:06.6	44	0.002	2.31	-34.19	2.31	-34.18	44	91.16	0.5	72.8	72.38	0.5	93.96	262.3	348.3
	183		13:58:08.5	44	0.003	2.29	-34.08	2.29	-34.06	44	91.16	0.6	72.8	72.36	0.6	95.56	263.8	348.3
	184		13:58:10.5	44	0.004	2.26	-33.96	2.26	-33.94	44	91.16	0.7	72.8	72.14	0.7	96.67	265.0	348.3
	185		13:58:12.5	44	0.005	2.24	-33.84	2.24	-33.82	44	91.16	0.8	72.8	72.01	0.8	97.44	265.7	348.3
	186		13:58:14.5	44	0.006	2.22	-33.72	2.21	-33.70	44	91.16	1.0	72.8	71.89	0.9	97.99	266.3	348.3
P-12b	187		17:27:06.2	45	0.016	1.97	-34.48	1.97	-34.46	45	91.12	0.5	71.4	70.81	0.5	92.34	260.6	348.2
	188		17:27:08.2	45	0.017	1.94	-34.36	1.94	-34.34	45	91.11	0.6	71.4	70.77	0.6	94.29	262.5	348.2
	189		17:27:10.2	45	0.018	1.92	-34.24	1.91	-34.22	45	91.11	0.7	71.4	70.65	0.7	95.58	263.8	348.2
	190		17:27:12.2	45	0.019	1.89	-34.12	1.89	-34.10	45	91.11	0.9	71.4	70.53	0.8	96.48	264.7	348.2
	191		17:27:14.2	45	0.020	1.87	-34.00	1.86	-33.97	45	91.10	1.0	71.4	70.48	1.0	97.16	265.4	348.2
	192		17:27:16.2	45	0.021	1.84	-33.88	1.84	-33.85	45	91.10	1.1	71.4	70.28	1.1	97.70	265.9	348.2
	193		17:27:18.2	45	0.022	1.82	-33.76	1.81	-33.73	45	91.09	1.2	71.4	70.15	1.2	98.12	266.3	348.2
	194		17:27:20.2	45	0.023	1.79	-33.64	1.79	-33.60	45	91.09	1.4	71.4	70.03	1.3	98.47	266.7	348.2
			DAY 317															
P-13a	197		07:21:13.2	45	0.012	2.00	-42.22	2.01	-42.21	45	91.12	0.2	71.8	71.61	0.2	63.58	231.8	348.2
	198		07:21:15.3	45	0.013	1.98	-42.09	1.98	-42.08	45	91.11	0.4	71.8	71.48	0.3	76.81	245.0	348.2
	199		07:21:17.4	45	0.014	1.95	-41.96	1.95	-41.95	45	91.11	0.5	71.8	71.35	0.5	83.40	251.6	348.2
	200		07:21:19.5	45	0.015	1.93	-41.84	1.93	-41.82	45	91.11	0.6	71.8	71.22	0.6	87.34	255.6	348.2
	201		07:21:21.7	45	0.016	1.90	-41.71	1.90	-41.69	45	91.10	0.7	71.8	71.08	0.7	90.00	258.3	348.2
	202		07:21:23.6	45	0.017	1.87	-41.59	1.87	-41.57	45	91.10	0.9	71.8	70.97	0.8	91.63	259.9	348.2
	203		07:21:25.6	45	0.018	1.85	-41.47	1.85	-41.45	45	91.10	1.0	71.8	70.84	1.0	92.92	261.1	348.2
	204		07:21:27.7	45	0.019	1.82	-41.34	1.82	-41.32	45	91.09	1.1	71.8	70.71	1.1	93.96	262.2	348.2
P-13b	205		10:50:17.8	46	0.028	1.58	-42.17	1.58	-42.16	46	91.04	0.7	70.4	69.79	0.6	88.64	256.8	348.2
	206		10:50:19.9	46	0.029	1.56	-42.05	1.56	-42.03	46	91.04	0.7	70.4	69.66	0.7	91.12	259.3	348.2
	207		10:50:22.0	46	0.030	1.53	-41.92	1.53	-41.90	46	91.03	0.8	70.4	69.53	0.8	92.82	261.0	348.1
	208		10:50:24.1	46	0.031	1.50	-41.80	1.50	-41.77	46	91.03	1.0	70.4	69.40	0.9	94.04	262.2	348.1
	209		10:50:26.2	46	0.033	1.48	-41.67	1.47	-41.64	46	91.02	1.1	70.4	69.27	1.1	94.99	263.1	348.1
	210		10:50:28.2	47	0.034	1.45	-41.54	1.45	-41.51	47	91.02	1.2	70.4	69.14	1.2	95.71	263.9	348.1
	211		10:50:30.4	47	0.035	1.42	-41.42	1.42	-41.38	47	91.01	1.4	70.4	69.01	1.3	96.32	264.5	348.1
	212		10:50:32.4	47	0.036	1.40	-41.29	1.39	-41.25	47	91.00	1.5	70.4	68.88	1.4	96.80	264.9	348.1
		SECONDARY PHOTO SITES																
			DAY 310															
S-1	21		15:26:12.9	46	-0.006	3.29	40.80	3.27	40.89	46	91.52	3.5	72.9	69.55	3.4	101.78	270.4	348.6
	22		15:26:15.0	46	-0.005	3.26	40.93	3.25	41.02	46	91.52	3.6	72.9	69.42	3.5	101.78	270.4	348.6
	23		15:26:17.1	46	-0.004	3.24	41.05	3.22	41.15	46	91.52	3.7	72.9	69.29	3.6	101.78	270.4	348.6
	24		15:26:19.2	46	-0.003	3.21	41.18	3.19	41.28	45	91.52	3.9	72.9	69.15	3.8	101.77	270.4	348.6
S-2a	25		18:53:59.9	47	-0.030	3.82	36.18	3.58	36.40	48	91.50	12.3	81.1	72.28	12.0	136.82	306.4	350.2
	26		18:54:02.2	46	-0.029	3.79	36.31	3.56	36.34	48	91.51	12.4	81.1	72.13	12.1	136.44	306.0	350.2
	27		18:54:04.4	46	-0.028	3.77	36.44	3.53	36.68	48	91.51	12.5	81.1	72.00	12.2	136.10	305.6	350.2
	28		18:54:06.7	46	-0.027	3.74	36.58	3.50	36.52	47	91.51	12.7	81.1	71.86	12.3	135.74	305.2	350.2
S-2b	29		22:23:12.8	46	-0.009	3.31	36.73	3.55	36.51	47	91.50	12.3	62.1	70.40	12.0	317.65	126.9	349.9
	30		22:23:14.7	46	-0.009	3.29	36.48	3.52	36.63	47	91.50	12.2	62.1	70.28	11.9	317.98	127.2	349.9
	31		22:23:16.7	46	-0.007	3.26	36.96	3.50	36.76	47	91.50	12.1	62.1	70.16	11.3	318.34	127.6	349.8
	32		22:23:18.7	46	-0.006	3.24	37.08	3.47	36.88	47	91.50	12.0	62.1	70.03	11.7	318.70	127.9	349.8
			DAY 313															
S-6	92		02:30:46.1	44	-0.049	3.96	4.35	4.28	4.41	45	91.32	13.2	78.6	76.07	12.8	10.89	138.9	181.1
S-7	93		09:27:37.3	44	-0.058	4.13	-0.35	0.26	-1.13	129	91.28	72.0	76.1	78.04	68.0	191.33	1.7	333.6
S-8	94		16:29:25.0	48	0.082	0.76	12.19	0.76	12.21	48	90.81	0.7	61.8	61.14	0.7	95.72	263.8	348.1
S-9	95		23:24:10.8	41	0.003	2.61	-0.74	2.62	-0.76	41	91.29	1.1	69.6	70.64	1.0	284.04	92.3	348.3

Table 2.4-8: Photo Supporting Data (Continued)

EXP NO.	TELEPHOTO TILT DIST MM 2%	TELEPHOTO SCALE FACTOR $X10^{-3}$ 2%	TELEPHOTO PHOTO CORNER COORDINATES A LAT DEG	A LONG DEG	B LAT DEG	B LONG DEG	C LAT DEG	C LONG DEG	D LAT DEG	D LONG DEG
179	1.2	0.014	2.63	-34.43	2.12	-34.53	2.14	-34.66	2.66	-34.55
180	2.3	0.014	2.61	-34.30	2.09	-34.41	2.12	-34.54	2.63	-34.43
181	3.5	0.014	2.58	-34.19	2.07	-34.29	2.10	-34.42	2.61	-34.32
182	4.8	0.014	2.56	-34.06	2.04	-34.17	2.07	-34.30	2.58	-34.19
183	6.1	0.014	2.53	-33.95	2.02	-34.05	2.05	-34.18	2.56	-34.07
184	7.4	0.014	2.51	-33.82	1.99	-33.93	2.02	-34.06	2.53	-33.95
185	8.7	0.014	2.48	-33.70	1.97	-33.81	1.99	-33.93	2.51	-33.83
186	9.9	0.014	2.46	-33.58	1.94	-33.69	1.97	-33.81	2.48	-33.71
187	5.1	0.014	2.21	-34.34	1.69	-34.45	1.72	-34.58	2.24	-34.48
188	6.3	0.014	2.19	-34.22	1.67	-34.33	1.69	-34.46	2.21	-34.35
189	7.6	0.014	2.16	-34.10	1.64	-34.21	1.67	-34.34	2.19	-34.23
190	8.9	0.014	2.14	-33.98	1.62	-34.09	1.64	-34.22	2.16	-34.11
191	10.2	0.014	2.11	-33.85	1.59	-33.96	1.62	-34.09	2.14	-33.98
192	11.5	0.014	2.08	-33.73	1.56	-33.84	1.59	-33.97	2.11	-33.86
193	12.8	0.014	2.06	-33.61	1.54	-33.72	1.56	-33.85	2.09	-33.74
194	14.1	0.014	2.03	-33.48	1.51	-33.59	1.54	-33.72	2.06	-33.61
197	2.5	0.013	2.26	-42.09	1.73	-42.20	1.76	-42.33	2.28	-42.22
198	3.7	0.013	2.23	-41.96	1.70	-42.07	1.73	-42.20	2.26	-42.09
199	5.0	0.013	2.20	-41.83	1.68	-41.94	1.71	-42.07	2.23	-41.96
200	6.3	0.013	2.18	-41.70	1.65	-41.81	1.68	-41.94	2.20	-41.83
201	7.7	0.013	2.15	-41.57	1.62	-41.67	1.65	-41.81	2.18	-41.70
202	8.9	0.013	2.12	-41.45	1.60	-41.56	1.63	-41.69	2.15	-41.58
203	10.2	0.013	2.10	-41.32	1.57	-41.43	1.60	-41.57	2.13	-41.46
204	11.6	0.013	2.07	-41.19	1.54	-41.30	1.57	-41.44	2.10	-41.33
205	5.9	0.013	1.84	-42.04	1.30	-42.15	1.33	-42.28	1.86	-42.17
206	7.2	0.013	1.81	-41.91	1.27	-42.02	1.30	-42.15	1.84	-42.04
207	8.6	0.013	1.78	-41.78	1.25	-41.89	1.27	-42.02	1.81	-41.91
208	9.9	0.013	1.76	-41.65	1.22	-41.76	1.25	-41.90	1.79	-41.78
209	11.3	0.013	1.73	-41.52	1.19	-41.63	1.22	-41.76	1.76	-41.65
210	12.6	0.013	1.70	-41.39	1.16	-41.50	1.19	-41.64	1.73	-41.52
211	14.0	0.013	1.68	-41.26	1.14	-41.37	1.16	-41.51	1.71	-41.39
212	15.4	0.013	1.65	-41.13	1.11	-41.24	1.14	-41.38	1.68	-41.27
21	35.9	0.013	3.53	41.01	2.99	40.90	3.02	40.76	3.55	40.87
22	37.3	0.013	3.50	41.14	2.96	41.03	2.99	40.89	3.52	41.00
23	38.6	0.013	3.47	41.27	2.94	41.16	2.97	41.02	3.50	41.13
24	40.0	0.013	3.45	41.40	2.91	41.29	2.94	41.15	3.47	41.26
25	129.4	0.013	3.84	36.52	3.28	36.41	3.32	36.27	3.87	36.39
26	130.7	0.013	3.81	36.67	3.25	36.56	3.29	36.41	3.84	36.53
27	131.9	0.013	3.79	36.80	3.23	36.69	3.26	36.55	3.81	36.66
28	133.2	0.013	3.76	36.94	3.20	36.83	3.23	36.69	3.79	36.80
29	129.7	0.013	3.81	36.64	3.27	36.53	3.29	36.39	3.85	36.50
30	128.6	0.013	3.78	36.76	3.24	36.64	3.27	36.51	3.82	36.62
31	127.5	0.013	3.76	36.88	3.22	36.77	3.25	36.63	3.80	36.74
32	126.4	0.013	3.73	37.00	3.19	36.89	3.22	36.76	3.77	36.86
92	138.9	0.014	4.55	4.54	4.01	4.43	4.04	4.30	4.58	4.40
93	1509.8	0.014								
94	7.2	0.013	1.02	12.33	0.47	12.22	0.49	12.08	1.05	12.19
95	11.2	0.015	2.85	-0.65	2.37	-0.75	2.39	-0.87	2.87	-0.77

EXP NO.	WIDE ANGLE TILT DIST MM 2%	WIDE ANGLE SCALE FACTOR $X10^{-3}$ 2%	WIDE ANGLE PHOTO CORNER COORDINATES A LAT DEG	A LONG DEG	B LAT DEG	B LONG DEG	C LAT DEG	C LONG DEG	D LAT DEG	D LONG DEG
179	0.2	0.002	2.87	-33.93	1.70	-34.17	1.91	-35.16	3.07	-34.91
180	0.3	0.002	2.84	-33.81	1.68	-34.05	1.88	-35.03	3.05	-34.79
181	0.5	0.002	2.82	-33.69	1.65	-33.93	1.86	-34.92	3.02	-34.68
182	0.6	0.002	2.79	-33.57	1.63	-33.81	1.83	-34.79	3.00	-34.55
183	0.8	0.002	2.77	-33.45	1.60	-33.69	1.81	-34.67	2.97	-34.43
184	1.0	0.002	2.74	-33.32	1.58	-33.57	1.78	-34.55	2.94	-34.31
185	1.1	0.002	2.72	-33.20	1.54	-33.44	1.76	-34.43	2.92	-34.19
186	1.3	0.002	2.70	-33.08	1.52	-33.32	1.73	-34.31	2.89	-34.07
187	0.7	0.002	2.45	-33.84	1.27	-34.09	1.48	-35.09	2.66	-34.84
188	0.8	0.002	2.43	-33.72	1.24	-33.96	1.46	-34.96	2.63	-34.72
189	1.0	0.002	2.40	-33.59	1.22	-33.84	1.43	-34.84	2.61	-34.59
190	1.2	0.002	2.38	-33.47	1.19	-33.72	1.41	-34.72	2.58	-34.47
191	1.3	0.002	2.35	-33.35	1.16	-33.59	1.38	-33.59	2.56	-34.35
192	1.5	0.002	2.33	-33.22	1.14	-33.47	1.35	-34.47	2.53	-34.22
193	1.7	0.002	2.30	-33.10	1.11	-33.35	1.33	-34.35	2.50	-34.10
194	1.9	0.002	2.28	-32.97	1.08	-33.22	1.30	-34.22	2.48	-33.98
197	0.3	0.002	2.50	-41.58	1.31	-41.83	1.52	-42.84	2.71	-42.59
198	0.5	0.002	2.47	-41.45	1.28	-41.70	1.49	-42.71	2.68	-42.46
199	0.7	0.002	2.45	-41.32	1.25	-41.57	1.46	-42.58	2.65	-42.33
200	0.8	0.002	2.42	-41.19	1.22	-41.44	1.44	-42.45	2.63	-42.20
201	1.0	0.002	2.39	-41.05	1.19	-41.30	1.41	-42.31	2.60	-42.07
202	1.2	0.002	2.37	-40.94	1.17	-41.19	1.38	-42.19	2.57	-41.95
203	1.3	0.002	2.35	-40.81	1.14	-41.06	1.36	-42.07	2.55	-41.83
204	1.5	0.002	2.32	-40.68	1.11	-40.93	1.33	-41.94	2.52	-41.70
205	0.8	0.002	2.09	-41.51	0.87	-41.77	1.08	-42.80	2.30	-42.55
206	0.9	0.002	2.06	-41.38	0.84	-41.64	1.06	-42.67	2.27	-42.42
207	1.1	0.002	2.04	-41.25	0.81	-41.51	1.03	-42.54	2.24	-42.29
208	1.3	0.002	2.01	-41.12	0.78	-41.38	1.00	-42.41	2.22	-42.16
209	1.5	0.002	1.98	-40.99	0.75	-41.25	0.97	-42.28	2.19	-42.03
210	1.7	0.002	1.96	-40.86	0.72	-41.12	0.95	-42.15	2.16	-41.90
211	1.8	0.002	1.93	-40.73	0.69	-40.99	0.92	-42.02	2.14	-41.77
212	2.0	0.002	1.91	-40.60	0.66	-40.86	0.89	-41.90	2.11	-41.64
21	4.7	0.002	3.78	41.54	2.55	41.29	2.78	40.26	3.97	40.50
22	4.9	0.002	3.76	41.67	2.52	41.42	2.75	40.39	3.94	40.63
23	5.1	0.002	3.73	41.80	2.49	41.55	2.73	40.52	3.91	40.76
24	5.2	0.002	3.71	41.93	2.46	41.68	2.70	40.65	3.89	40.89
25	17.0	0.002	4.10	37.07	2.73	36.86	3.07	35.74	4.26	36.03
26	17.1	0.002	4.07	37.21	2.71	37.01	3.05	35.89	2.23	36.17
27	17.3	0.002	4.05	37.35	2.68	37.14	3.02	36.02	4.20	36.31
28	17.5	0.002	4.02	37.49	2.65	37.28	2.99	36.16	4.17	36.45
29	17.0	0.002	4.05	37.16	2.89	36.87	3.04	35.86	4.38	36.06
30	16.9	0.002	4.02	37.28	2.86	36.99	3.02	35.97	4.36	36.18
31	16.7	0.002	4.00	37.40	2.84	37.11	2.99	36.10	4.33	36.30
32	16.6	0.002	3.97	37.52	2.81	37.24	2.97	36.22	4.30	36.43
92	18.2	0.002	4.85	5.11	3.64	4.76	3.32	3.84	5.07	3.99
93	198.0	0.002								
94	1.0	0.002	1.28	12.87	0.01	12.61	0.24	11.55	1.49	11.81
95	1.5	0.002	3.07	-0.20	1.99	-0.42	2.17	-1.34	3.26	-1.12

Table 2.4-8: Photo Supporting Data (Continued)

PHOTO		TIME OF EXPOSURE		SPACECRAFT				PRINCIPAL GROUND POINT		SLANT DIST	SUN AZIM	EMISSION ANGLE	PHASE ANGLE	INCIDENCE ANGLE	TILT ANGLE	TILT AZIM	SWING ANGLE	NORTH DEVIATION
SITE NO.	EXP NO.	S/C	GMT	ALT	ALT RT	LAT	LONG	LAT	LONG									
		SECONDS	HR:MIN:SEC	KM	KM/SEC	DEG	DEG	DEG	DEG	KM	DEG	DEG	DEG	DEG	DEG	DEG	DEG	DEG
		ESTIMATED ERROR ± .03		1.1	.001	.01	.006	.01	.006	1.1	.01	.12	.12	.01	.12	.01	.10	.10
		SECONDARY PHOTO SITES (Continued)																
S-10	112		DAY 314 13:17:11.8	42	-0.032	3.36	-12.09	3.36	-12.11	42	91.28	0.7	74.3	74.96	0.7	283.84	92.3	348.5
S-11	137		DAY 315 03:09:15.4	51	-0.101	4.89	-27.57	4.90	-27.63	51	90.94	2.0	81.5	83.47	1.9	283.04	92.1	349.1
S-12	162		DAY 316 00:05:42.7	46	0.058	1.06	-20.05	5.60	-20.05	147	90.92	74.1	80.8	65.41	69.6	0.03	177.5	357.4
S-13	195		DAY 317 00:22:55.7	48	-0.053	3.57	-46.20	3.58	-46.28	48	91.11	3.0	76.3	79.22	2.9	282.06	90.6	348.5
S-15	213		14:16:09.2	48	-0.056	3.57	-53.84	8.11	-52.88	151	91.09	73.5	96.1	78.93	68.8	11.75	179.0	329.0
S-16	214		17:45:15.0	48	-0.040	3.16	-53.71	3.16	-53.80	48	91.13	0.2	77.8	77.95	0.2	291.29	99.7	348.4
S-17	215		21:12:53.5	51	-0.068	3.81	-58.99	7.23	-58.27	119	91.03	66.4	95.5	80.76	62.9	11.79	178.8	334.2
		FARSIDE PHOTO SITES																
S-3	33		DAY 311 02:54:26.4	1453	0.319	-9.93	174.29	-10.1	174.4	1453	273.40	0.3	69.9	70.06	0.2	161.50	158.3	176.8
S-4	34		06:22:53.6	1450	0.320	-9.95	172.3	5.0	173.8	1576	267.97	31.7	69.9	71.15	16.6	5.97	356.4	169.5
S-5	75		DAY 312 10:12:18.0	1466	0.315	-9.73	158.4	-20.7	158.2	1533	277.20	23.4	69.9	70.76	12.4	180.86	182.2	181.2
S-14	196		DAY 317 04:58:05.0	1517	0.293	-8.77	100.7	-8.82	101.0	1517	272.68	0.6	69.9	70.58	0.4	90.17	96.5	177.3

Table 2.4-8: Photo Supporting Data (Continued)

EXP NO.	TELEPHOTO										WIDE ANGLE									
	TILT DIST	SCALE FACTOR	PHOTO CORNER COORDINATES								TILT DIST	SCALE FACTOR	PHOTO CORNER COORDINATES							
			A		B		C		D				A		B		C		D	
			LAT	LONG	LAT	LONG	LAT	LONG	LAT	LONG			LAT	LONG	LAT	LONG	LAT	LONG	LAT	LONG
	MM	$X10^{-3}$	DEG	DEG	DEG	DEG	DEG	DEG	DEG	DEG	MM	$X10^{-3}$	DEG	DEG	DEG	DEG	DEG	DEG	DEG	DEG
	2%	2%									2%	2%								
112	7.2	0.014	3.60	-12.00	3.11	-12.10	3.13	-12.22	3.62	-12.12	0.9	0.002	3.82	-11.53	2.71	-11.75	2.90	-12.69	4.02	-12.47
137	20.5	0.012	5.18	-27.49	4.59	-27.61	4.62	-27.76	5.21	-27.64	2.7	0.002	5.46	-26.93	4.12	-27.19	4.33	-28.34	5.70	-28.08
162	1639.6	0.013									215.0	0.002								
195	30.9	0.013	3.85	-46.15	3.29	-46.26	3.32	-46.40	3.88	-46.29	4.1	0.002	4.10	-45.62	2.86	-45.88	3.05	-46.95	4.34	-46.69
213	1573.8	0.012									206.4	0.002								
214	1.9	0.013	3.42	-53.67	2.87	-53.78	2.90	-53.92	3.45	-53.81	0.3	0.002	3.68	-53.14	2.43	-53.39	2.64	-54.46	3.90	-54.20
215	1193.6	0.012									156.5	0.002								
33	2.4	0.000	-18.73	171.51	-1.25	172.7	-1.49	177.0	-19.0	176.1	0.3	0.000	-31.72	149.26	-15.0	155.5	12.8	-164.0	-34.4	163.0
34	182.2	0.000	-4.09	170.20	19.4	173.2	18.3	178.9	-4.8	174.5	23.9	0.000	-11.5	153.8	*	*	*	*	-16.8	-172.9
75	134.3	0.000	-32.3	155.43	-11.7	155.80	-11.57	160.2	-32.2	161.4	17.6	0.000	*	*	-0.25	140.7	-0.18	174.5	*	*
196	15.4	0.000	-17.8	98.2	0.4	99.1	0.2	103.7	-18.1	103.0	2.0	0.000	-31.8	75.0	17.5	80.5	16.0	124.3	-34.4	125.5

* CORNER OF MOON

2.5 OPERATIONAL PERFORMANCE

Photographic operations pertinent to the evaluation and use of Mission II photography are discussed in this section. Detailed evaluation of the photo subsystem operation during the mission is included as part of Mission II final report, Boeing Document D2-100752-3, Volume III.

2.5.1 MISSION PLANNING

Site locations, together with predicted orbital parameters and photo subsystem operational constraints, provided the basis for establishing the film management and film budget plan shown in Table 2.5-1. Because Mission II followed the nominal plan closely, very few film budget changes were required. The nominal plan was followed exactly until Orbit 90 (Site IIP-11). Sites IIP-11 and -12 were then shifted one orbit later, to Orbits 91 and 94, and Site IIS-13 was moved to Orbit 95, for better target coverage. These changes required some rescheduling of film processing, but presented no operational difficulties. Minor changes in processing times were made to correct for processing rate veriations and to maintain the scheduled readout index. The observed readout index was the final criterion for film management, which was entirely satisfactory throughout the mission.

2.5.2 SPACECRAFT OPERATION AND CONTROL

2.5.2.1 Photo Sequence

All photo command sequences were checked on-line for possible constraint or logic violations. Such factors as V/H sensor operation near the terminator were checked and, if necessary, sequence modifications were recommended. Most sites were taken with a standard sequence, similar to that used for Mission I.

2.5.2.2 Camera-On Time Determination

To obtain an actual exposure as close as possible to the time desired, the stored program command (SPC) camera-on time was calculated as follows:

The exposure time desired was first obtained from Flight Path Analysis and Command FPAC). For single frame, V/H sensor-off photos, this time was entered into the stored program sequence. Due to the nature of the V/H sensor cycle, a half-frame bias was introduced to center the actual exposure times about the desired time, on the average. This bias was one-half the expected frame interval time. Thus, the time programmed for a photo pass was the desired time minus the half-frame bias.

It was not known by the cognizant personnel during Mission II that this particular photo sybsystem had an additional V/H sensor-determined delay between the programmed camera-on pulse, and the time code interrogation and shutter operations. The actual exposure times, therefore, were late by approximately 0.3 $\pm$ 0.1 second. For V/H sensor-off photos, this delay becomes 0.9 second; these photos were late by that amount.

2.5.2.3 Exposure Control

Exposure control began with mission design, and the preparation of a lighting strategy study to determine the effects of illumination on the signal-to-noise ratio for Lunar Orbiter photography. At that time, the nominal mission geometry was used to determine a set of nominal shutter speeds that were used for planning purposes, and as operational inputs prior to on-line determinations.

Vertical Photography

The photo quality prediction computer program (QUAL) was again used, as in Mission I, to assist in determining shutter speeds for all vertical photography. Since this program requires considerable run time, especially when time-shared, an additional option was made available that computes only the predicted spacecraft film densities. This output was available in minutes and provided preliminary determinations of the optimum shutter speed. In the case of secondary sites, the final shutter speed was generally determined from these predicted film densities.

In many cases, a shutter speed yielding densities in the 0.4 to 0.7 range could be selected and no further analysis was required for photography control. In borderline situations, QUAL was run with the cone and slope resolution options for the shutter speeds in question. Shutter speed was then selected for best resolution. A nominal 1-sigma smear value (125 microns/second at 3-degree crab angle) was used for these cases. Albedos determined by the U. S. Geological Survey were used for most sites.

High light transmission of the 80-mm lens, relative to the 610-mm lens, greatly complicated

Table 2.5-1: Film Budget Plan

PHASE: Orbital (SEAL)

Site No.	Orbit No.	Event (Frames)			Total Frames Accumulated			Frame Numbers			Stereo Pairs
		Take	Process	Readout	Readout	Extra In Storage Looper	Bimat Thru Processor	Exposed	Wide-Angle and Time Code Readout	Telephoto Readout	
	51	11	11				2	-7 to +4			
P-1 S-1	52	16 4	19			1	21	5 - 20 21 - 24			
S-2	53	4	2	0.5M	0.5	3	23	25 - 28	5	7p - 6p	A_1
S-2	54	4	2	0.5MG	1.0	5	25	29 - 32	7	9p - 8p	B_1
S-3	55	1	2	0.5G	1.5	4	27	33	9	11p - 10p	C_1 A_2
S-4	56	1	2	0.4GW	1.9	3	29	34	11	13p - 12p	B_2
P-2	57	8	4	0.4W	2.3	7	33	35 - 42	13	14p	D_1 C_2
	58		3	0.9W	3.2	4	36		17	18p	D_2
P-3	59	8	8	0.4M	3.6	4	44	43 - 50	20	21p	
P-3	60	8	8	0.4M	4.0	4	52	51 - 58	28	29p	
P-4	61	8	4	0.4MG	4.4	8	56	59 - 66	36	37p	E_1
P-5	62	8	4	0.4G	4.8	12	60	67 - 74	40	41p	E_2
	63		4	0.7GW	5.5	8	64		44	45p	F_1
S-5	64	1	3	0.7W	6.2	6	67	75	48	49p	F_2
	65		2	0.8W	7.0	4	69		51	52p	G_1
P-6	66	8	2	0.5M	7.5	10	71	76 - 83	53	54p	H_1
P-6	67	8	2	0.5M	8.0	16	73	84 - 91	55	56p	G_2
	68		2	0.9MG	8.9	14	75		57	58p	H_2
S-6	69	1	2	0.7G	9.6	13	77	92	59	60p	I_1
	70		2	0.9GW	10.5	11	79		61	62p	J_1
S-7	71	1	2	0.8W	11.3	10	81	93	63	64p	I_2
	72		2	1W	12.3	8	83		65	66	J_2
S-8	73	1	2	0.8M	13.1	7	85	94	67	68p	K_1

Table 2.5-1: Film Budget Plan (Continued)

PHASE: Orbital (SEAL)

Site No.	Orbit No.	Event (Frames) Take	Process	Readout	Total Frames Accumulated Readout	Extra In Storage Looper	Bimat Thru Processor	Frame Numbers Exposed	Wide-Angle and Time Code Readout	Telephoto Readout	Stereo Pairs
	74	1	2	1M	14.1	5	87		69	70	
S-9	75	8	4	0.9MC	15.0	2	91	95	71	72p	K_2
P-7	76	8	2	0.9G	15.9	8	93	96-103	75	76p	
P-7	77		4	1GW	16.9	12	97	104-111	77	78	M_1
	78	1	4	1W	17.9	8	101		81	82	M_2
S-10	79	8	4	1W	18.9	5	105	112	85	86	N_1
P-8	80	8	8	1M	19.9	5	113	113-120	89	90	N_2
P-8	81	8	4	1M	20.9	9	117	121-128	97	98	O_1
P-8	82	1	4	1MG	21.9	13	121	129-136	101	102	O_2
S-11	83		4	1G	22.9	10	125	137	105	106	P_1
	84	8	5	1GW	23.9	5	130		109	110	P_2
P-9	85	8	4	1W	24.9	9	134	138-145	114	115	Q_1
P-10	86	8	5	1W	25.9	12	139	146-153	118	119	Q_2
P-10	87		4	1M	26.9	16	143	154-161	123	124	R_1
	88	1	4	1M	27.9	12	147		127	128	R_2
S-12	89		4	1MG	28.9	9	151	162	131	132	S_1
	90	8	4	1G	29.9	5	155		135	136	S_2
P-11	91	8	8	1GW	30.9	5	163	163-170	139	140	T_1
P-11	92	8	9	1W	31.9	4	172	171-178	147	148	T_2
P-12	93	8	4	1W	32.9	8	176	179-186	156	157	U_1
P-12	94		4	1M	33.9	12	180	187-194	160	161	U_2
	95	1	3	1M	34.9	9	184		164	165	V_1
S-13	96		3	1MG	35.9	7	186	195	167	168	V_2
S-14	97	1	2	0.9G	36.8	6	188	196	170	171p	W
P-13	98	8	4	1GW	37.8	10	192	197-204	172	173	W^1
P-13	99	8	4	1W	38.8	14	196	205-212	176	177	X^2
S-15	100	1	4	1W	39.8	11	200	213	180	181	X^1_2
S-16	101	1	6	1M	40.8	6	206	214	184	185	
S-17	102	1	3	1M	41.8	4	209	215	190	191	
	103	16	7b	1M		13	216		200	201	
	104		8b	1G		5	224		208	209	
	105		4			0	226				
	105	3				0					

*Notes: (By Orbit Number)

General: Duration of readout is based on giving the second" readout – drive on" command as early as 30 minutes after completing the reverse attitude maneuver following photography, whichever is later.

Although readout is indicated every orbit, such an accomplishment is not committed. Readout will be scrubbed when it interfers with necessary tracking or mission control.

P in "Frame Numbers" "Readout" indicates partial frame.

Initials following numbers in "Event" "Readout" signify the DSIF station in receiving position; G = Goldstone, M = Madrid, W = Woomera.

exposure control. In several cases, satisfactory exposure could not be achieved in both cameras. When this occurred for a multiple-pass site, the shutter speed was changed between orbits to optimize exposure for each camera in at least one orbit. QUAL did not fully reflect this problem in that the 80-mm results had to be discounted slightly.

Table 2.5-2, a tabulation of the appropriate prime site data used in QUAL and selected shutter speeds, also lists the corresponding nominal mission design data and the actual values determined during postmission analysis. Table 2.5-3 lists similar data for the secondary sites.

Oblique Photography

The several oblique secondary sites (IIS-2, -7, -12, -15, and -17) could not be analyzed with QUAL, and the exposure had to be calculated directly from the illumination geometry and the photometric function. The calculation was reduced to a shutter speed nomograph, Figure 2.5-1, which yielded exposure and optimum shutter speed directly. Inputs to the nomographs are albedo, phase angle, and an angle, α, which is the projection of the surface normal into the phase angle plane.

α is measured between the surface normal and the camera axis and represents the tilt of the surface toward or away from the sunline. α is positive for a surface facing away from the Sun. α can be calculated from the formula

$$\alpha = -\tan^{-1} \frac{\cos i}{\cos e \sin g} - \cot g$$

where: i = incidence angle (between surface normal and sunline)
e = emission angle (between surface normal and camera axis)
g = phase angle (between camera axis and sunline)

The above angles and signs correspond to the FPAC photo command program (GCPL) definitions.

For convenience, one nomograph was modified to indicate spacecraft film densities for each shutter speed. Results obtained with the nomograph generally appeared valid when compared to the reassembled pictures available for in-flight analysis.

Average-Density Data

To obtain a quantitative comparison of predicted versus actual film densities, the video engineers were requested, during priority readout, to take a number of average-density readings in the exposed portions of the frames. These measurements consisted of a minimum of six readings in each telephoto and wideangle frame on the GRE film. To compare spacecraft film densities – as obtained from QUAL – with these averages, the densities were converted to GRE film densities using the calibration shown in Figure 2.5-2. Table 2.5-4 gives these comparisons. The averages for the 80-mm system are, in most cases, lower due to the higher transmission of this lens.

By the start of command preparation for Site P-5, enough average-density data had been accumulated to indicate an underexposure trend in the 610-mm photos. The shift amounted to 0.1 and 0.2 density, computed for the spacecraft film, relative to the QUAL predictions. Table 2.5-3 indicates that a shift of this magnitude occurred for most, but not all, prime sites. Before Site P-5, this trend had no operational effect, but P-5 was marginal with a shutter speed between 0-04 and 0.02; 0.04 was finally selected to provide good detail coverage, at the expense of overexposed wide-angle photos. High-resolution coverage was favored because of the nature of the target (Ranger VIII impact area). Similar problems arose for Sites IIP-12 and -13. However, these were two-pass targets and the shutter speed could be changed between passes to provide one orbit each of good telephoto and good wide-angle data.

Postmission QUAL Results

As an estimate of actual photo subsystem performance, QUAL has been run for the actual prime site photo conditions. The results are shown in the following output sheets (Figures 2.5-3 through 2.5-17). The photo geometry was taken from the postmission EVAL run and is tabulated in Table 2.5-2.

Table 2.5-2: Lunar Orbiter Mission II — Prime-Site Parameter Summary

Site No.	Selected Albedo	Phase Angle Degrees			Altitude KM			Shutter Speed		Rad. Dose	Smear Nominal	
	NASA Preferred	Nominal Mission	Predicted	Actual	Nominal Mission	Predicted	Actual	Nominal Mission	Actual	Rads	Rate*	Angle**
IIP-1	0.088	74.5	72.9	72.9	51.2	48.0	47.4	1/25	1/25	1.0	125	60°
IIP-2	0.088	68.4	68.0	67.8	48.3	45.0	44.6	1/50	1/50	1.0	125	60°
IIP-3a	0.084	76.3	75.6	75.6	50.5	48.0	47.5	1/25	1/25	1.0	125	60°
IIP-3b	0.084	76.3	74.4	74.4	50.5	46.3	45.7	1/25	1/25	1.0	125	60°
IIP-4	0.111	78.6	77.7	77.7	52.3	50.5	49.2	1/25	1/25	1.0	125	60°
IIP-5	0.086	68.8	68.8	69.1	46.7	43.6	42.9	1/50	1/25	1.0	125	60°
IIP-6a	0.087	61.0	62.6	62.6	50.9	48.5	47.0	1/50	1/50	1.0	125	60°
IIP-6b	0.087	61.0	61.1	61.1	50.9	50.9	49.1	1/50	1/50	1.0	125	60°
IIP-7a	0.098	69.7	70.1	70.2	44.2	42.2	41.0	1/50	1/50	1.25	125	60°
IIP-7b	0.098	69.7	68.4	68.7	44.2	42.8	41.6	1/50	1/50	1.25	125	60°
IIP-8a	0.092	60.8	63.1	63.1	51.2	47.2	47.0	1/50	1/50	1.25	125	60°
IIP-8b	0.092	60.8	61.7	61.7	51.2	50.5	49.6	1/50	1/50	1.25	125	60°
IIP-8c	0.092	60.8	60.2	60.2	51.2	53.3	52.6	1/50	1/50	1.25	125	60°
IIP-9	0.093	65.8	66.1	66.1	46.8	45.1	44.7	1/50	1/50	1.25	125	60°
IIP-10a	0.091	77.8	76.9	76.9	48.3	44.8	44.4	1/25	1/25	1.25	125	60°
IIP-10b	0.091	77.8	75.5	75.5	48.3	43.8	43.4	1/25	1/25	1.25	125	60°
IIP-11a	0.105	62.1	62.9	62.9	52.5	51.0	52.0	1/50	1/50	1.25	125	60°
IIP-11b	0.105	62.1	61.5	61.5	52.5	54.1	55.4	1/50	1/50	1.25	125	60°
IIP-12a	0.087	74.1	72.9	72.8	47.6	43.6	44.2	1/25	1/25	1.25	125	60°
IIP-12b	0.087	74.1	71.4	71.4	47.6	43.9	44.9	1/25	1/50	1.25	125	60°
IIP-13a	0.073	71.1	71.8	71.8	49.2	45.7	45.3	1/25	1/25	1.25	125	60°
IIP-13b	0.073	71.1	70.4	70.4	49.2	46.5	46.4	1/25	1/50	1.25	125	60°

* Microns / Sec.
** This angle is QUAL Input angle and represents smear 30 degrees off flight direction.

Table 2.5-3: Secondary-Site Parameter Summary

Site	Selected Albedo	Phase Angle		Altitude		Slant Range	α	Shutter Speed
		Predicted	Actual	Predicted	Actual			
IIS-1	0.096	72.9	72.9	46.3	45.9	46.0	−4°	1/25
IIS-2a	0.088	81.1	81.1	47.1	46.5	47.6	−9°	1/25
IIS-2b		62.2	62.1	46.0	45.6	46.6	+8.1°	1/50
IIS-3	0.120	69.9	69.9	1451	1453	1453	~ 0°	1/50
IIS-4	0.120	69.9	69.9	1451	1450	1576	~ 0°	1/50
IIS-5	0.120	69.9	69.9	1466	1466	1534	−1°	1/50
IIS-6	0.137	78.7	78.6	44.1	43.9	45.0	−5.1°	1/50
IIS-7	0.092	76.1	76.1	44.9	44.2	129.1	−31°	1/50
IIS-8	0.139	61.8	61.8	49.1	47.7	47.7	~ 0°	1/100
IIS-9	0.105	69.6	69.6	41.9	41.3	41.3	~ 0°	1/50
IIS-10.2	0.092	74.7	74.3	42.0	42.3	42.3	~ 0°	1/50
IIS-11	0.105	81.5	81.5	51.0	51.2	51.3	~ 0°	1/25
IIS-12	0.120	80.8	80.8	45.7	45.7	146.8	−53.5°	1/100
IIS-13	0.074	76.8	76.3	45.6	47.9	47.9	~ 0°	1/25
IIS-14	0.120	70.0	69.9	1511	1496	1497	~ 0°	1/50
IIS-15	0.070	96.1	96.0	49.8	48.8	150.8	−36.7°	1/25
IIS-16	0.072	77.8	77.8	48.3	47.6	47.6	~ 0°	1/25
IIS-17	0.100	95.4	95.5	52.0	50.9	119.0	−26.4	1/25

2.5.2.4 Photo Time Correlation

The following procedure was adopted to obtain correct GMTs for each photo frame.

1) After completion of readout and processing of the GRE film, the video engineer read the recorded time code and reported it to the photo data analyst as part of his preliminary analysis.
2) The photo data analyst then converted the binary number represented by the time code to decimal clock time using conversion tables.
3) The decimal clock was furnished to the programmer analyst as the imput for a TIML computer run. The TIML program makes the necessary corrections to obtain true GMT. As modified for Mission II, the TIML output lists the input clock time, the corresponding GMT, and actuation time of the two shutters.
4) After obtaining the GMT, the photo data analyst entered it on the photo identification form. The completed form was then mailed to Eastman Kodak in time to be available prior to the arrival of the GRE film from the DSSs. The times were subsequently checked against the scheduled camera-on times by the photo acquisition specialist.

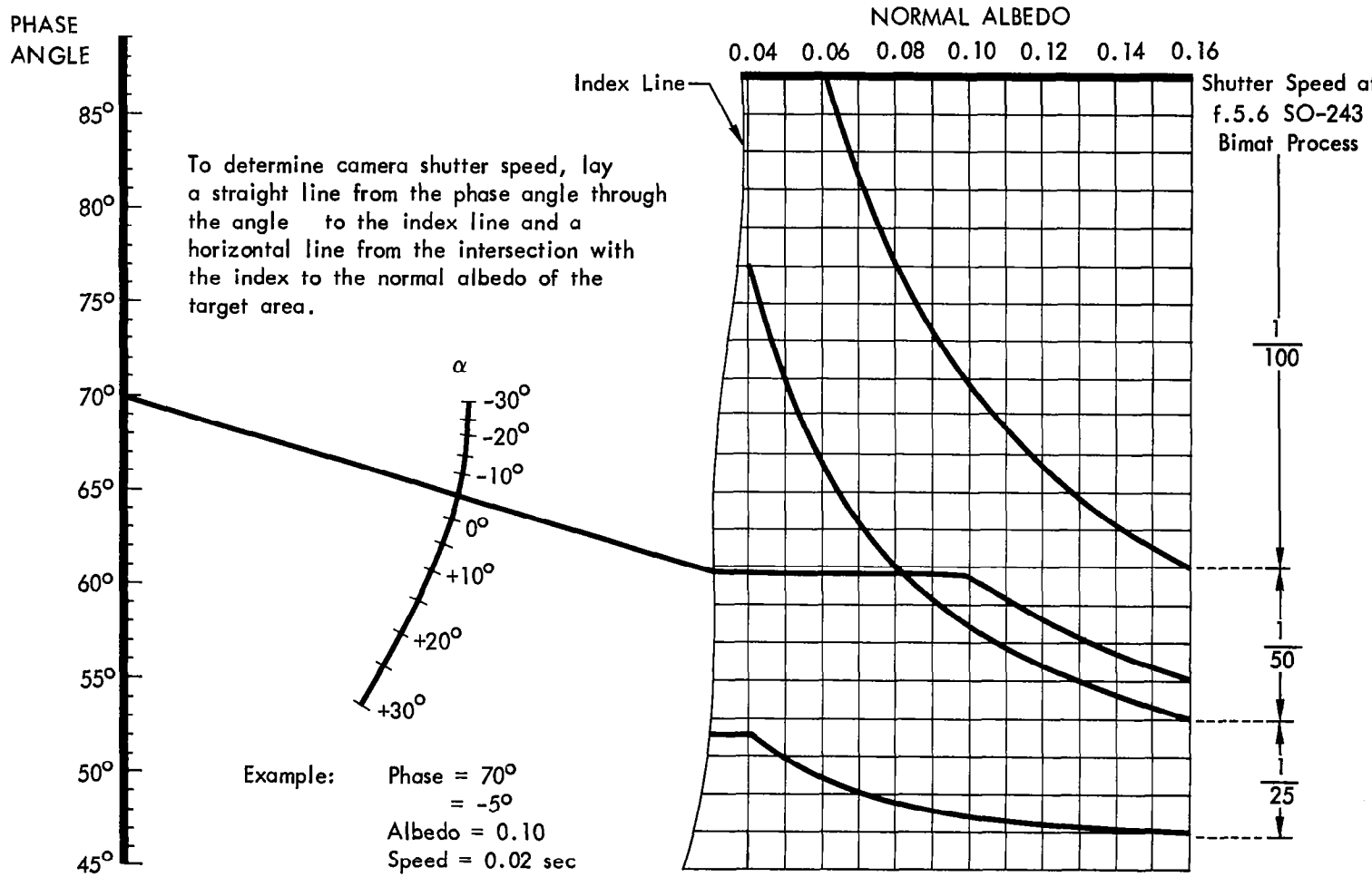

Figure 2.5-1: Shutter Speed Nomogram

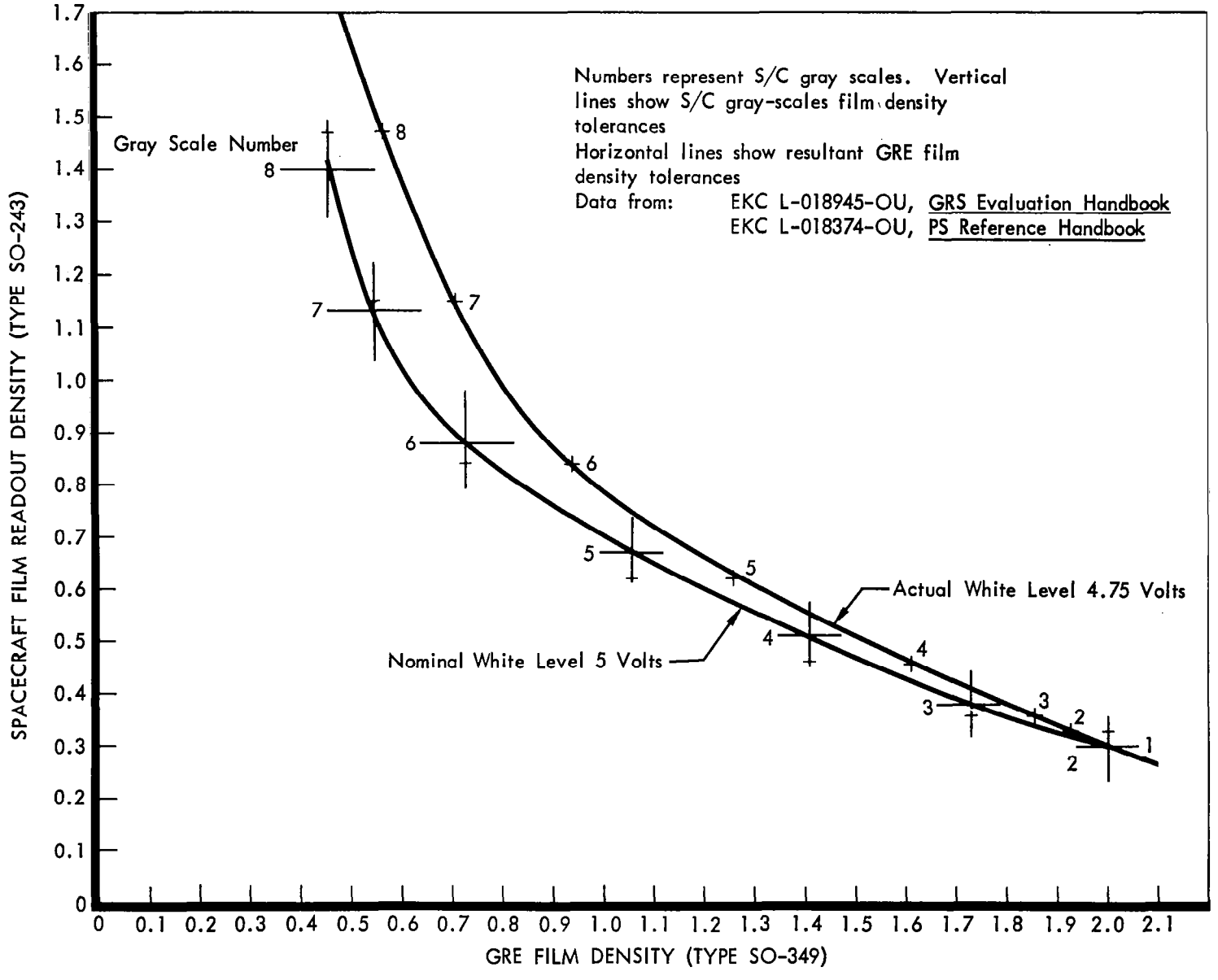

Figure 2.5-2: Spacecraft Film Density vs. GRE Film Density

Table 2.5-4: GRE Film Density				
SITE	WIDE ANGLE (80-mm)		TELEPHOTO (610-mm)	
	Average	QUAL	Average	QUAL
P-1	0.87	0.85	1.47	1.12
P-1	0.87	0.85	1.47	1.12
P-2	0.76	1.13 1.41	1.59	1.49 1.73
P-3a	0.96	0.98	1.49	1.33
P-4	0.84	0.88	1.41	1.18
P-5	0.58	0.83 0.72	1.01	1.08 0.90
P-6a	0.74	0.87	1.48	1.17
P-7b	0.63	1.04	1.44	1.39
P-8a	0.57	0.90	1.23	1.22
P-8b	0.51	0.85	0.94	1.13
P-8c	0.52	0.81	1.16	1.07
P-11a	0.48	1.01 0.81	1.02	1.37 1.07
P-11b	0.53	0.93 0.77	1.07	1.26 0.98
P-11a	0.63	0.80	1.17	1.05

2.5.3 RECONSTRUCTION OPERATIONS

Reconstruction of the photographs was carried out by the same method used for Mission I and described in the final report, Volume II, Paragraph 2.5.5. The following discussion concerns operations specific to Mission II.

2.5.3.1 Use of White Level as Reference

The video gain optimization procedure is predicated upon proper exposure of edge data and upon proper spacecraft processing. Eastman Kodak documents specify a background density of 0.30. This spacecraft film density, which corresponds to a video white level signal of 5.0 volts, should result in a GRE film density of 2.0. The optimization procedure used during the first part of the mission was based upon proper exposure and processing of edge data. Optimum video gain in the spacecraft causes the GRE signal to just clip. As the spacecraft's clip level is set at 5.2 volts, and the peak to peak variation of the "W" pattern (Refer to Paragraph 2.5.3.3) is 0.15 volt, the average of the white level signal was felt to be 5.00 volts.

Based upon the edge data step table readings through Readout Sequence 025, Operations Directive B-34, issued on November 23, 1966, required changing the optimum white level voltage from 5.0 to 4.75, as the edge data was improperly exposed to a density of 0.33. The effect on the GRE film for the various steps is tabulated in Table 2.5-5.

Use of the new optimization started with Readout Sequence 043. Achievement of optimum gain was the responsibility of video engineers at the Deep Space Station. The optimization voltage is based upon static scanning (dynamic scanning could produce a somewhat different voltage because the film may or may not be clamped) and upon proper exposure and processing in the focus stop area of the film. If these are not achieved, the "white level" voltage is uncertain.

Starting with Readout Sequence 087, data was obtained to permit correlation of white-level voltage variation and gray-scale variation in areas of the spacecraft film near processing variations. These data are plotted in Figures 2.5-18 through 2.5-21. Attention is drawn to the considerable variation in white level between the Bimat pull-off and the processor stop line and to the fact that the gray scale densities appear to track the white level variations very well. During Mission I, when the white level voltage was held suspect in areas near processing stoplines, the magnitude of white level variance was not so apparent. Based upon the data gathered toward the end of Mission II, it has been decided to collect and plot data on white level variation and three gray scale density readings at the beginning and at the end of each readout, at the edges of moderate-resolution frames, and at 10- and 20-minute intervals following the trailing edge of the moderate-resolution frames.

Table 2.5-5: Edge Data Densities - GRE Film		
Step	R/O Densities S/C Film	Predicted GRE Densities (Exclusive of Kine Flare)
1	0.30	2.00
2	0.33	1.92
3	0.36	1.85
4	0.46	1.61
5	0.62	1.26
6	0.84	0.94
7	1.15	0.71
8	1.47	0.57
9	1.78	0.50

Figure 2.5-3: Photo Quality Predict Program (QUAL) Output, Site IIP-1

```
ORBIT NUMBER   0      SITE NUMBER  1      FLIGHT NUMBER  2      TIME 000/00/00/00      RUN NUMBER 00000000

                      LUNAR LONGITUDE= 999.99        LUNAR LATITUDE= 999.99

INITIAL CONDITIONS --- ALBEDO= 0.088      PHASE ANGLE= 72.9 DEGREES      ALTITUDE=  47.4 KILOMETERS

                      RADIATION=  1.0 RADS    SMEAR RATE=   125. MICRONS/SEC    SMEAR ANGLE=  60.0 DEGREES

PREDICTED S/C FILM DENSITY FOR 24 INCH CAMERA AT ALL SHUTTER SPEEDS - SLOW= 0.76  MEDIUM= 0.40  FAST= 0.27

PREDICTED S/C FILM DENSITY FOR  3 INCH CAMERA AT ALL SHUTTER SPEEDS - SLOW= 1.00  MEDIUM= 0.54  FAST= 0.31

                              * * * * * OPTIONS AND RESULTS * * * * *

  SLOW SHUTTER SPEED       SLOPE TARGET       GRE OUTPUT POINT      24 INCH LENS
        ITERATION NUMBER= 0            SLOPE=  1.00 DEGREES      SIGNAL-TO-NOISE RATIO=  7.57
        ITERATION NUMBER= 1            SLOPE=  0.13 DEGREES

  SLOW SHUTTER SPEED       CONE TARGET        GRE OUTPUT POINT      24 INCH LENS
        ITERATION NUMBER= 1         DIAMETER=  1.29 METERS       SIGNAL-TO-NOISE RATIO=  6.24
        ITERATION NUMBER= 2         DIAMETER=  0.89 METERS       SIGNAL-TO-NOISE RATIO=  2.96
        ITERATION NUMBER= 3         DIAMETER=  0.90 METERS

  SLOW SHUTTER SPEED       SLOPE TARGET       GRE OUTPUT POINT      80 MM   LENS
        ITERATION NUMBER= 0            SLOPE=  1.00 DEGREES      SIGNAL-TO-NOISE RATIO=  0.58
        ITERATION NUMBER= 1            SLOPE=  1.66 DEGREES

  SLOW SHUTTER SPEED       CONE TARGET        GRE OUTPUT POINT      80 MM   LENS
        ITERATION NUMBER= 1         DIAMETER= 12.17 METERS       SIGNAL-TO-NOISE RATIO= 18.60
        ITERATION NUMBER= 2         DIAMETER=  4.89 METERS       SIGNAL-TO-NOISE RATIO=  2.27
        ITERATION NUMBER= 3         DIAMETER=  5.63 METERS       SIGNAL-TO-NOISE RATIO=  3.29
        ITERATION NUMBER= 4         DIAMETER=  5.37 METERS
```

Figure 2.5-4: Photo Quality Predict Program (QUAL) Output, Site IIP-2

```
ORBIT NUMBER   0      SITE NUMBER  2      FLIGHT NUMBER  2      TIME 000/00/00/00      RUN NUMBER 00000000

                      LUNAR LONGITUDE= 999.99        LUNAR LATITUDE= 999.99

INITIAL CONDITIONS --- ALBEDO= 0.088      PHASE ANGLE= 67.8 DEGREES      ALTITUDE=  44.6 KILOMETERS

                      RADIATION=  1.0 RADS    SMEAR RATE=   125. MICRONS/SEC    SMEAR ANGLE=  60.0 DEGREES

PREDICTED S/C FILM DENSITY FOR 24 INCH CAMERA AT ALL SHUTTER SPEEDS - SLOW= 0.95  MEDIUM= 0.52  FAST= 0.30

PREDICTED S/C FILM DENSITY FOR  3 INCH CAMERA AT ALL SHUTTER SPEEDS - SLOW= 1.20  MEDIUM= 0.71  FAST= 0.38

                              * * * * * OPTIONS AND RESULTS * * * * *

  MEDIUM SHUTTER SPEED     SLOPE TARGET       GRE OUTPUT POINT      24 INCH LENS
        ITERATION NUMBER= 0            SLOPE=  1.00 DEGREES      SIGNAL-TO-NOISE RATIO=  4.11
        ITERATION NUMBER= 1            SLOPE=  0.24 DEGREES

  MEDIUM SHUTTER SPEED     CONE TARGET        GRE OUTPUT POINT      24 INCH LENS
        ITERATION NUMBER= 1         DIAMETER=  1.11 METERS       SIGNAL-TO-NOISE RATIO=  3.98
        ITERATION NUMBER= 2         DIAMETER=  0.96 METERS       SIGNAL-TO-NOISE RATIO=  3.03
        ITERATION NUMBER= 3         DIAMETER=  0.96 METERS

  MEDIUM SHUTTER SPEED     SLOPE TARGET       GRE OUTPUT POINT      80 MM   LENS
        ITERATION NUMBER= 0            SLOPE=  1.00 DEGREES      SIGNAL-TO-NOISE RATIO=  0.45
        ITERATION NUMBER= 1            SLOPE=  2.13 DEGREES

  MEDIUM SHUTTER SPEED     CONE TARGET        GRE OUTPUT POINT      80 MM   LENS
        ITERATION NUMBER= 1         DIAMETER=  8.41 METERS       SIGNAL-TO-NOISE RATIO=  7.72
        ITERATION NUMBER= 2         DIAMETER=  5.24 METERS       SIGNAL-TO-NOISE RATIO=  2.72
        ITERATION NUMBER= 3         DIAMETER=  5.51 METERS
```

Figure 2.5-5: Photo Quality Predict Program (QUAL) Output, Site IIP-3

```
ORBIT NUMBER  0     SITE NUMBER  3     FLIGHT NUMBER  2     TIME 000/00/00/00     RUN NUMBER 00000000

                    LUNAR LONGITUDE= 999.99     LUNAR LATITUDE= 999.99

INITIAL CONDITIONS --- ALBEDO= 0.084     PHASE ANGLE= 75.6 DEGREES     ALTITUDE=  47.5 KILOMETERS

                    RADIATION=  1.0 RADS     SMEAR RATE=  125. MICRONS/SEC     SMEAR ANGLE=  60.0 DEGREES

PREDICTED S/C FILM DENSITY FOR 24 INCH CAMERA AT ALL SHUTTER SPEEDS - SLOW= 0.59  MEDIUM= 0.33  FAST= 0.25

PREDICTED S/C FILM DENSITY FOR  3 INCH CAMERA AT ALL SHUTTER SPEEDS - SLOW= 0.80  MEDIUM= 0.43  FAST= 0.28

                    * * * * * OPTIONS AND RESULTS * * * * *

  SLOW SHUTTER SPEED      SLOPE TARGET      GRE OUTPUT POINT     24 INCH LENS
       ITERATION NUMBER= 0          SLOPE=  1.00 DEGREES      SIGNAL-TO-NOISE RATIO=  8.82
       ITERATION NUMBER= 1          SLOPE=  0.11 DEGREES

  SLOW SHUTTER SPEED       CONE TARGET      GRE OUTPUT POINT     24 INCH LENS
       ITERATION NUMBER= 1       DIAMETER=  1.31 METERS      SIGNAL-TO-NOISE RATIO=  8.38
       ITERATION NUMBER= 2       DIAMETER=  0.78 METERS      SIGNAL-TO-NOISE RATIO=  2.98
       ITERATION NUMBER= 3       DIAMETER=  0.79 METERS

  SLOW SHUTTER SPEED      SLOPE TARGET      GRE OUTPUT POINT     80 MM  LENS
       ITERATION NUMBER= 0          SLOPE=  1.00 DEGREES      SIGNAL-TO-NOISE RATIO=  0.66
       ITERATION NUMBER= 1          SLOPE=  1.42 DEGREES

  SLOW SHUTTER SPEED       CONE TARGET      GRE OUTPUT POINT     80 MM  LENS
       ITERATION NUMBER= 1       DIAMETER=  9.99 METERS      SIGNAL-TO-NOISE RATIO= 15.67
       ITERATION NUMBER= 2       DIAMETER=  4.37 METERS      SIGNAL-TO-NOISE RATIO=  2.30
       ITERATION NUMBER= 3       DIAMETER=  4.99 METERS      SIGNAL-TO-NOISE RATIO=  3.26
       ITERATION NUMBER= 4       DIAMETER=  4.79 METERS
```

Figure 2.5-6: Photo Quality Predict Program (QUAL) Output, Site IIP-4

```
ORBIT NUMBER  0     SITE NUMBER  4     FLIGHT NUMBER  2     TIME 000/00/00/00     RUN NUMBER 00000000

                    LUNAR LONGITUDE= 999.99     LUNAR LATITUDE= 999.99

INITIAL CONDITIONS --- ALBEDO= 0.111     PHASE ANGLE= 77.7 DEGREES     ALTITUDE=  49.2 KILOMETERS

                    RADIATION=  1.0 RADS     SMEAR RATE=  125. MICRONS/SEC     SMEAR ANGLE=  60.0 DEGREES

PREDICTED S/C FILM DENSITY FOR 24 INCH CAMERA AT ALL SHUTTER SPEEDS - SLOW= 0.65  MEDIUM= 0.36  FAST= 0.26

PREDICTED S/C FILM DENSITY FOR  3 INCH CAMERA AT ALL SHUTTER SPEEDS - SLOW= 0.87  MEDIUM= 0.46  FAST= 0.29

                    * * * * * OPTIONS AND RESULTS * * * * *

  SLOW SHUTTER SPEED      SLOPE TARGET      GRE OUTPUT POINT     24 INCH LENS
       ITERATION NUMBER= 0          SLOPE=  1.00 DEGREES      SIGNAL-TO-NOISE RATIO=  9.04
       ITERATION NUMBER= 1          SLOPE=  0.10 DEGREES

  SLOW SHUTTER SPEED       CONE TARGET      GRE OUTPUT POINT     24 INCH LENS
       ITERATION NUMBER= 1       DIAMETER=  1.35 METERS      SIGNAL-TO-NOISE RATIO= 10.34
       ITERATION NUMBER= 2       DIAMETER=  0.73 METERS      SIGNAL-TO-NOISE RATIO=  2.95
       ITERATION NUMBER= 3       DIAMETER=  0.74 METERS

  SLOW SHUTTER SPEED      SLOPE TARGET      GRE OUTPUT POINT     80 MM  LENS
       ITERATION NUMBER= 0          SLOPE=  1.00 DEGREES      SIGNAL-TO-NOISE RATIO=  0.64
       ITERATION NUMBER= 1          SLOPE=  1.35 DEGREES

  SLOW SHUTTER SPEED       CONE TARGET      GRE OUTPUT POINT     80 MM  LENS
       ITERATION NUMBER= 1       DIAMETER= 11.15 METERS      SIGNAL-TO-NOISE RATIO= 20.73
       ITERATION NUMBER= 2       DIAMETER=  4.24 METERS      SIGNAL-TO-NOISE RATIO=  2.24
       ITERATION NUMBER= 3       DIAMETER=  4.91 METERS      SIGNAL-TO-NOISE RATIO=  3.31
       ITERATION NUMBER= 4       DIAMETER=  4.67 METERS
```

Figure 2.5-7: Photo Quality Predict Program (QUAL) Output, Site IIP-5

```
ORBIT NUMBER  0      SITE NUMBER  5      FLIGHT NUMBER  2      TIME 000/00/00/00      RUN NUMBER 00000000

                    LUNAR LONGITUDE= 999.99        LUNAR LATITUDE= 999.99

INITIAL CONDITIONS --- ALBEDO= 0.086      PHASE ANGLE= 69.1 DEGREES      ALTITUDE=   42.9 KILOMETERS

                    RADIATION=  1.0 RADS    SMEAR RATE=   125. MICRONS/SEC    SMEAR ANGLE=  60.0 DEGREES

PREDICTED S/C FILM DENSITY FOR 24 INCH CAMERA AT ALL SHUTTER SPEEDS - SLOW= 0.90  MEDIUM= 0.48  FAST= 0.29

PREDICTED S/C FILM DENSITY FOR  3 INCH CAMERA AT ALL SHUTTER SPEEDS - SLOW= 1.14  MEDIUM= 0.66  FAST= 0.36

                          * * * * * OPTIONS AND RESULTS * * * * *

  SLOW SHUTTER SPEED      SLOPE TARGET      GRE OUTPUT POINT      24 INCH LENS
        ITERATION NUMBER= 0          SLOPE=  1.00 DEGREES     SIGNAL-TO-NOISE RATIO=  5.12
        ITERATION NUMBER= 1          SLOPE=  0.19 DEGREES

  SLOW SHUTTER SPEED       CONE TARGET      GRE OUTPUT POINT      24 INCH LENS
        ITERATION NUMBER= 1        DIAMETER=  1.31 METERS       SIGNAL-TO-NOISE RATIO=  6.28
        ITERATION NUMBER= 2        DIAMETER=  0.91 METERS       SIGNAL-TO-NOISE RATIO=  2.99
        ITERATION NUMBER= 3        DIAMETER=  0.91 METERS

  SLOW SHUTTER SPEED      SLOPE TARGET      GRE OUTPUT POINT      80 MM   LENS
        ITERATION NUMBER= 0          SLOPE=  1.00 DEGREES     SIGNAL-TO-NOISE RATIO=  0.40
        ITERATION NUMBER= 1          SLOPE=  2.38 DEGREES

  SLOW SHUTTER SPEED       CONE TARGET      GRE OUTPUT POINT      80 MM   LENS
        ITERATION NUMBER= 1        DIAMETER= 12.83 METERS       SIGNAL-TO-NOISE RATIO= 15.19
        ITERATION NUMBER= 2        DIAMETER=  5.70 METERS       SIGNAL-TO-NOISE RATIO=  2.57
        ITERATION NUMBER= 3        DIAMETER=  6.16 METERS
```

Figure 2.5-8: Photo Quality Predict Program (QUAL) Output, Site IIP-6

```
ORBIT NUMBER  0      SITE NUMBER  6      FLIGHT NUMBER  2      TIME 000/00/00/00      RUN NUMBER 00000000

                    LUNAR LONGITUDE= 999.99        LUNAR LATITUDE= 999.99

INITIAL CONDITIONS --- ALBEDO= 0.087      PHASE ANGLE= 62.6 DEGREES      ALTITUDE=   47.0 KILOMETERS

                    RADIATION=  1.0 RADS    SMEAR RATE=   125. MICRONS/SEC    SMEAR ANGLE=  60.0 DEGREES

PREDICTED S/C FILM DENSITY FOR 24 INCH CAMERA AT ALL SHUTTER SPEEDS - SLOW= 1.12  MEDIUM= 0.63  FAST= 0.35

PREDICTED S/C FILM DENSITY FOR  3 INCH CAMERA AT ALL SHUTTER SPEEDS - SLOW= 1.36  MEDIUM= 0.85  FAST= 0.45

                          * * * * * OPTIONS AND RESULTS * * * * *

MEDIUM SHUTTER SPEED      SLOPE TARGET      GRE OUTPUT POINT      24 INCH LENS
        ITERATION NUMBER= 0          SLOPE=  1.00 DEGREES     SIGNAL-TO-NOISE RATIO=  3.81
        ITERATION NUMBER= 1          SLOPE=  0.26 DEGREES

MEDIUM SHUTTER SPEED       CONE TARGET      GRE OUTPUT POINT      24 INCH LENS
        ITERATION NUMBER= 1        DIAMETER=  1.17 METERS       SIGNAL-TO-NOISE RATIO=  3.20
        ITERATION NUMBER= 2        DIAMETER=  1.13 METERS

MEDIUM SHUTTER SPEED      SLOPE TARGET      GRE OUTPUT POINT      80 MM   LENS
        ITERATION NUMBER= 0          SLOPE=  1.00 DEGREES     SIGNAL-TO-NOISE RATIO=  0.29
        ITERATION NUMBER= 1          SLOPE=  3.20 DEGREES

MEDIUM SHUTTER SPEED       CONE TARGET      GRE OUTPUT POINT      80 MM   LENS
        ITERATION NUMBER= 1        DIAMETER=  9.47 METERS       SIGNAL-TO-NOISE RATIO=  6.58
        ITERATION NUMBER= 2        DIAMETER=  6.39 METERS       SIGNAL-TO-NOISE RATIO=  2.78
        ITERATION NUMBER= 3        DIAMETER=  6.64 METERS
```

Figure 2.5-9: Photo Quality Predict Program (QUAL) Output, Site IIP-7

```
ORBIT NUMBER   0      SITE NUMBER  7      FLIGHT NUMBER  2      TIME 000/00/00/00      RUN NUMBER 00000000

                      LUNAR LONGITUDE= 999.99       LUNAR LATITUDE= 999.99

INITIAL CONDITIONS --- ALBEDO= 0.098      PHASE ANGLE= 70.2 DEGREES      ALTITUDE=   41.0 KILOMETERS

                      RADIATION=  1.2 RADS    SMEAR RATE=   125. MICRONS/SEC    SMEAR ANGLE=  60.0 DEGREES

PREDICTED S/C FILM DENSITY FOR 24 INCH CAMERA AT ALL SHUTTER SPEEDS - SLOW= 0.95  MEDIUM= 0.51  FAST= 0.30

PREDICTED S/C FILM DENSITY FOR  3 INCH CAMERA AT ALL SHUTTER SPEEDS - SLOW= 1.20  MEDIUM= 0.71  FAST= 0.38

                                * * * * * OPTIONS AND RESULTS * * * * *

MEDIUM SHUTTER SPEED       SLOPE TARGET       GRE OUTPUT POINT      24 INCH LENS
        ITERATION NUMBER= 0           SLOPE=  1.00 DEGREES      SIGNAL-TO-NOISE RATIO=  5.45
        ITERATION NUMBER= 1           SLOPE=  0.18 DEGREES

MEDIUM SHUTTER SPEED        CONE TARGET       GRE OUTPUT POINT      24 INCH LENS
        ITERATION NUMBER= 1        DIAMETER=  1.02 METERS       SIGNAL-TO-NOISE RATIO=  4.51
        ITERATION NUMBER= 2        DIAMETER=  0.83 METERS       SIGNAL-TO-NOISE RATIO=  3.03
        ITERATION NUMBER= 3        DIAMETER=  0.83 METERS

MEDIUM SHUTTER SPEED       SLOPE TARGET       GRE OUTPUT POINT      80 MM  LENS
        ITERATION NUMBER= 0           SLOPE=  1.00 DEGREES      SIGNAL-TO-NOISE RATIO=  0.62
        ITERATION NUMBER= 1           SLOPE=  1.56 DEGREES

MEDIUM SHUTTER SPEED        CONE TARGET       GRE OUTPUT POINT      80 MM  LENS
        ITERATION NUMBER= 1        DIAMETER=  7.74 METERS       SIGNAL-TO-NOISE RATIO=  8.84
        ITERATION NUMBER= 2        DIAMETER=  4.51 METERS       SIGNAL-TO-NOISE RATIO=  2.66
        ITERATION NUMBER= 3        DIAMETER=  4.79 METERS
```

Figure 2.5-10: Photo Quality Predict Program (QUAL) Output, Site IIP-8

```
ORBIT NUMBER   0      SITE NUMBER  8      FLIGHT NUMBER  2      TIME 000/00/00/00      RUN NUMBER 00000000

                      LUNAR LONGITUDE= 999.99       LUNAR LATITUDE= 999.99

INITIAL CONDITIONS --- ALBEDO= 0.092      PHASE ANGLE= 61.7 DEGREES      ALTITUDE=   49.6 KILOMETERS

                      RADIATION=  1.2 RADS    SMEAR RATE=   125. MICRONS/SEC    SMEAR ANGLE=  60.0 DEGREES

PREDICTED S/C FILM DENSITY FOR 24 INCH CAMERA AT ALL SHUTTER SPEEDS - SLOW= 1.18  MEDIUM= 0.70  FAST= 0.38

PREDICTED S/C FILM DENSITY FOR  3 INCH CAMERA AT ALL SHUTTER SPEEDS - SLOW= 1.43  MEDIUM= 0.92  FAST= 0.49

                                * * * * * OPTIONS AND RESULTS * * * * *

MEDIUM SHUTTER SPEED       SLOPE TARGET       GRE OUTPUT POINT      24 INCH LENS
        ITERATION NUMBER= 0           SLOPE=  1.00 DEGREES      SIGNAL-TO-NOISE RATIO=  3.30
        ITERATION NUMBER= 1           SLOPE=  0.30 DEGREES

MEDIUM SHUTTER SPEED        CONE TARGET       GRE OUTPUT POINT      24 INCH LENS
        ITERATION NUMBER= 1        DIAMETER=  1.23 METERS       SIGNAL-TO-NOISE RATIO=  3.02
        ITERATION NUMBER= 2        DIAMETER=  1.23 METERS

MEDIUM SHUTTER SPEED       SLOPE TARGET       GRE OUTPUT POINT      80 MM  LENS
        ITERATION NUMBER= 0           SLOPE=  1.00 DEGREES      SIGNAL-TO-NOISE RATIO=  0.24
        ITERATION NUMBER= 1           SLOPE=  3.81 DEGREES

MEDIUM SHUTTER SPEED        CONE TARGET       GRE OUTPUT POINT      80 MM  LENS
        ITERATION NUMBER= 1        DIAMETER= 10.83 METERS       SIGNAL-TO-NOISE RATIO=  6.96
        ITERATION NUMBER= 2        DIAMETER=  7.11 METERS       SIGNAL-TO-NOISE RATIO=  2.79
        ITERATION NUMBER= 3        DIAMETER=  7.36 METERS
```

Figure 2.5-11: Photo Quality Predict Program (QUAL) Output, Site IIP-9

```
ORBIT NUMBER   0      SITE NUMBER  9      FLIGHT NUMBER  2      TIME 000/00/00/00      RUN NUMBER 00000000

                      LUNAR LONGITUDE= 999.99       LUNAR LATITUDE= 999.99

INITIAL CONDITIONS --- ALBEDO= 0.093      PHASE ANGLE= 66.1 DEGREES      ALTITUDE=   44.7 KILOMETERS

                      RADIATION=  1.2 RADS    SMEAR RATE=   125. MICRONS/SEC    SMEAR ANGLE=  60.0 DEGREES

PREDICTED S/C FILM DENSITY FOR 24 INCH CAMERA AT ALL SHUTTER SPEEDS - SLOW= 1.05  MEDIUM= 0.58  FAST= 0.33

PREDICTED S/C FILM DENSITY FOR  3 INCH CAMERA AT ALL SHUTTER SPEEDS - SLOW= 1.29  MEDIUM= 0.78  FAST= 0.42

                              * * * * * OPTIONS AND RESULTS * * * * *

MEDIUM SHUTTER SPEED       SLOPE TARGET       GRE OUTPUT POINT       24 INCH LENS
        ITERATION NUMBER= 0           SLOPE=  1.00 DEGREES       SIGNAL-TO-NOISE RATIO=  3.68
        ITERATION NUMBER= 1           SLOPE=  0.27 DEGREES

MEDIUM SHUTTER SPEED        CONE TARGET       GRE OUTPUT POINT       24 INCH LENS
        ITERATION NUMBER= 1         DIAMETER=  1.11 METERS         SIGNAL-TO-NOISE RATIO=  3.81
        ITERATION NUMBER= 2         DIAMETER=  0.99 METERS         SIGNAL-TO-NOISE RATIO=  3.02
        ITERATION NUMBER= 3         DIAMETER=  0.98 METERS

MEDIUM SHUTTER SPEED       SLOPE TARGET       GRE OUTPUT POINT       80 MM   LENS
        ITERATION NUMBER= 0           SLOPE=  1.00 DEGREES       SIGNAL-TO-NOISE RATIO=  0.37
        ITERATION NUMBER= 1           SLOPE=  2.56 DEGREES

MEDIUM SHUTTER SPEED        CONE TARGET       GRE OUTPUT POINT       80 MM   LENS
        ITERATION NUMBER= 1         DIAMETER=  8.39 METERS         SIGNAL-TO-NOISE RATIO=  6.69
        ITERATION NUMBER= 2         DIAMETER=  5.62 METERS         SIGNAL-TO-NOISE RATIO=  2.74
        ITERATION NUMBER= 3         DIAMETER=  5.88 METERS
```

Figure 2.5-12: Photo Quality Predict Program (QUAL) Output, Site IIP-10

```
ORBIT NUMBER   0      SITE NUMBER 10      FLIGHT NUMBER  2      TIME 000/00/00/00      RUN NUMBER 00000000

                      LUNAR LONGITUDE= 999.99       LUNAR LATITUDE= 999.99

INITIAL CONDITIONS --- ALBEDO= 0.091      PHASE ANGLE= 76.9 DEGREES      ALTITUDE=   44.4 KILOMETERS

                      RADIATION=  1.2 RADS    SMEAR RATE=   125. MICRONS/SEC    SMEAR ANGLE=  60.0 DEGREES

PREDICTED S/C FILM DENSITY FOR 24 INCH CAMERA AT ALL SHUTTER SPEEDS - SLOW= 0.58  MEDIUM= 0.33  FAST= 0.25

PREDICTED S/C FILM DENSITY FOR  3 INCH CAMERA AT ALL SHUTTER SPEEDS - SLOW= 0.78  MEDIUM= 0.42  FAST= 0.27

                              * * * * * OPTIONS AND RESULTS * * * * *

  SLOW SHUTTER SPEED       SLOPE TARGET       GRE OUTPUT POINT       24 INCH LENS
        ITERATION NUMBER= 0           SLOPE=  1.00 DEGREES       SIGNAL-TO-NOISE RATIO=  7.27
        ITERATION NUMBER= 1           SLOPE=  0.12 DEGREES

  SLOW SHUTTER SPEED        CONE TARGET       GRE OUTPUT POINT       24 INCH LENS
        ITERATION NUMBER= 1         DIAMETER=  1.22 METERS         SIGNAL-TO-NOISE RATIO=  9.08
        ITERATION NUMBER= 2         DIAMETER=  0.70 METERS         SIGNAL-TO-NOISE RATIO=  2.97
        ITERATION NUMBER= 3         DIAMETER=  0.71 METERS

  SLOW SHUTTER SPEED       SLOPE TARGET       GRE OUTPUT POINT       80 MM   LENS
        ITERATION NUMBER= 0           SLOPE=  1.00 DEGREES       SIGNAL-TO-NOISE RATIO=  0.72
        ITERATION NUMBER= 1           SLOPE=  1.23 DEGREES

  SLOW SHUTTER SPEED        CONE TARGET       GRE OUTPUT POINT       80 MM   LENS
        ITERATION NUMBER= 1         DIAMETER=  9.24 METERS         SIGNAL-TO-NOISE RATIO= 16.32
        ITERATION NUMBER= 2         DIAMETER=  3.96 METERS         SIGNAL-TO-NOISE RATIO=  2.30
        ITERATION NUMBER= 3         DIAMETER=  4.52 METERS         SIGNAL-TO-NOISE RATIO=  3.26
        ITERATION NUMBER= 4         DIAMETER=  4.34 METERS
```

Figure 2.5-13: Photo Quality Predict Program (QUAL) Output, Site IIP-11

```
ORBIT NUMBER   0      SITE NUMBER 11      FLIGHT NUMBER  2      TIME 000/00/00/00      RUN NUMBER 00000000

                      LUNAR LONGITUDE= 999.99        LUNAR LATITUDE= 999.99

INITIAL CONDITIONS --- ALBEDO= 0.105      PHASE ANGLE= 62.9 DEGREES      ALTITUDE=   52.0 KILOMETERS

                      RADIATION=  1.2 RADS    SMEAR RATE=   125. MICRONS/SEC    SMEAR ANGLE=  60.0 DEGREES

PREDICTED S/C FILM DENSITY FOR 24 INCH CAMERA AT ALL SHUTTER SPEEDS - SLOW= 1.24  MEDIUM= 0.74  FAST= 0.40

PREDICTED S/C FILM DENSITY FOR  3 INCH CAMERA AT ALL SHUTTER SPEEDS - SLOW= 1.48  MEDIUM= 0.97  FAST= 0.53

                              * * * * * OPTIONS AND RESULTS * * * * *

MEDIUM SHUTTER SPEED       SLOPE TARGET       GRE OUTPUT POINT      24 INCH LENS
        ITERATION NUMBER= 0          SLOPE=  1.00 DEGREES      SIGNAL-TO-NOISE RATIO=  2.99
        ITERATION NUMBER= 1          SLOPE=  0.33 DEGREES

MEDIUM SHUTTER SPEED        CONE TARGET       GRE OUTPUT POINT      24 INCH LENS
        ITERATION NUMBER= 1       DIAMETER=  1.27 METERS      SIGNAL-TO-NOISE RATIO=  2.97
        ITERATION NUMBER= 2       DIAMETER=  1.28 METERS

MEDIUM SHUTTER SPEED       SLOPE TARGET       GRE OUTPUT POINT      80 MM   LENS
        ITERATION NUMBER= 0          SLOPE=  1.00 DEGREES      SIGNAL-TO-NOISE RATIO=  0.25
        ITERATION NUMBER= 1          SLOPE=  3.65 DEGREES

MEDIUM SHUTTER SPEED        CONE TARGET       GRE OUTPUT POINT      80 MM   LENS
        ITERATION NUMBER= 1       DIAMETER= 12.07 METERS      SIGNAL-TO-NOISE RATIO=  9.02
        ITERATION NUMBER= 2       DIAMETER=  6.96 METERS      SIGNAL-TO-NOISE RATIO=  2.68
        ITERATION NUMBER= 3       DIAMETER=  7.36 METERS
```

Figure 2.5-14: Photo Quality Predict Program (QUAL) Output, Site IIP-12a

```
ORBIT NUMBER   0      SITE NUMBER 12a     FLIGHT NUMBER  2      TIME 000/00/00/00      RUN NUMBER 00000000

                      LUNAR LONGITUDE= 999.99        LUNAR LATITUDE= 999.99

INITIAL CONDITIONS --- ALBEDO= 0.087      PHASE ANGLE= 72.8 DEGREES      ALTITUDE=   44.2 KILOMETERS

                      RADIATION=  1.2 RADS    SMEAR RATE=   125. MICRONS/SEC    SMEAR ANGLE=  60.0 DEGREES

PREDICTED S/C FILM DENSITY FOR 24 INCH CAMERA AT ALL SHUTTER SPEEDS - SLOW= 0.76  MEDIUM= 0.40  FAST= 0.27

PREDICTED S/C FILM DENSITY FOR  3 INCH CAMERA AT ALL SHUTTER SPEEDS - SLOW= 0.99  MEDIUM= 0.54  FAST= 0.31

                              * * * * * OPTIONS AND RESULTS * * * * *

 SLOW SHUTTER SPEED       SLOPE TARGET       GRE OUTPUT POINT      24 INCH LENS
        ITERATION NUMBER= 0          SLOPE=  1.00 DEGREES      SIGNAL-TO-NOISE RATIO=  6.24
        ITERATION NUMBER= 1          SLOPE=  0.16 DEGREES

 SLOW SHUTTER SPEED        CONE TARGET       GRE OUTPUT POINT      24 INCH LENS
        ITERATION NUMBER= 1       DIAMETER=  1.20 METERS      SIGNAL-TO-NOISE RATIO=  6.21
        ITERATION NUMBER= 2       DIAMETER=  0.83 METERS      SIGNAL-TO-NOISE RATIO=  2.96
        ITERATION NUMBER= 3       DIAMETER=  0.84 METERS

 SLOW SHUTTER SPEED       SLOPE TARGET       GRE OUTPUT POINT      80 MM   LENS
        ITERATION NUMBER= 0          SLOPE=  1.00 DEGREES      SIGNAL-TO-NOISE RATIO=  0.65
        ITERATION NUMBER= 1          SLOPE=  1.49 DEGREES

 SLOW SHUTTER SPEED        CONE TARGET       GRE OUTPUT POINT      80 MM   LENS
        ITERATION NUMBER= 1       DIAMETER= 11.31 METERS      SIGNAL-TO-NOISE RATIO= 18.41
        ITERATION NUMBER= 2       DIAMETER=  4.57 METERS      SIGNAL-TO-NOISE RATIO=  2.28
        ITERATION NUMBER= 3       DIAMETER=  5.24 METERS      SIGNAL-TO-NOISE RATIO=  3.28
        ITERATION NUMBER= 4       DIAMETER=  5.01 METERS
```

Figure 2.5-15: Photo Quality Predict Program (QUAL) Output, Site IIP-12b

```
ORBIT NUMBER   0      SITE NUMBER 12b     FLIGHT NUMBER  2      TIME 000/00/00/00      RUN NUMBER 00000000

                      LUNAR LONGITUDE= 999.99        LUNAR LATITUDE= 999.99

INITIAL CONDITIONS --- ALBEDO= 0.087      PHASE ANGLE= 71.4 DEGREES      ALTITUDE=   44.9 KILOMETERS

                      RADIATION=  1.2 RADS    SMEAR RATE=   125. MICRONS/SEC    SMEAR ANGLE=  60.0 DEGREES

PREDICTED S/C FILM DENSITY FOR 24 INCH CAMERA AT ALL SHUTTER SPEEDS - SLOW= 0.82  MEDIUM= 0.44  FAST= 0.28

PREDICTED S/C FILM DENSITY FOR  3 INCH CAMERA AT ALL SHUTTER SPEEDS - SLOW= 1.06  MEDIUM= 0.59  FAST= 0.33

                              * * * * * OPTIONS AND RESULTS * * * * *

MEDIUM SHUTTER SPEED       SLOPE TARGET       GRE OUTPUT POINT      24 INCH LENS
        ITERATION NUMBER= 0          SLOPE=  1.00 DEGREES       SIGNAL-TO-NOISE RATIO=  4.39
        ITERATION NUMBER= 1          SLOPE=  0.23 DEGREES

MEDIUM SHUTTER SPEED       CONE TARGET        GRE OUTPUT POINT      24 INCH LENS
        ITERATION NUMBER= 1       DIAMETER=  1.21 METERS          SIGNAL-TO-NOISE RATIO=  4.73
        ITERATION NUMBER= 2       DIAMETER=  0.96 METERS          SIGNAL-TO-NOISE RATIO=  3.06
        ITERATION NUMBER= 3       DIAMETER=  0.95 METERS

MEDIUM SHUTTER SPEED       SLOPE TARGET       GRE OUTPUT POINT      80 MM  LENS
        ITERATION NUMBER= 0          SLOPE=  1.00 DEGREES       SIGNAL-TO-NOISE RATIO=  0.58
        ITERATION NUMBER= 1          SLOPE=  1.67 DEGREES

MEDIUM SHUTTER SPEED       CONE TARGET        GRE OUTPUT POINT      80 MM  LENS
        ITERATION NUMBER= 1       DIAMETER=  8.51 METERS          SIGNAL-TO-NOISE RATIO=  9.56
        ITERATION NUMBER= 2       DIAMETER=  4.77 METERS          SIGNAL-TO-NOISE RATIO=  2.69
        ITERATION NUMBER= 3       DIAMETER=  5.03 METERS
```

Figure 2.5-16: Photo Quality Predict Program (QUAL) Output, Site IIP-13a

```
ORBIT NUMBER   0      SITE NUMBER 13a     FLIGHT NUMBER  2      TIME 000/00/00/00      RUN NUMBER 00000000

                      LUNAR LONGITUDE= 999.99        LUNAR LATITUDE= 999.99

INITIAL CONDITIONS --- ALBEDO= 0.073      PHASE ANGLE= 71.8 DEGREES      ALTITUDE=   45.3 KILOMETERS

                      RADIATION=  1.2 RADS    SMEAR RATE=   125. MICRONS/SEC    SMEAR ANGLE=  60.0 DEGREES

PREDICTED S/C FILM DENSITY FOR 24 INCH CAMERA AT ALL SHUTTER SPEEDS - SLOW= 0.69  MEDIUM= 0.37  FAST= 0.26

PREDICTED S/C FILM DENSITY FOR  3 INCH CAMERA AT ALL SHUTTER SPEEDS - SLOW= 0.91  MEDIUM= 0.49  FAST= 0.30

                              * * * * * OPTIONS AND RESULTS * * * * *

 SLOW SHUTTER SPEED        SLOPE TARGET       GRE OUTPUT POINT      24 INCH LENS
        ITERATION NUMBER= 0          SLOPE=  1.00 DEGREES       SIGNAL-TO-NOISE RATIO=  5.98
        ITERATION NUMBER= 1          SLOPE=  0.17 DEGREES

 SLOW SHUTTER SPEED        CONE TARGET        GRE OUTPUT POINT      24 INCH LENS
        ITERATION NUMBER= 1       DIAMETER=  1.25 METERS          SIGNAL-TO-NOISE RATIO=  6.40
        ITERATION NUMBER= 2       DIAMETER=  0.85 METERS          SIGNAL-TO-NOISE RATIO=  2.98
        ITERATION NUMBER= 3       DIAMETER=  0.86 METERS

 SLOW SHUTTER SPEED        SLOPE TARGET       GRE OUTPUT POINT      80 MM  LENS
        ITERATION NUMBER= 0          SLOPE=  1.00 DEGREES       SIGNAL-TO-NOISE RATIO=  0.56
        ITERATION NUMBER= 1          SLOPE=  1.73 DEGREES

 SLOW SHUTTER SPEED        CONE TARGET        GRE OUTPUT POINT      80 MM  LENS
        ITERATION NUMBER= 1       DIAMETER= 10.71 METERS          SIGNAL-TO-NOISE RATIO= 14.19
        ITERATION NUMBER= 2       DIAMETER=  4.93 METERS          SIGNAL-TO-NOISE RATIO=  2.46
        ITERATION NUMBER= 3       DIAMETER=  5.44 METERS          SIGNAL-TO-NOISE RATIO=  3.16
        ITERATION NUMBER= 4       DIAMETER=  5.30 METERS
```

Figure 2.5-17: Photo Quality Predict Program (QUAL) Output, Site IIP-13b

```
ORBIT NUMBER   0      SITE NUMBER 13b     FLIGHT NUMBER  2      TIME 000/00/00/00      RUN NUMBER 00000000
                      LUNAR LONGITUDE= 999.99        LUNAR LATITUDE= 999.99
INITIAL CONDITIONS -- ALBEDO= 0.073      PHASE ANGLE= 70.4 DEGREES      ALTITUDE=   46.4 KILOMETERS
                      RADIATION=  1.2 RADS    SMEAR RATE=   125. MICRONS/SEC    SMEAR ANGLE=  60.0 DEGREES
PREDICTED S/C FILM DENSITY FOR 24 INCH CAMERA AT ALL SHUTTER SPEEDS - SLOW= 0.74  MEDIUM= 0.40  FAST= 0.27
PREDICTED S/C FILM DENSITY FOR  3 INCH CAMERA AT ALL SHUTTER SPEEDS - SLOW= 0.97  MEDIUM= 0.53  FAST= 0.31
                                  * * * * * OPTIONS AND RESULTS * * * * *
MEDIUM SHUTTER SPEED       SLOPE TARGET       GRE OUTPUT POINT      24 INCH LENS
        ITERATION NUMBER= 0          SLOPE=  1.00 DEGREES      SIGNAL-TO-NOISE RATIO=  3.65
        ITERATION NUMBER= 1          SLOPE=  0.27 DEGREES
MEDIUM SHUTTER SPEED       CONE TARGET        GRE OUTPUT POINT      24 INCH LENS
        ITERATION NUMBER= 1       DIAMETER=  1.31 METERS       SIGNAL-TO-NOISE RATIO=  4.46
        ITERATION NUMBER= 2       DIAMETER=  1.08 METERS       SIGNAL-TO-NOISE RATIO=  3.08
        ITERATION NUMBER= 3       DIAMETER=  1.06 METERS
MEDIUM SHUTTER SPEED       SLOPE TARGET       GRE OUTPUT POINT      80 MM  LENS
        ITERATION NUMBER= 0          SLOPE=  1.00 DEGREES      SIGNAL-TO-NOISE RATIO=  0.49
        ITERATION NUMBER= 1          SLOPE=  1.98 DEGREES
MEDIUM SHUTTER SPEED       CONE TARGET        GRE OUTPUT POINT      80 MM  LENS
        ITERATION NUMBER= 1       DIAMETER=  8.79 METERS       SIGNAL-TO-NOISE RATIO=  8.51
        ITERATION NUMBER= 2       DIAMETER=  5.22 METERS       SIGNAL-TO-NOISE RATIO=  2.72
        ITERATION NUMBER= 3       DIAMETER=  5.48 METERS
```

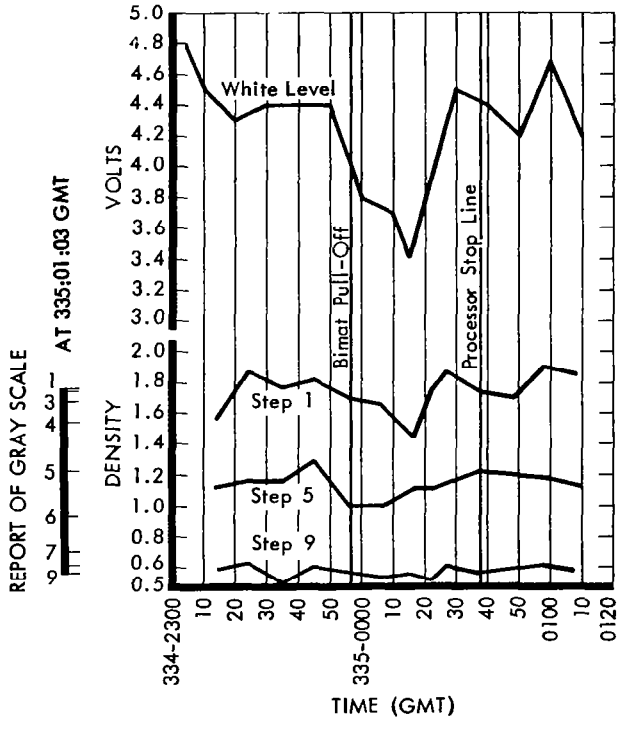

Figure 2.5-18: White Level and Gray Scale Variation Near Processing Defects Readout Sequence 087

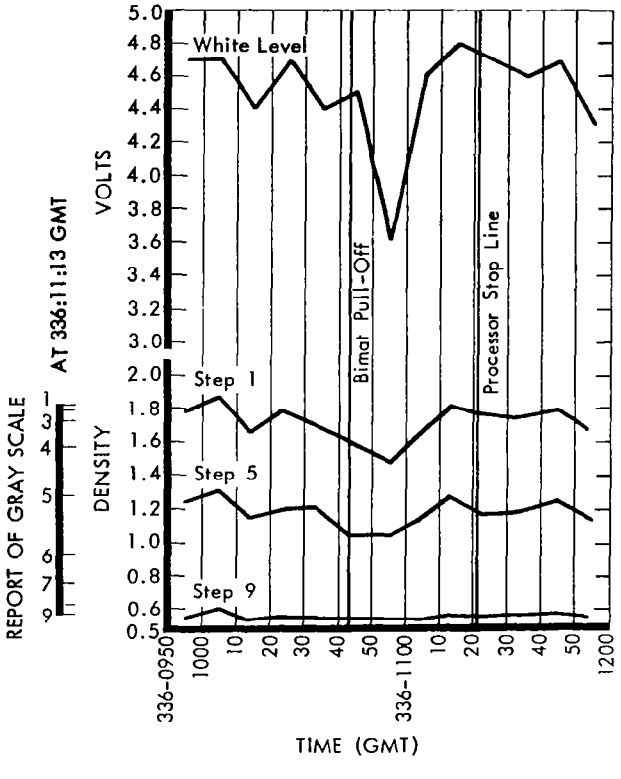

Figure 2.5-19: White Level and Gray Scale Variation Near Processing Defects Readout Sequence 097

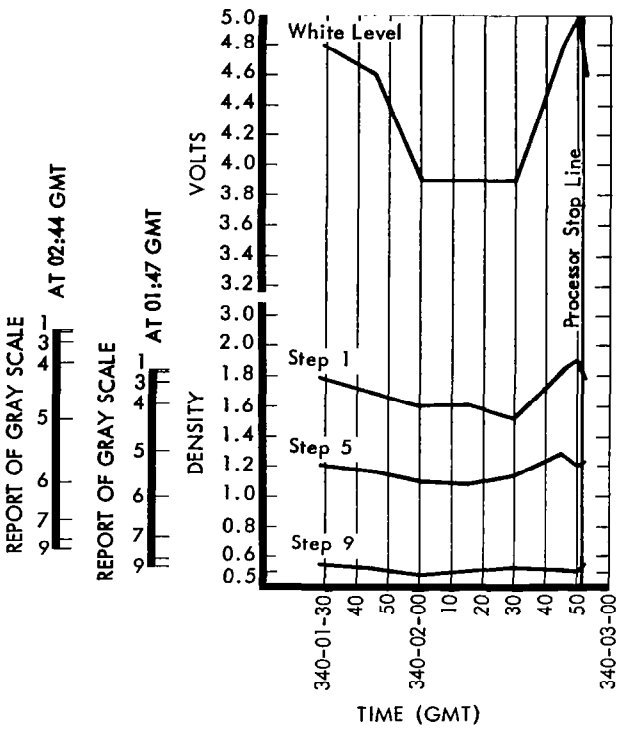

Figure 2.5-20: White Level and Gray Scale Variation Readout Sequence 122

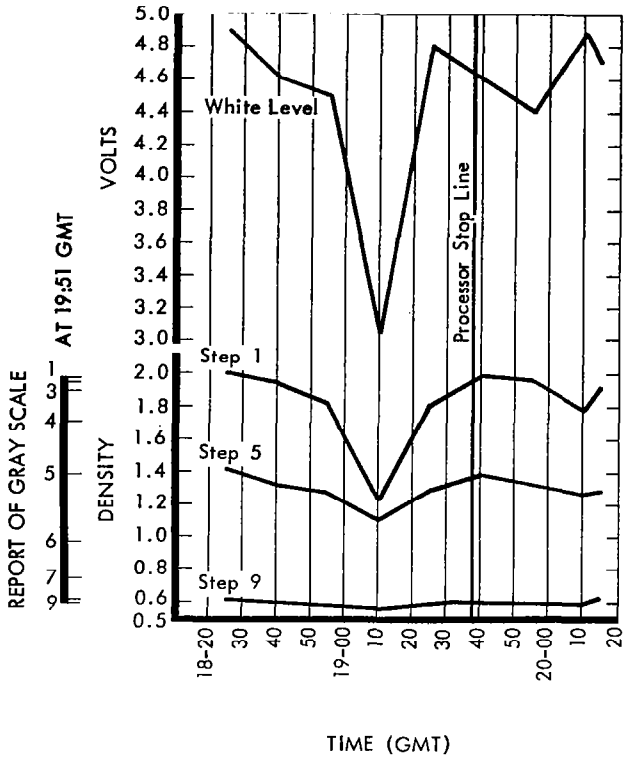

Figure 2.5-21: White Level and Gray Scale Variation Readout Sequence 127

2.5.3.2 Decrease in White Level During Readout

A phenomenon, not reported earlier, became apparent during Readout Sequences 115, 116, and 117 (Refer to Figure 2.5-22). The white level at the end of readout 115 was, reportedly, 4.3 volts. At the beginning of the next readout, 116, the white level was 4.7 volts. During the 120-minute readout, the white level average value decreased steadily and ended at 4.1 volts. At the beginning of Sequence 117, in the focus stop position, the white level jumped to 4.5 volts.

One gain increase brought this value up to 4.9 volts. Again the average white level decreased during readout and was 4.0 at the end of readout. The probable cause of this is photomultiplier tube degradation. Various methods of compensation are being considered for Mission III. The procurement specification states maximum "on" time of 93 minutes. But even before 93 minutes the decrease was considerable. The gray scale data is too scattered to draw any conclusions. If more data existed, it might be possible to separate photo video chain (PVC) decrease from the change in density. No processor stop lines or other Bimat processing defects were reported by the video engineer for these frames readout in sequences 115, 116, and 117.

2.5.3.3 Variation of Density as A Function of W Signature

Focus of the line-scan tube affects the level of the video signal during a scan across the width of a framelet. Ideally, the level would be constant for a constant film density. However, the angular sweep of the light spot produces a variation in intensity. Optimum focus produces a small variation that takes the form of a low rounded "W" on the GRE A-scope. This variation is reflected as a density variation across the framelet on the reconstructed record. As a result of the "W" focus pattern, the density variation can range from a maximum of 2.0 in the peak density to a minimum of 1.7. Therefore, care was taken by the video engineer to make measurements in a framelet that had a complete gray scale within it. Even with this precaution, because of the nonsymmetry of the "A" pattern (an "A" framelet's densities are the mirror image of a "B" framelet's), the spread in gray scales read from various framelets makes correlation difficult.

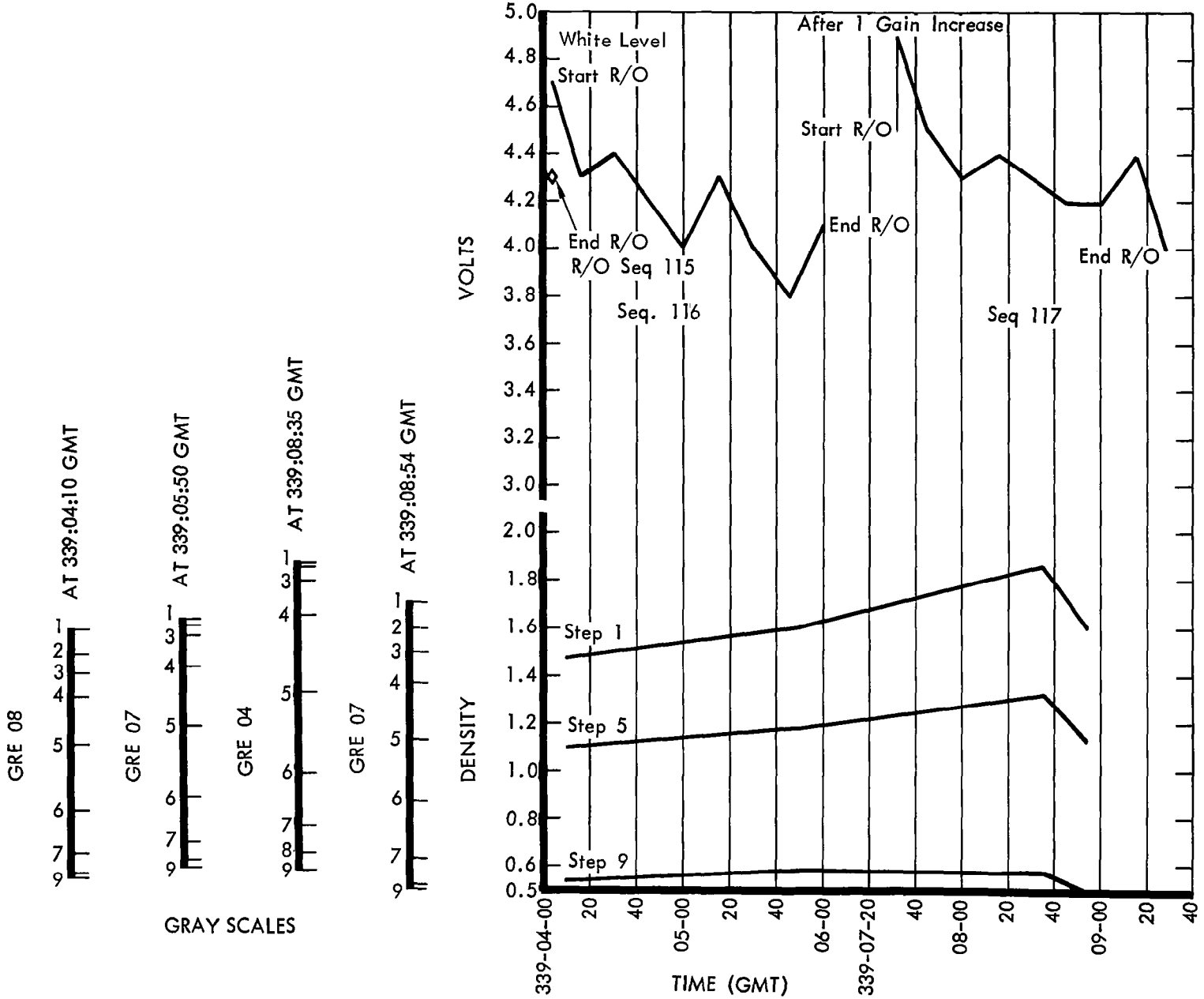

Figure 2.5-22: White Level Variation, Readout Sequences 115, 116, and 117

2.6 CONCLUSIONS

The photographic portion of Lunar Orbiter Mission II is considered to be very nearly a complete success. All scheduled sites were photographed and 98.5% of the photography was reconstructed before readout was terminated when the traveling-wave-tube amplifier (TWTA) failed to turn on.

A few frames of Site IIP-7 were affected by an unusual amount of lace defect in processing.

The specified resolution was achieved at all sites in both wide-angle and telephoto coverage. Fall-off of resolution was noted toward frame edges as expected due to optical and photometric factors, and in frames or portion of frames where exposure level was near or beyond limiting values. In some localized areas surface topography resulted in more nearly grazing illumination that increased contrasts. In such instances, features smaller than system specifications requirements can be detected.

The location of Ranger VIII was photographed successfully. The impact point has been identified by the NASA Lunar Orbiter photo data screening group as one of two small, bright craters. This location may be found near the center of Telephoto Frame 70, about 2.25 framelet widths from the side opposite the edge data and close to the junction of framelets 601 and 602.

The attempt to obtain convergent stereo coverage at Site IIS-2 was successful, although readout scanning characteristics introduce distortions that degrade stereo quality. Side overlap at eight primary sites was sufficient to provide stereo coverage of some telephoto photographs.

The oblique coverage obtained at four secondary sites photographed by single dualframes is of excellent quality. Frame 162 of Site IIS-12, Copernicus, and Frame 213 of Site IIS-16, Marius, are particularly outstanding.

NASA-Langley, 1967 — 31 CR-931

"The aeronautical and space activities of the United States shall be conducted so as to contribute . . . to the expansion of human knowledge of phenomena in the atmosphere and space. The Administration shall provide for the widest practicable and appropriate dissemination of information concerning its activities and the results thereof."

—NATIONAL AERONAUTICS AND SPACE ACT OF 1958

NASA SCIENTIFIC AND TECHNICAL PUBLICATIONS

TECHNICAL REPORTS: Scientific and technical information considered important, complete, and a lasting contribution to existing knowledge.

TECHNICAL NOTES: Information less broad in scope but nevertheless of importance as a contribution to existing knowledge.

TECHNICAL MEMORANDUMS: Information receiving limited distribution because of preliminary data, security classification, or other reasons.

CONTRACTOR REPORTS: Scientific and technical information generated under a NASA contract or grant and considered an important contribution to existing knowledge.

TECHNICAL TRANSLATIONS: Information published in a foreign language considered to merit NASA distribution in English.

SPECIAL PUBLICATIONS: Information derived from or of value to NASA activities. Publications include conference proceedings, monographs, data compilations, handbooks, sourcebooks, and special bibliographies.

TECHNOLOGY UTILIZATION PUBLICATIONS: Information on technology used by NASA that may be of particular interest in commercial and other non-aerospace applications. Publications include Tech Briefs, Technology Utilization Reports and Notes, and Technology Surveys.

Details on the availability of these publications may be obtained from:

SCIENTIFIC AND TECHNICAL INFORMATION DIVISION

NATIONAL AERONAUTICS AND SPACE ADMINISTRATION

Washington, D.C. 20546